Perfluorinated Amphiphilic Block Copolymers: Structure Formation and Biomedical Applications

Dissertation

Zur Erlangung des akademischen Grades

Doktor-Ingenieur (Dr. -Ing.)

vorgelegt dem

Zentrum für Ingenieurwissenschaften

der Martin-Luther-Universität Halle-Wittenberg

als organisatorische Grundeinheit für Forschung und Lehre im Range einer Fakultät

(§75 Abs. 1 HAG LSA, §19 Abs. 1 Grundordnung)

von Herrn M. Sc. Chiranjeevi Peetla

geb. am 20.07.1977 in Valigonda (India)

Gutachter:

1. Prof. Dr. Jörg Kressler
2. Prof. Dr. Bernd Steuhn

Halle (Saale), den 10-5-2010

Dedicated to my family

Acknowledgements

First of all I would like to express my sincere gratitude to Prof. Dr. Joerg Kressler for giving me an opportunity to work in his group. I am grateful to him for his constant encouragement, valuable suggestions, and inspiration throughout my PhD.

I would like to express my cordial appreciation to Dr. Karsten Busse for his valuable instructions and suggestions throughout my stay in Halle. Special thanks and appreciation are due to my colleagues Dr. H. Hussain, and Dr. Nasir Mahamood for their fruitful discussions related to my research work. I am very thankful to all other colleagues Dr. H. Kausche, Dr. Z. Funke, Dr. H. Budde, Dr. S. Kaiser, Dr. Yanjiao jiang for their cooperation and nice company during my stay. Sincere thanks are extended to Mrs. Claudia Hochbach and Yvonne mobius for their help in solving my day to day problems which any student might face in a foreign land. I would like to acknowledge SFB 418 for financial support of this work.

Finally, I wish to pay my gratitude to my loving family members for their encouragement throughout my studies. I would like to express special thanks to my wife Padmaja. She helped me to concentrate on completing this dissertation and supported mentally during the course of this work. Without her help and encouragement, this study would not have been completed.

This dissertation is based on the following publications:

Chapter 3

1. Peetla C, Busse K, Kressler J. Structured Hydrogels Formed by Amphiphilic Block Copolymers. Polym, Prepr. *(Am. Chem. Soc., Poly. Mat. Eng. Sci),* 90(1), 394-395, 2004.

Chapter 4

2. Peetla C, Graf K. H, Kressler J. Langmuir Monolayer and Langmuir-Blodgett Films of Amphiphilic Triblock Copolymers with Water Soluble Middle Block. *Coll. & Polym. Sci.,* 285, 27-37, 2006.

3. Peetla C, Busse K, Kressler J. Nanostructures in Langmuir Monolayer and Langmuir-Blodgett Films of Amphiphilic Triblock Copolymers with Water Soluble Middle Block. Polym, Prepr. (*Am. Chem. Soc., Poly. Mat. Eng. Sci),* 95, 678-679, 2006.

Chapter 5

4. Busse K, **Peetla C,** Kressler J. Water Surface Covering of Fluorinated Amphiphilic Triblock Copolymers: Surface Pressure-Area and X-ray Reflectivity Investigations. *Langmuir,* 23, 6975-6982, 2007.

Table of Contents

Chapter 4. Langmuir Monolayer and Langmuir-Blodgett Films of Amphiphilic Triblock Copolymers with Water Soluble Middle Block

Chapter 5. Water Surface covering of Fluorinated Amphiphilic Triblock Copolymers: Surface Pressure-Area and X-ray Reflectivity Investigations

Chapter 6. Perfluorinated block copolymer interaction with lipid monolayer

Chapter 1

General Introduction

1.1. Block copolymer self-assembly

Self-assembly is the autonomous organization of components into patterns or structures without human intervention.[1, 2] Self-assembling molecules are amphiphilic in structure. In general, amphiphilicity is imparted to a molecule by spatially segregating the hydrophobic and hydrophilic portions either along the length of the molecule or on distinct faces of a structured molecule.[3,] The hydrophilic portion can be charged (anionic cationic, or zwitterionic) or uncharged. The concept of using amphiphilicity to drive molecular assembly is taken from nature, where amphiphilic molecules such as lipids, peptides, and proteins serve as building blocks to form an astonishing range of complex structures such as lipid membranes, folded proteins, structured nucleic acids, protein aggregates, molecular machines.[1] Self assembly is one of the most general strategies currently available for generating highly ordered nanostructures. Therefore, it plays a significant role in many fields: chemistry, physics, biology, materials science, and nanotechnology. Similar to many self-assembling materials such as surfactants or liquid crystals, block copolymers undergo mesophase transitions due to the changes of external fields. Block copolymers (BCPs) are composed of two or more chemically distinct, and immiscible, polymer blocks covalently bound together. For instance, A-B diblock composed of a linear chain of type A monomers bound on one end to a linear chain of type B monomers. Thermodynamic incompatibility between the A and B blocks drives A-B block molecules to self-organize via microphase separation in which the contact between similar blocks is maximized and between dissimilar blocks it is minimized.[4-8] Macrophase separation is prevented by the entropic forces stemming

from the covalent bonds holding the A and B blocks together. Theories of the morphology transition of diblock copolymers at equilibrium have been studied for more than three decades.[9,10] The nano structure morphology and the domain spacing within the nanostructures depends on the segment size, molecular weight, and the strength of interaction between the blocks represented by the Flory–Huggins interaction parameter χ[11, 12]
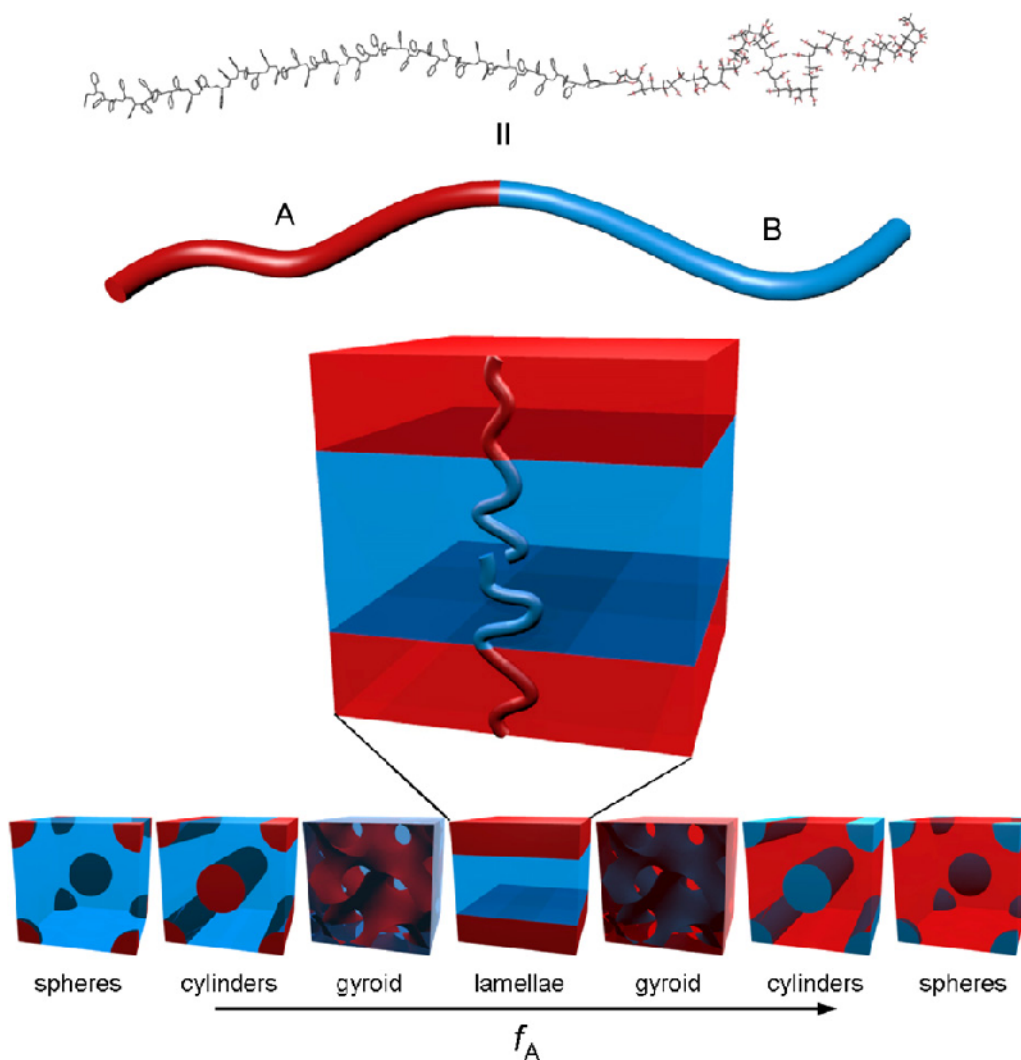
Figure 1.1. Schematic of thermodynamically stable diblock copolymer phases. The A–B diblock copolymer, such as the PS-*b*-PMMA molecule represented at the top, is depicted as a simple two-color chain for simplicity. The chains self-organize such that contact between the immiscible blocks is minimized, with the structure determined primarily by the relative lengths of the two polymer blocks (f_A) (reprinted with copy right permission from ref 13).

The temperature-dependent Flory–Huggins interaction parameter, χ_{AB} describes the free energy cost of contact between dissimilar monomers that governs this process. In addition, the degree of polymerization, N, and the relative composition fractions, f_A and f_B, where $f_A = N_A/N$ and $f_A + f_B = 1$. Common periodic phases for A–B diblocks, with increasing f_A, include bodycentered cubic A spheres in a B matrix, hexagonally packed A cylinders in a B matrix, bicontinuous gyroid, and lamellae.[13] Fig. 1.1. depicts these morphologies with the diblock molecules represented as simplified two-color chains.

Hamley[14] has reviewed recent developments in the use of block copolymer self-assembly to create morphologies that can be used to template the fabrication of nanostructures in other materials. In addition, the patterning of semiconductor surfaces using block copolymer film masks and the use of block copolymer micelles as 'nanoreactors' to prepare metal and semiconductor nanoparticles are discussed. In a separate review, Darling etal.[13] discussed the detailed experimental and theoretical studies aimed at controlling the alignment of BCPs in the bulk, in thin films, and in 3-D confinement. Recently, Tsori etal.[15] has shown that rather simple theoretical treatments can accurately model BCP behavior in the melt, thus opening up opportunities for exploratory studies in this area. Lecommandoux etal.[16] has reviewed the physics of block copolymers in solutions and in the bulk. In particular, they have shown that beyond the classical results on flexible–flexible block copolymer chains, the architecture (rigidity of the blocks, cyclization, etc) as well as external parameters (temperature, pH, ionic strength) play an important role in the different phases of a material made from block copolymers with controlled architectures. All these reviews shows the increasing importance of the block copolymer self assembly.

1.1. Amphiphilic block copolymer self-assembly in water

Block copolymers with sequences of hydrophilic monomers covalently bound to sequences of hydrophobic monomers are called amphiphilic block copolymers (ABCs). In aqueous environment these block copolymers self-assemble to minimize contact between hydrophobic segments and water.[17] The morphology of the resulting aggregate structure, (also known as micelle) depends on molecular architecture of the copolymer, and temperature. For instance, Pluronics 85 (PEO_{27}-b-PPO_{39}-b-PEO_{27}) forms spherical micelles at room temperature,[18] with increasing temperature shape of the micelles was found to be changed from spherical to rod like micelles. The concentration at which micellization occurs is known as critical micelle concentration (*cmc*). Fig.1.2. shows schematic drawing of micelles structures formed by ABCs with different molecular architecture in water. Simple AB, ABA type block copolymers form spherical micelles whereas BAB type of block copolymers form flower like micelles,[19] in which A, B represents hydrophilic and hydrophobic blocks respectively. The *cmc* is higher for the BAB triblock copolymer than the reverse architecture (ABA). This is due to the entropy loss associated with the looping of the middle block. Over the past decade micellization behavior of various ABCs has been extensively investigated and reported.[12-15]
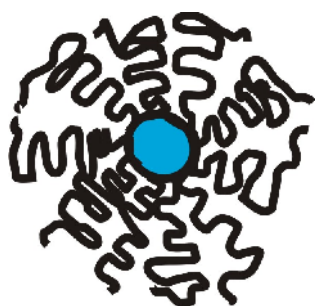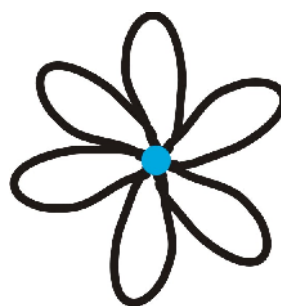
Spherical micelle   Flower micelle

Figure 1.2. Schematic drawing of micelles structures formed by ABCs with different molecular architecture in water.

At higher copolymer concentrations these ABCs form gels. Sol – gel transition of ABCs have been shown to depend on hydrophilic/hydrophobic block ratios,[20] molecular architecture, and temperature.[21] In general, sol – gel transition has shown to occur either with increasing concentarion/temperature of the copolymer for following reasons; dense micellar packing[22] entanglements among hydrophilic blocks of the spherical micelle [23] and physical network formation.[24] Hydrophobic domains of the ABCs gels are arranged in specific pattern to form structured gels. Usually, ABCs gelation behaviour is studied by rheology and the gel structures are investigated by different methods such as real space (imaging) and reciprocal space (scattering).[25, 26] In real space techniques electron microscopy (TEM technique)[27] is widely used, where as in reciprocal space techniques small angle scattering techniques small angle scattering (SAXS)[28-30] small angle neutron scattering (SANS)[31-32]are employed.

Pluronics are ABA type triblock copolymers, they are known as temperature-sensitive polymer. They exhibit sol – gel transition behavior with increasing temperature. Aqueous Pluronic solutions are known to undergo sol-gel transition through a shift from unimer to micelle. Sol - gel transition behaviour was extensively studied by rheology and SAXS, SANS experiments[28-32]. Two different pluronics; pluronic 127, and pluronic 85 have shown to form structured gels at higher concentration and/or temperature in water. However, in pluronic 127 sol-gel transition was observed due to entanglements among the hydrophilic blocks, whereas in pluronic 85 it was due to close packing of micelles. This difference in gelation behaviour was attributed to difference in the length of hydrophilic blocks, in pluronic 85 the hydrophilic block are shorter compared Pluronic 127. Pluronic 94, Pluronic 103 contains short hydrophilic (PEO) block and longer hydrophobic (PPO) block than Pluorinc 85. Pluronic with short hydrophilic blocks form two gel states i.e. they form hard gels at lower temperature and soft gel state at higher temperature.[32, 33]

The most widely studied BAB type triblock copolymers are hydrophobically modified water soluble polymers (HMWSP) commonly known as associate thickeners (AT), e.g.

Hydrophobically modified ethoxylated urethanes, (HEUR)[34-36]. These triblock copolymers consist of poly(ethylene glycol) chain extended by small hydrophobic urethanes and terminated by hydrophobic alcohols. Typically hydrophobic groups range from n-$C_{12}H_{25}$ to n-$C_{22}H_{45}$. Other BAB type block copolymers which have been studied include the poly(ethyleneoxide)-*b*-poly(butyleneoxide)[37], PPO-*b*-PEO-*b*-PPO, and fluorocarbon end-capped HEUR[38]. BAB type block copolymers form loops (the hydrophobic end blocks are in the same micelle) and bridges (the hydrophobic end block are in the different micelle) in water. Fig. 1.3. shows typical lyotrophic phases exhibited by amphiphilic block copolymers in water.

| Cubic phase gel | Hexagonal phase gel | Lamellar phase gel |
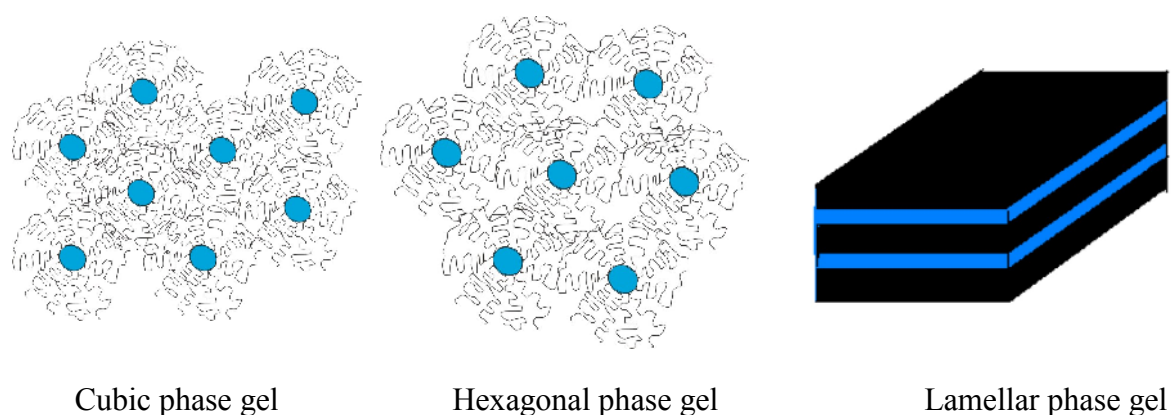
Figure 1.3. Schematic drawing of typical lyotrophic phases exhibited by amphiphilic block copolymers in water.

Several studies showed that the gel properties can be tuned by changing different parameters such as the kind of monomers that are used, the length of the different blocks, and external parameters such as the polymer concentration, pH, and temperature.[39-40] For instance, Hietala et al.[39] studied rheological behavior poly(acrylic acid)-*b*-polystyrene (PAA-*b*-PS) star block copolymers hydrogels. They have investigated the effect of star block copolymer

concentration, temperature by rheology. Higher concentration leads to stronger elastic networks at room temperature, whereas higher temperature has an opposite effect i.e. gel - solution transition. SAXS experiments of the hydrogels, confirm this observation by showing two distinct scattering correlation peaks for concentrated samples indicating hydrophobic association (gel formation) at room temperature. At higher temperatures intensity of the scattering correlation peaks was found to decrease indicating the loss of the network structure due to thermal motion (solution). In contrast, hydrogels of ABA type triblock copolymers with thermosensitive poly(*N*-(2-hydroxypropyl) methacrylamide lactate) A-blocks and a hydrophilic poly(ethylene glycol) B-block have been reported to be became stronger with increasing temperature and concentration.[40] Gelation occurred rapidly upon increasing the temperature to 37 °C.

In separate study,[41] the gelation behavior of poly-L-lysine-*b*-poly-L-leucine diblock and poly-L-lysine-*b*-poly-L-leucine-*b*-poly-L-lysine triblock copolypeptides was investigated by rheological properties. It was showed that the rodlike helical secondary structure poly-L-leucine blocks was critical for gelation and the mechanical properties of the gels can be tuned through the molecular architecture of the block copolypeptides and also by carefully mixing different polypeptides in solution.

1.3. Amphiphilic block copolymer self assembly at the air-water interface and on solid substrates

ABCs are widely used as stabilizing agents in pharmaceutical formulations, personal care products and detergents. Therefore it is essential to understand the processes near the interfaces to fully exploit these block copolymer in pharmaceutical, and other nano-technological applications.[42, 43] The interfacial properties of the ABCs have been widely investigated by the Langmuir technique. Langmuir monolayers are prepared by spreading ABCs at the air-water interface from chloroform solutions.[44] Upon spreading, ABCs form monolayers at the air-water interface; the hydrophobic block (block with lowest surface energy) will preferentially accumulate at the interface, where as the hydrophilic block (block with lowest interfacial energy) will be attracted to the aqueous subphase.[45] ABCs monolayers have attracted much attention because various kinds of nano-scale aggregates with predictable morphologies can be formed by controlling the molecular weight, molecular structure, relative length of each block, and concentration of the spreading solution.[46-49] In addition, the Langmuir technique allows the control of the nanostructures formed at the air-water interface by compression or expansion of monolayer through moving barriers. The barriers can either increase or decrease the area available for the molecules. The properties of monolayers can be derived from the surface pressure - area measurements. The conformational changes of the polymer chains and the two dimensional aggregate formation at the interface can be observed in situ by surface-sensitive techniques such as x-ray reflectivity, neutron reflectivity, brewster angle microscopy (BAM).[50, 51]

Langmuir monolayer behavior of PEO based block copolymer with different hydrophobic blocks; poly(propylene oxide) (PPO),[52] poly(ethyl ethylene) (PEE),[53, 54] poly(hydrogenated isoprene) (PhI) [55], poly(1,1-diethylsilabutane) (PdESB) [56] or poly(styrene) (PS)[57, 58] on water surface are extensively investigated. Typically the Langmuir isotherm of

these copolymers shows three distinct regions with one phase-transition. Alexander et al.[59] described the phase transition as the formation of pancake-like structures at large molecular areas transforming into brushes at lower molecular areas with an intermediate plateau region corresponding to the dissolution of the PEO block. Upon compression, the hydrophobic blocks aggregate at the interface, while the hydrophilic PEO block dissolves into the water sub-phase.

The Langmuir monolayers and two dimensional aggregate structures formed at interface can be transferred on to the solid substrates such as mica, silicon. Controlled patterning of amphiphilic block copolymers can be achieved using Langmuir-Blodgett technique.[60-62] The Langmuir-Blodgett (LB) technology is perhaps the most promising of such techniques because it allows the fabrication of ultra thin, highly ordered films on solid substrates. In the LB method, a one molecule thick layer (Langmuir monolayer) spread at the air-water interface is transferred onto a solid substrate, a process that can be repeated several times with the same substrate to form multilayer films. Njikang etal.[63] investigated self assembling behavior of arborescent PS-g-PEO copolymers. Based on AFM images of block copolymers LB films; they have concluded that by changing the composition and the structure of arborescent PS-g-PEO copolymers, the association behavior can be modified to favor the formation of either ribbon-like superstructures of uniform width, large island-like clusters with a wide size distribution, or non-associated micelles of uniform size.

PS-*b*-PEO block copolymers with different molecular architecture are shown to form surface micelles. Well-organized structures can be formed, when the microphase segregation of the polymer is driven through the choice of solvent and grafting density on the solids[63] Three different mechanisms were reported to explain the domain formation in linear ABCs LB films. According to Goncalves da Silva et al.[64] block copolymers form micelles in the spreading solution already. Upon spreading they form surface micelles, which become more

densely packed with increasing surface pressure. In contrast, An et al.[65] and Israelachvili[66] suggested that the polymers were spread as unimers onto the subphase and aggregate upon compression. Cox et al.[67] stated that linear block copolymers deposit as a combination of both models. PS-*b*-PMMA diblock copolymers, in which both PS and PMMA blocks are water-insoluble, the copolymer molecules remain at the air-water interface and self-assemble at high surface coverage, forming surface micelles. At low surface pressures, the surface active PMMA forms an expanded monolayer at the interface and the hydrophobic PS block forms condensed globules.[68] Upon compression, the PMMA chains are forced to densely pack with the ester groups oriented toward the water subphase, while the glassy PS block anchors the polymer floating film to the interface and thus ensure the stability of surface aggregates.

Sevaral authors showed that block copolymer characteristic parameters such as polymer architecture, chain length/polarity, and external parameters such as surface density, subphase pH can all strongly influence their self-assembly at the A/W interface and on the solid substrates.

Joncheray etal.[69] studied self assembling behavior of two different dendrimerlike block copolymers based on polystyrene and poly(*tert*-butylacrylate) (PS-*b*-P*t*BA) or poly(acrylic acid) (PS-*b*-PAA) at air-water interface and on the solid substrates. PS-*b*-P*t*BA forms thermodynamically stable Langmuir monolayers and self-assembles into circular surface micelles upto 24 mN/m whereas, PS-*b*-PAA did not form stable monolayers at high pH. This was attributed to lack of surface activity of poly(acrylic acid). It is surface-active only under acidic pH conditions. Under acidic conditions, the isotherm showed the presence of a pseudoplateau at 5 mN/m characteristic of a phase transition that corresponds to a pancake-to-brush transition, with the progressive aqueous dissolution of the PAA segments underneath the anchoring PS cores. Circular surface micelles for pressures below the pseudoplateau with a very low aggregation number (Fig.1.4).
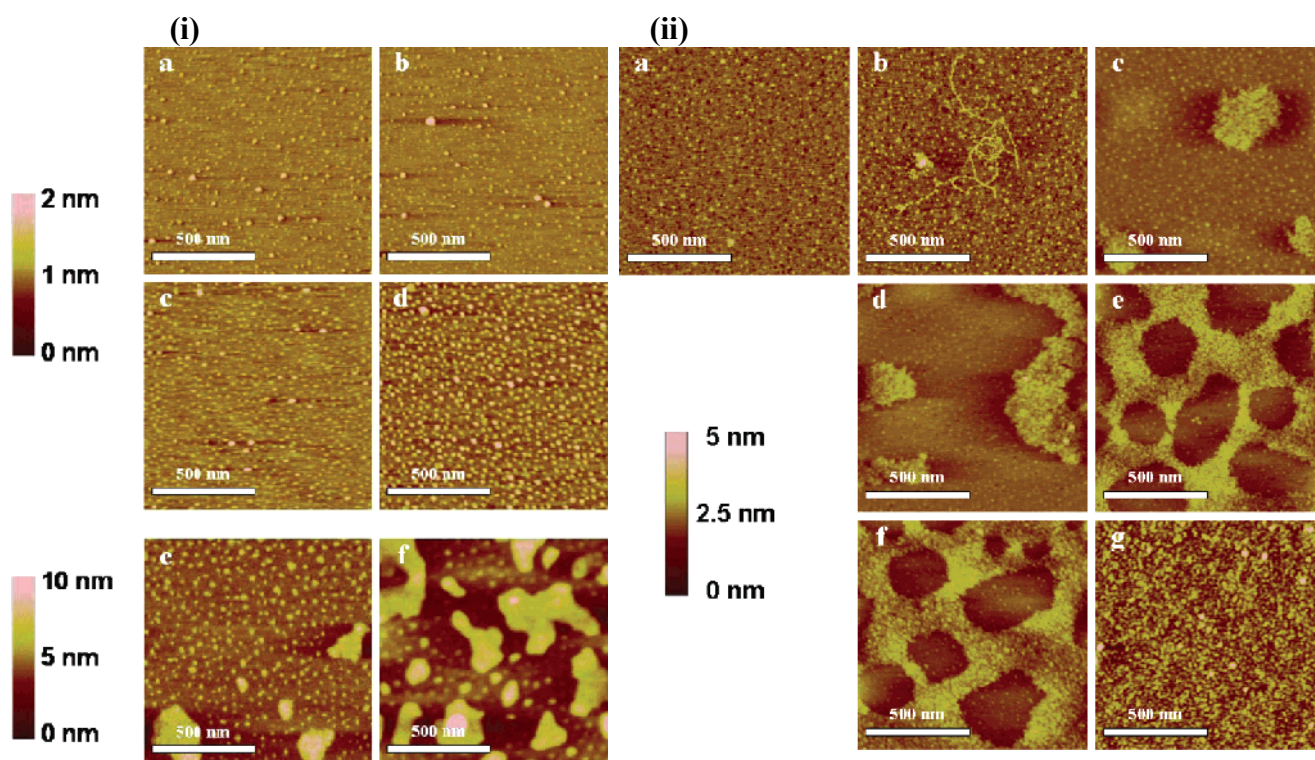
Figure 1. 4. (i). Topographic AFM images of PS-*b*-P*t*BA LB films transferred at 5 mN/m (a),

10 mN/m (b), 15 mN/m (c), 20 mN/m (d), 24 mN/m (middle of plateau, MMA) 20 000 Å2)

(e), and 40 mN/m (f). (ii). Topographic AFM images of PS-*b*-PAA LB films transferred at 2

mN/m (a), 4 mN/m (b), 4.5 mN/m (c), 5 mN/m (d), 5.5 mN/m (e), 6 mN/m (f), and 8 mN/m

(g). reprinted with copy right permission from ref-69.

Xie et al.[70] investigated the interfacial behavior of poly(isoprene)-*b*-poly(ethylene

oxide) (PI-*b*-PEO) and   poly(isoprene)-*b*-poly(acrylic acid) PI-*b*-PAA diblock copolymers

mixed layers using the Langmuir balance technique and neutron reflectivity. From the result it

was concluded that the monolayer behavior depends on pH and hydrogen –bonding

complexation. At pH 2.5 the π-*A* isotherm of PI-*b*-PEO and PI-*b*-PAA mixed monolayers did

not show pseudoplateau region corresponding to PEO segment desorption. This behavior was

attributed to hydrogen-bonding complexation between the undissociated carboxylic acids and

the PEO. It appears that desorption of PEO segments is hindered as a consequence of this complexation.

1.4. Applications of block copolymers

Block copolymers micelles are known for their potential biomedical applications.[71-73]. They form micelles in the range of 10-100 nm in diameter, which can mimic naturally occurring biological transport systems such as lipoproteins. Due to their nano-size they can facilitates their extravasations at tumor sites while avoiding renal clearance and reticuloendothelial uptake.[72] Block copolymer micelles are highly stable in aqueous solutions due to their intrinsic low cmc, which prevents dissociation of micelles upon dilution into blood stream after intravenous injection. ABCs gels are being used as delivery systems or separation media in biological or pharmaceutical applications.[74] In block copolymer gels hydrophobic and hydrophilic domains are regular distributed on nano meter scale, thus provide mechanical properties to the gels. It is established that capillary electrophoresis method is superior to conventional slab gel electrophoresis method for the separation of biopolymers such as proteins and DNA fragments. Gel phases of Pluronic F127 ($E_{99}P_{69}E_{99}$. with E and P being oxyethylene and oxypropylene respectively) in 1 X TBE buffer (Tris-Borate EDTA) was used successfully in separating double stranded DNA fragments and single-stranded oligonucletides size markers by capillary electrophoresis method[75, 76] Being a typical amphiphilic block copolymer, $E_{99}P_{69}E_{99}$ tends to self-associate into micellar structures, at room temperatures they form cubic liquid crystalline gel in buffer solution used for DNA separation. At low temperatures below 5 °C they are in solution of very low viscosity which facilitates filling the gel into the capillaries.

Amphiphilic block copolymers are being investigated for their application in stabilisation of emulsions and foam for biomedical applications.[77-79] ABA type of amphiphilic block copolymers showed promising properties when compared to protein stabilisers.[80] ABA type

triblock copolymers forms polymer brushes at interfaces. The reason for considering amphiphilic block copolymers as more advantageous to other stabilisers is their strong adsorption to oil-water and air-water interfaces, providing effective steric barrier which prevents flocculation or coalescence of emulsion droplets or foam bubbles. Poloxomer 188 (P188) type block copolymers have been shown to be effective against injuries. Poloxomer 188 effectively seals the damaged membranes of skeletal muscle cells, thus prevents leakage of intracellular components. Sealing capability of P188 was shown by using Langmuir lipid monolayers as model membrane system.[81].

Block copolymers, are known to interact with cell membranes. Several studies have been shown that pluronics cause pronounced chemosensitization of tumor cells which exhibit drug resistance to anticancer drugs.[82] This effect was attributed to inhibition of the P-glycoprotein responsible for drug efflux by interacting with the membrane lipids surrounding this protein. In addition, these block copolymers showed membrane destabilizing ability. Membrane destabiling ability was depedent on both pluronic bulk hydrophobicity and the chemical microstructure.[83] Pluronics have shown to cause higher acceleration of doxorubicin permeation than polysurfactants.

1.5. Conclusions

My thesis research focused primarily on investigating the self assembly of perfluorinated block copolymer in water, at the air-water interface, on solid substrates and potential biomedical application. I have used diblock and triblock perfluorinated amphiphilic block copolymer: poly(ethyleneoxide)-*b*-poly(pefluoro hexyl ethyl methacrylate) (PEO-PFMA) with different molecular parameters. The triblock copolymers consist of water soluble PEO in the middle with hydrophobic PFMA outer blocks. Self assembling behavior of these block copolymers was studied using dynamic light scattering (DLS), rheology, Langmuir film balance, atomic force microscopy (AFM), and most advanced X-ray scatterings methods such as SAXS and XR. Amphiphilic block copolymer molecular properties and the basic principles of the various methods used will be discussed in the next chapter. Chapter 3, Chapter 4, Chapter 5, and Chapter 6 form the core of this thesis.

DLS and rheology data showed that the perfluorinated ABA triblock copolymers can form physical gels. The hydrophobic block has effect on gel strength, whereas the hydrophilic block influences the critical gel concentration. SAXS data indicated improved longrange order with increasing concentration of triblock copolymer in water. Amphiphilic triblock copolymers can also form stable monolayers at air-water interface. It is observed that a small PFMA content (less than 13 wt% of the copolymer) can influence the brush formation of the PEO block. An extended plateau for all copolymers shows the typical phase-transition from pancake to brush for the PEO chains. An additional plateau in the brush regime is attributed to rearrangement of PFMA blocks from horizontal to vertical. The plateau observed in the brush regime was assigned for horizontal to perpendicular rearrangement of flexible hydrophobic PFMA chain at the air-water interface. The water soluble $PEO_{10}F9$ triblock copolymer shows no second pseudo plateau in the isotherm and no enrichment of FMA parts could be observed at the air-water interface during compression. The triblock copolymers can ($PEO_{20}F9$) penetrate when the lipid packing density is low. Assuming that the lipid monolayer at low

lipid packing density mimics the damaged cell bilayer, the penetration of block copolymers helps the damaged membrane to regain barrier control. At higher lipid density, the block copolymer was squeezed out of the DPhPC lipid monolayer. This extraordinary ability of block copolymer to selectively insert when needed and leave once the membrane regained its structural integrity are major features that promise perfluorinated block copolymer ($PEO_{20}F9$) to be a good therapeutic agent for various biomedical applications.

Chapter 2

Experimental

2.1. Perfluorinated amphiphilic block copolymers

In this study, we have used PEO-PFMA diblock, triblock copolymers. The chemical structure of the triblock copolymers used in this study was shown in Fig. 2.1. Triblock copolymers consist of water soluble PEO in the middle with hydrophobic PFMA outer blocks. The block copolymers used in this study were synthesized and characterized in accordance to the previously reported procedure.[84] PEO with 5 Kg mol^{-1}, 10 Kg mol^{-1}, 20 Kg mol^{-1} were used. Molecular properties of the block copolymers were presented in Table 2.1. The reported molar mass (M_n) values are based on size exclusion chromatography (SEC) data where the calibration is carried out using PEO standards. Table 2.1. shows the block copolymer molar mass are lower than molar mass of the PEO homopolymer used for synthesis of the copolymer. For example, PEO$_{10}$F9 has a molar mass of 9.4 kg mol^{-1} whereas the PEO middle block has a molar mass of 10 kg mol^{-1}. The lower molar mass of copolymer is the result of decreased hydrodynamic volume in SEC experiments due to the contraction of fluorine containing blocks.[84] The abbreviation scheme PEOxFy has been used, where x represented PEO molar mass in kg mol^{-1} and y represented PFMA wt% in the block copolymer. In the case of diblock copolymers, an additional -D is added to the name. For instance, PEO$_{20}$F4 is a triblock copolymer with 4 wt% PFMA in the outer blocks and 20 kg mol^{-1} PEO middle block. PEO$_5$F32-D is a diblock copolymers with 5 kg mol^{-1} and 32 wt% of PFMA block.
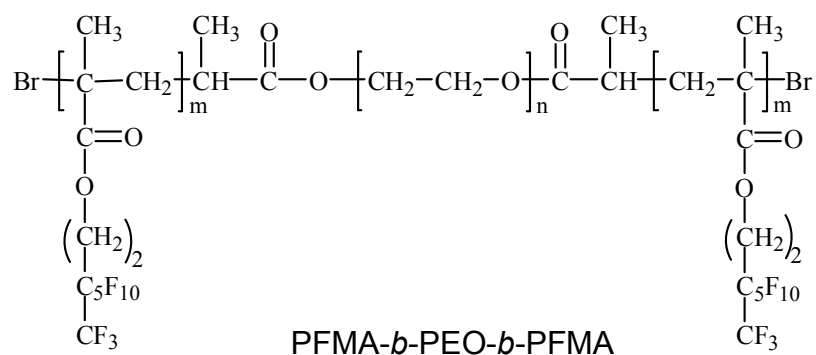
Figure. 2.1. Chemical structure of PFMA-*b*-PEO–*b*-PFMA triblock copolymer.

Table.1. Molecular characteristic of copolymers

Copolymer	M_n [a) Kg mol^{-1}]	PFMA [b) wt%]	M_w/M_n
PEO$_5$F32-D	7.6	31.9	1.26
PEO$_{10}$F5	9.3	5	1.3
PEO$_{10}$F9	9.4	9	1.33
PEO$_{10}$F13	9.7	13	1.27
PEO$_{10}$F41	16	40.3	1.32
PEO$_{20}$F4	27.2	4	1.4
PEO$_{20}$F9	26.5	9	1.3
PEO$_{20}$F13	26.7	13	1.31
PEO$_{20}$F69	65	68.7	1.30

a) SEC results from THF using PEO standards.

b) ^{1}H NMR results.

2.2. Dynamic Light Scattering

Dynamic light scattering (DLS) is a common technique used for the investigation of structures of polymers in solution, colloidal suspensions, gels and other more complex systems. Here we explain the basic principle through which radii distribution of colloids in solvents can be measured. The Dynamic Light Scattering technique investigates the relationships between the normalized time autocorrelation function $g^{(2)}(\tau)$ and delay time τ. The time dependence of scattered light is analyzed in terms of the time autocorrelation function $(I(t)I(t+\tau))$, where $I(t)$ and $I(t+\tau)$ are the scattered intensities of light at time t and t $/\tau$ and τ is the delay time. Results are typically expressed in terms of the normalized time autocorrelation function.

$$g^2(\tau) = \frac{(I(t)\,I(t+\tau))}{(I(t))^2} \qquad (1)$$

According to the light scattering theories,[85] the correlation function of the monodisperse sample can analyzed using following equation.

$$g^2(\tau) = B + \beta.\exp(-2\Gamma\tau) \qquad (2)$$

Where B is the baseline of the correlation function at infinite delay, β is the correlation function amplitude at zero delay, and Γ is the decay rate. Γ is the decay rate, and it is related to D and q with following equation.

$$D = \frac{\Gamma}{q^2} \qquad (3)$$

D is the macromolecular translational diffusion coefficient of the particles and q is the magnitude of the scattering vector. It is given by

$$q = \frac{4\pi n}{\lambda}\sin\theta/2 \qquad (4)$$

Where n is the solvent index of refraction, λ is the vacuum wavelength of the incident light, and θ is the scattering angle. Details of the particle size distribution can then be obtained via the Stokes-Einstein equation.

$$R_h = \frac{kT}{6\pi\eta D} \qquad (5)$$

Where k is Boltzmann's constant, T is the temperature in K, and η is the solvent viscosity. In our measurements, intensity time-correlation function $g^2(\tau)$ of dilute and semi dilute solutions of tri block copolymers was measured at scattering angles 50° -130° with an ALV-5000 goniometer equipped with a Nd/YAG DPSS-200 laser at a wavelength of 532 nm. For concentrated tri block copolymer solutions the intensity time-correlation function $g^2(\tau)$ was measured at scattering angle 90° with ALV-5000 equipped with a 22mW He-Ne laser at a wavelength 632.8 nm. The normalized field autocorrelation function $g^1(\tau)$ was derived from the $g^2(\tau)$ via the Siegert relation.[85]

2.3. Rheology

The word rheology is derived form the Greek word "rheos", to flow, and is the study of flow and deformation of a material. Experimentally rheology is the study of the effects of shear on a system. There are two types of behaviour that systems can exhibit i.e. elastic and viscous. In elastic behaviour, systems act as a spring, returning the energy imparted to it, in viscous behaviour it acts as a damper and dissipate the applied energy as heat. Gels show both these effects and are thus viscoelastic materials. Here we explain experimental observations of Winter and Chambon[86] for the determination of gel point of cross linked systems by rheological measurements. Chambon and Winter observed that the relaxation pattern of cross linked polymeric systems at the gel point shows self-similarity at long times,

$$G(t) = St^{-n} \qquad \lambda_c < t < \infty \qquad (6)$$

where S is called the stiffness and n is the relaxation exponent. The low limit λ_c is the relaxation time characterizing the crossover to glass transition (or the crossover to entanglement if present). The dynamic moduli G′ and G″ according to the theory of linear viscoelasticity of polymers are given by

$$G'(\omega) = \omega \int_o^\infty G(t) \sin(\omega t)\, dt \qquad (7)$$

$$G''(\omega) = \omega \int_O^\infty G(t) \cos(\omega t)\, dt \qquad (8)$$

Substitution of equation (1) into equations (2) and (3) leads to

$$G'(\omega) = \frac{S\pi\omega_n}{2\Gamma(n)\sin(\frac{1}{2}\pi n)} \qquad (9)$$

$$G''(\omega) = \frac{S\pi\omega_n}{2\Gamma(n)\cos(\frac{1}{2}\pi n)} \qquad (10)$$

$$\frac{G''}{G'} = \tan(\delta) = \tan(\frac{1}{2}\pi n) \qquad (11)$$

where $\Gamma(n)$ is the Legendre gamma function. The storage and loss moduli G′ and G″, of a gelling system at the gel point obey a scaling law with the same exponent n.

$$G'(\omega), \text{ and } G''(\omega) \; \alpha \; \omega^n \qquad (12)$$

$$\text{Tan } \delta = \frac{G''(\omega)}{G'(\omega)} = \tan(\frac{n\pi}{2}) \qquad (13)$$

Therefore parallel and straight lines with slopes n are obtained at the gel point upon plotting both dynamic moduli vs frequency on double logarithmic scales (see Fig 2.2 (a)). As a result, the phase angle δ at the gel point is independent of frequency. To determine the gel point, several frequency sweeps of the phase angle need to be performed before and after the gel point. The crossover of the phase angle δ lines at each frequency plotted in the way as shown in Fig. 2.2 (b) determines the gel time and the phase angle δ at the gel point.
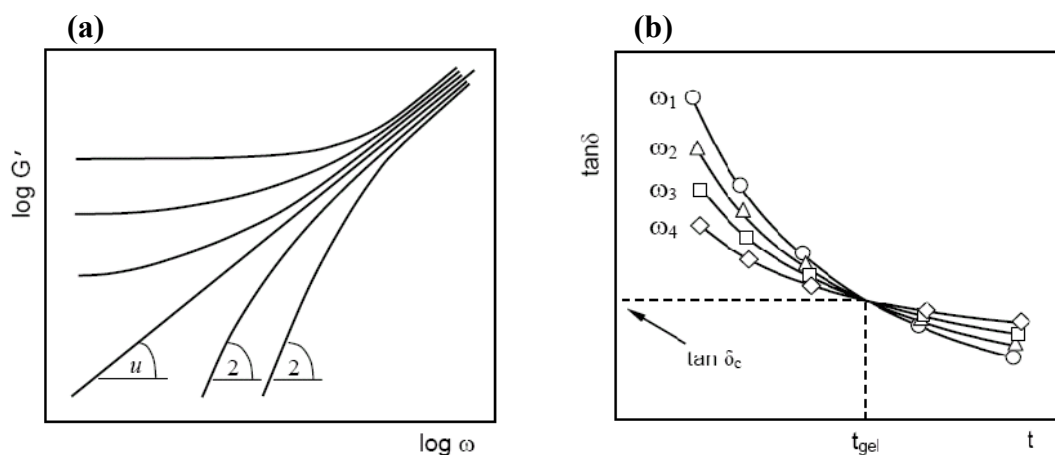
Figure 2.2. (a) Development of storage modulus as a function of frequency during gelation, at the gel point, a straight line with slope n is found for the log G' vs log ω curve. (b). Viscoelastic loss tangent as a function of time at several frequencies. The crossover of the line marks the gel time.

The relaxation exponent n is hence obtained from Eq. 13. The Winter and Chambon method has been successfully applied to both chemical[87] and physical[88] gelling systems. This method was also successfully extended to cases where the sol-gel transition occurs at a critical concentration[89] or a critical temperature[90] instead of a gel time, where the frequency dependence of the loss tangent or phase angle was measured at different concentrations or temperatures.

Concentrated solutions of perfluorinated amphiphilic block copolymer were investigated using rheometric scientific instrument equipped with water bath temperature control was used with a cone and plate geometry with 0.4 radians cone angle and 40 mm diameter. Sample loading is achieved by lowering the upper part of sample holder (cone) slowly. After placing the sample at the center of the bottom plate all the experiments were carried at strain rate less than 10%. The strain level was determined in the strain sweep test so that all the measurements were carried out within linear viscoelastic regime.

2.4. Langmuir- Blodgett technique

A Langmuir monolayer is a layer of amphiphilic molecules oriented with their hydrophilic heads on one side of the layer and their hydrophobic tails on the opposite. The change of surface tension caused by the presence of a Langmuir monolayer on a water surface is called its surface pressure (π). The surface pressure (π) - mean molecular area (mmA) isotherms of copolymers were collected using Teflon Langmuir trough system (KSV. Ltd, Helsinki, Finland) equipped with two moving barriers and Wilhelmy plate. The maximum available surface area of the Langmuir trough is (512 ×150) 76800 mm^2. Water used as subphase was distilled water which was subsequently passed through a water purification system from Purelab option system (ELGA Ltd. Celle, Germany) equipped with an organic removal cartridge, (conductance 0.06 $\mu S\ cm^{-1}$) maximum compression of pure water subphase gave surface pressures <0.05 $mN\ m^{-1}$. The temperature of the water subphase was maintained at 23±0.5°C using a circulated water bath system.

Copolymers (2 mg mL^{-1}) were dissolved in HPLC grade chloroform and predetermined amounts were spread evenly over the surface of subphase in 1-2 μL small drops using a Hamilton's digital microsyringe. Compression at a constant rate of 5 mm min^{-1} was started after 20 min to ensure the full evaporation of solvent. To obtain the complete copolymer isotherm different amounts of copolymer solutions were spread for each measurement. Different parts of isotherms overlap each other within the experimental error. The experimental setup was enclosed in a box so that the humidity is maintained at constant and surface contamination from outside air was avoided.

For Langmuir-Blodgett (LB) film preparation cleaned substrates were immersed into subphase prior to the monolayer deposition. Monolayer was compressed until desired transfer surface pressure was reached, then allowed to equilibrate for 10 min. Monolayers were deposited onto silicon substrates by vertically extracting the silicon wafer through the film at a constant rate of 1 mm min^{-1} and keeping film surface pressure constant

2.5. Tapping-mode atomic force microscopy (TM-AFM)

Tapping-mode atomic force microscopy (TM-AFM) measures topography by tapping the surface with an oscillating probe tip so that the tip makes contact with sample only for short duration in each oscillation cycle.[91,92] TM-AFM technique was used to investigate ABCs, LB film surface morphology, LB film morphology of lipids. We used Nanoscope multimode AFM in tapping mode (Digital Instruments, Santa Barbara, CA). Cantilevers from MikroMasch were 125 μm long with resonance frequency of approximately 325 Hz and radius of curvature less than 10 nm. Images were captured with lateral scan frequency 1-2 Hz, and set point ratio of 0.95. Acquired images were flattened using second order flattening routine in digital instruments software. In my thesis I have collected and presented two types of data from the instrument, height image and phase image. These two types of images from tapping mode atomic force microscopy can be explained as following.

2..4.1. Height image. The vertical position of the probe tip is monitored by noting changes in the length of the z-axis on the xyz-scanning piezo tube. Input voltage to the scanning piezo tube is proportional to the length of the tube. The change in the z-axis is plotted as a topographical map of the sample surface. Height data is good measure of the height of surface features but does not show distinct edges of these features.

2.4.2. Phase image. This type of imaging monitors the change in phase offset, or phase angle, of the input drive signal [to the drive piezo] with respect to the phase offset of the oscillating cantilever. The phase of the drive signal is compared to the phase of the cantilever response signal on the photodiode detector. The phase offset between the two signals is defined as zero for the cantilever oscillating freely in air. As the probe tip engages the sample surface, the phase offset of the oscillating cantilever changes by some angle with respect to the phase offset of the input drive signal. As regions of differing elasticity are encountered on the sample surface, the phase angle between the two signals changes. These changes in phase

offset are due to differing amounts of damping experienced by the probe tip as it rasters across the sample surface. These differences are plotted as the so-called "phase image".

Figure 2.3. Schematic representation of major components of AFM showing the feed back loop for Tapping mode operation.[93]

2.6. Small angle x-ray scattering (SAXS)

Scattering measures a large volume of material, primarily determined by the size of the beam, which typically ranges from centimetres (neutron) to micrometers (microfocus X-ray). Within this volume, the distribution of the scattering centres is represented by the intensity as a function the scattering variable q.[94]

$$q = \frac{4\pi \sin(\theta)}{\lambda} \qquad (14)$$

SAXS probes length scales of 1-100 nm. This range covers typical nanostructures of block copolymers. For structures with a well-defined separation of centres a sharp peak is observed. Regular well-defined structures result in sharp intensities at characteristic intervals along the q axis. These "spacings" are given by the symmetry of the lattice[95]. For less regular structures a broader feature is observed reflecting the distribution of centres.

Ratios q/q* for Bragg reflections from various structures

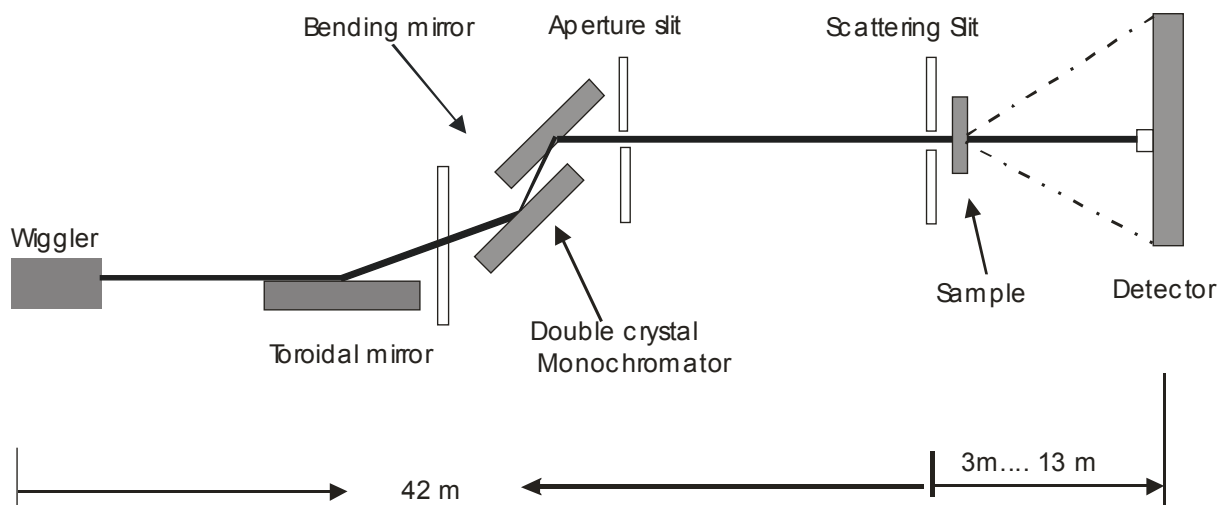| Structure	Ratio q/q*
Lamellar	1:2:3:4:5:6…..
Hexagonal	$1:\sqrt{3}:2=\sqrt{4}:\sqrt{7}:3=\sqrt{9}:\sqrt{11}\ldots$
Cubic bcc	$1:\sqrt{2}:\sqrt{3}:2=\sqrt{4}:\sqrt{5}:\sqrt{6}\ldots\ldots$
Cubic fcc	$1:\sqrt{(4/3)}:\sqrt{(8/3)}:\sqrt{(11/3)}:2=\sqrt{(12/3)}:\sqrt{(16/3)}\ldots$

Figure 2.4. Schematic diagram of the SAXS beamline (BW4) in the Hasylab, DESY.

(Diagram reproduced from the beamline description of BW4 at Hasylab, DESY.)

Concentrated solutions of perfluorinated amphiphilic block copolymer were investigated using BW-4 SAXS beamline in the Hasylab, Hamburg Germany. BW-4 SAXS beamline in the Hasylab uses pinhole collimation, double-focusing mirrors, and a double-crystal monochromator at a 38-pole wiggler line (see Figure 2.4). The sample to detector distance can be selected in the range from 3 to 13 m. At the short distance, the scattering angles from 1.24 to 50 rad can be observed. At 13 m distance, scattering angles from 0.12 to 10 mrad can be achieved.

2.7. X-ray reflectivity

X-ray reflectivity (XRR) provides information on film thickness, the roughness (fluctuations) of the interfaces, and the laterally averaged electron-density profile perpendicular to the interfaces.[96,97] The x-ray reflectivity geometry is shown in Fig 2.4a. Under specular conditions the exit angle θo is equal to the impinging angle θi; then the momentum transfer q is normal to the surface. The intensity of an electromagnetic wave reflected at an ideally sharp interface is called the fresnel reflectivity R_F, At large angles the reflected intensity decays as q^{-4}. Due to

the rapid decrease in intensity with increasing angle, the range of q in reflectivity

measurements is small, typically $q_{max} \approx 6$ nm–1 (see Fig. 2.4b).

(a)   **(b)**
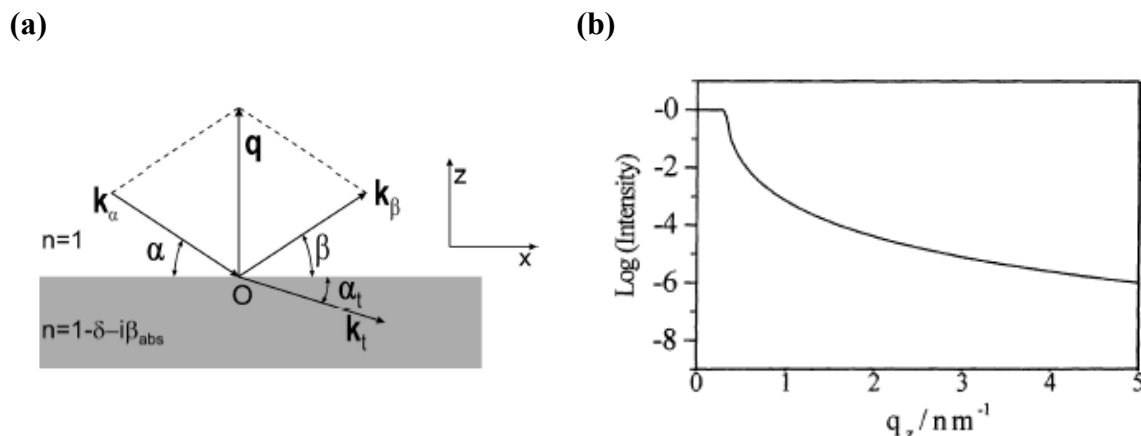

Figure 2.5. *(*a) Scattering geometry for x-ray reflectivity experiment. (b) Fresnel reflectivity of a single smooth interface*.

X-ray reflectivity measurements were carried out at the BW1beam line at HASYLAB (DESY,

Hamburg, Germany) using a liquid surface diffractometer with an incident wavelength of i)

1.3037 Å. A thermostated Langmuir trough equipped with a Wilhelmy film balance to

measure the surface pressure and a single barrier to change the surface area were mounted

on the diffractometer. The instrumental details are given in an article by J. Als-Nielsen.[98] To

avoid beam damage, the sample was displaced after several minutes of irradiation; i.e., a

single profile was measured on four neighboring positions. The data were corrected for

background scattering, and the obtained reflectivity curves were fitted using the

Parratt algorithm[99] embedded in a program by Mr. Braun (Parratt- The Reflectivity Tool,

kindly provided by HMI, Berlin).[100]

Chapter 3

Perfluorinated block copolymer hydrogels

3.1. Introduction

Amphiphilic block copolymer hydrogels are know for their pharmaceutical and biomedical applications such as drug delivery[101-105] systems, tissue engineering,[106,107] separation media.[108] In addition to, biocompatibility, most important prerequisites for block copolymer hydrogel to be useful in biomedical applications   are regular distribution of nano sized hydrophobic and hydrophilic domains, and their mechanical strength, Therefore, experimental investigations on structures and dynamics of hydrogels formed by amphiphilic diblock, triblock copolymers have been extensively reported.[109-116]

Generally amphiphilic block copolymers contains biocompatible poly(ethylene oxide)[117] as a water soluble block with various other biocompatible hydrophobic blocks such as poly (propylene oxide),[118,119] poly(L-lactide),[120,121] poly(oxybutylene),[110] and poly(D,L methyl glycolide)[122] are considered for biomedical applications. So for there are no reports found on amphiphilic block copolymers containing fluorinated hydrophobic blocks attached to PEO block, except in telechelic polymers which are widely studied for their applications such as rheology modifiers,[123, 124] and sustained drug delivery.[125]

ABA triblock copolymers in middle block selective solvents have been extensively reported.[126-135]   In general it is reported that ABA triblock copolymer chain in middle block selective solvents can form a loop (both A blocks belong to the same micellar core), a bridge (each block in different core), or a dangling chain similar to that of diblock chain. So triblock copolymers in middle block selective solvents can form physical gels through transient network formation.[136,137] The principal difference between chemical and physical gels lie in

the life time and the functionality of the network junction. Chemical bonds are considered to be permanent, whereas the physical network junctions have finite life time. The chemical gels form continuously with increasing extent of reaction where as the physical gelation process depends on the type of transition i.e. it may even jump from solution to gel if the network junctions are created by a first order transition. The transient nature of the physical network junction makes it difficult to study physical gels near their gel point.[130-135] It is even difficult to give a clear definition of the gel point because its molecular weight is finite even if it forms infinite cluster and it is soluble even beyond gel point. So usually, physical gels are characterized by using rheology.[130-135]

In this study, we report on rheology and possible structure formation of PFMA-*b*-PEO-*b*-PFMA triblock copolymer hydrogels. These block copolymers are ABA type triblock copolymers with water soluble (PEO) middle block and water insoluble end blocks (PFMA). Dilute aqueous solution properties of PEO-PFMA diblock, triblock copolymers were reported earlier.[138] We have investigated association behaviour of PEO-PFMA triblock copolymers with increasing block copolymer concentration in water using dynamic light scattering (DLS). Sol-gel transition, and abrupt rheological transition from visco elastic solid behaviour at room temperature to solid like behaviour at 35°C temperature was shown by rheology. SAXS data indicated formation of longrange structures in our triblock copolymer hydrogels.

3.2. Experimental

3.2.1. Sample preparation

In a vial, weighed amounts of block copolymer (PFMA- PEO-PFMA) were dissolved in BI-distilled water by stirring. The stirring time was dependent on water solubility of block copolymers. Samples were stored at room temperature for more than 48 hrs before measuring. So that the bubbles formed during mechanical stirring are removed.

3.2.2. DLS measurements

For dilute and semi dilute solutions of tri block copolymers under investigation the intensity time-correlation function $g^2(\tau)$ was measured at scattering angles 50° -130° with an ALV-5000 goniometer equipped with a Nd/YAG DPSS-200 laser at a wavelength of 532nm. For concentrated tri block copolymer solutions the intensity timecorrelation function $g^2(\tau)$ was measured at scattering angle 90° with ALV-5000 equipped with a 22mW He-Ne laser at a wavelength 632.8nm. The normalized field autocorrelation function $g^1(\tau)$ was derived from the $g^2(\tau)$ via the Siegert relation.[139]

3.2.3. Rheology measurements.

Rheometric scientific instrument equipped with water bath temperature control was used with a cone and plate geometry with 0.4 radians cone angle and 40 mm diameter for rheology measurements. Evaporation from the sample restricts the measure temperature, and temperature with drying was unavoidable during loading of the sample on the rheometer, which takes 5 -10 min. So the actual concentration of the sample might be slightly higher than indicated and all the data shown in figures are for experiments performed at 25°C unless and other wise indicated. Sample loading is achieved by lowering the upper part of sample holder

(cone) slowly. After placing the sample at the centre of the bottom plate all the experiments were carried at strain rate less than 10%.

3.2.4. SAXS

Concentrated solutions of perfluorinated amphiphilic block copolymer were investigated using BW-4 SAXS beamline in the Hasylab, Hamburg Germany. BW-4 SAXS beamline in the Hasylab uses pinhole collimation, double-focusing mirrors, and a double-crystal monochromator at a 38-pole wiggler line.

3.3. Results and Discussion

3.3.1. Effect of polymer concentration and hydrophobic block chain length on association behaviour of block copolymers in water.

Dilute aqueous solutions (i.e. triblock copolymer concentration < 1% w/v) of the triblock copolymers under investigation showed micelles in the range of 10 - 20 nm and clusters in the size range of 80 - 90 nm.[127] In dilute concentration regime; at particular concentration of triblock copolymer in water no significant difference was found in micelle size and cluster size with respect to hydrophobic and hydrophiphilic (middle block) block length. However, concentration of triblock copolymer had significant effect on cluster size.

For instance, Fig. 3.1.shows decay rate distribution of 1% w/v $PEO_{10}F5$ triblock in water. It shows two peaks one peak with broad distribution (fast mode) and another very small peak (slow mode) indicating bimodal distribution. CONTIN analysis of the data shows that the fast and slow modes corresponds to the hydrodynamic radii (R_h), 12 (micelle) and 200 nm (cluster) respectively.
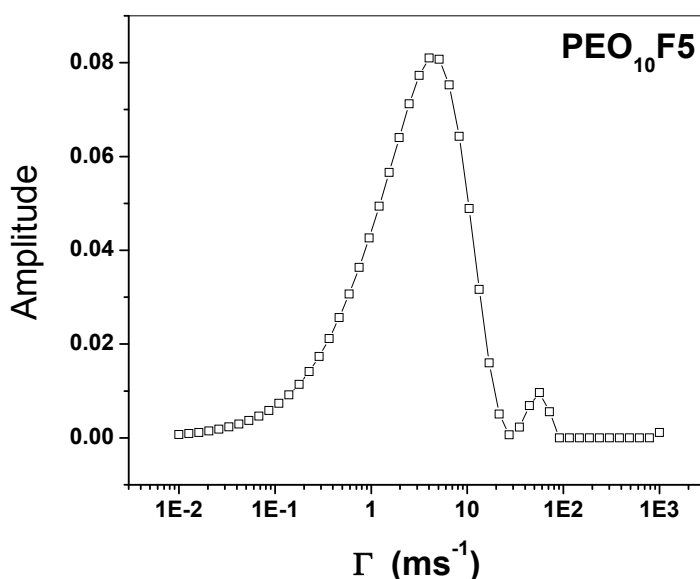

Figure 3.1. Decay rate distribution of 1% w/v $PEO_{10}F5$ triblock in water at 90º angle.

This increase in size of clusters for $PEO_{10}F5$ triblock copolymer motivated investigate the possibility of hydrogel formation as the clusters were assumed as interconnected micelles.
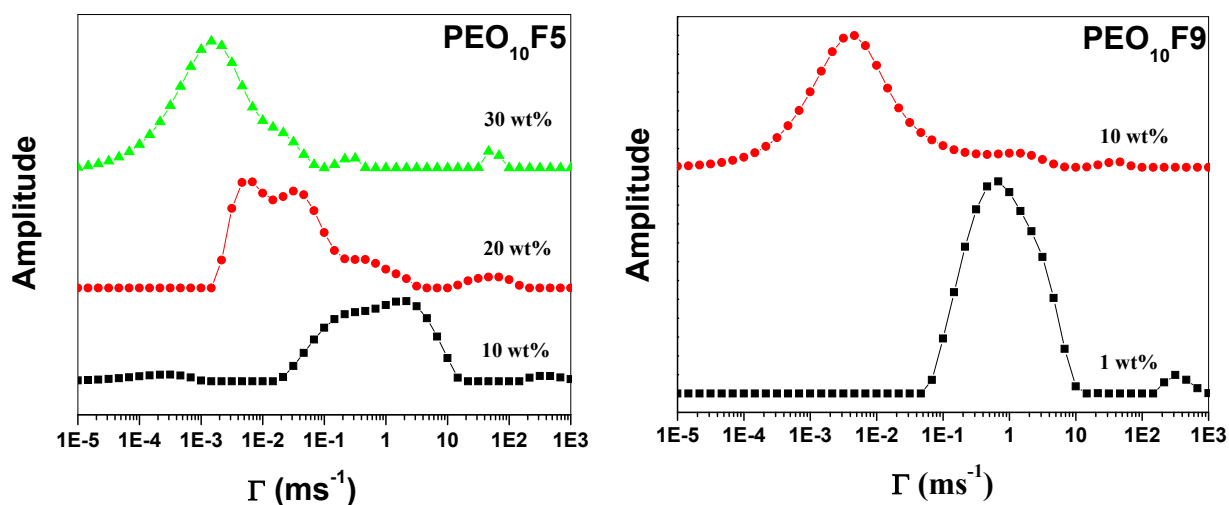

Figure 3.2. Decay rate distributions at 90° angle for $PEO_{10}F5$, $PEO_{10}F9$ copolymers at different concentrations.

Fig. 3.2. Shows decay rate distributions measured at 90° angle for $PEO_{10}F5$ and $PEO_{10}F9$ at different concentration. Peak corresponding to clusters shifts towards slower decay rates (Fig. 3.2.), i.e. with gradual increase in concentration, size of the cluster increased. This indicates network formation; however there was not significant increase in viscosity. Very highconcentrated $PEO_{10}F5$ (up to 30 % w/v) copolymer in water did not show any visible increasing in viscosity, whereas $PEO_{10}F9$ and $PEO_{10}F13$ formed gels above 15% w/v concentration. This signifies the role of hydrophobic chain length on the association behaviour of the block copolymers in water.

3.3.2. Effect of polymer concentration and hydrophobic, hydrophilic block chain length on rheological properties of block copolymer aqueous gels.

Steady-state viscosity measurements were carried out in order to characterize the flow behavior of $PEO_{10}F5$, $PEO_{10}F9$, and $PEO_{10}F13$ aqueous solutions. Fig. 3.3 shows the steady state viscosity of the block copolymer at different concentrations. These block copolymers differ in their hydrophobic block chain length.
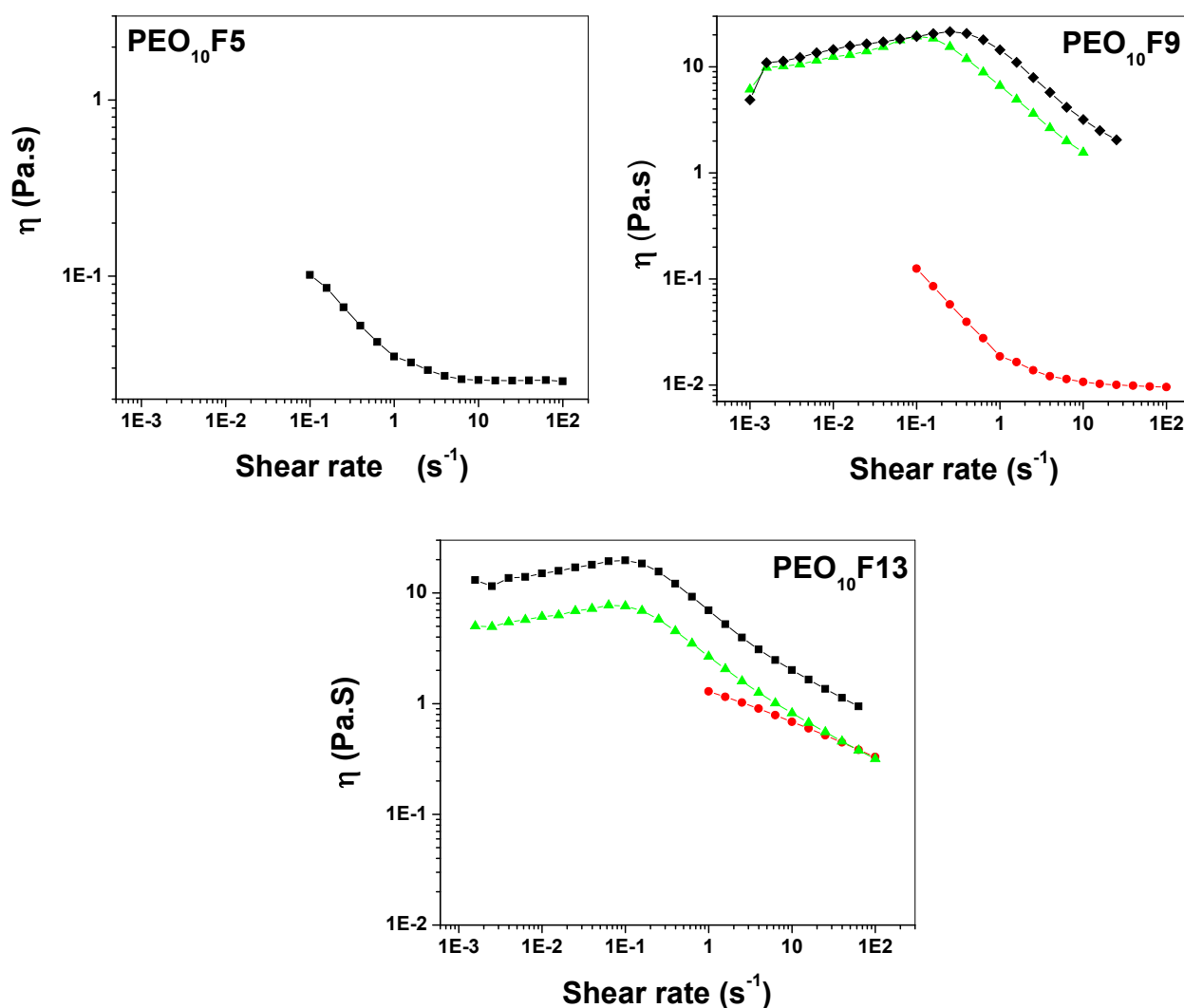

Figure 3.3. Shear rate dependent viscosity for $PEO_{10}F5$, $PEO_{10}F9$ and $PEO_{10}F13$ at different copolymer concentration. ($\bullet$) 14 wt%, 17.5 wt% ($\blacktriangle$), 25 wt% ($\blacksquare$).

In the entire shear rate region; shear thinning was observed at low concentration 14 % w/v for $PEO_{10}F9$ and $PEO_{10}F13$, and at very high concentration 25 % w/v of $PEO_{10}F5$ (Fig. 3.3). Shear thinning is due to the yield stress. Copolymer with lowest hydrophobic content $PEO_{10}F5$ showed very low viscosity at very high (25 % w/v) copolymer concentration, whereas at 14 % w/v, $PEO_{10}F9$, showed similar viscosity, and $PEO_{10}F13$ showed slightly higher viscosity. Increase in viscosity with increasing hydrophobic chain length clear indicates the role of hydrophobic blocks in the network formation. Viscosity of $PEO_{10}F5$ was very low even at 25 % w/v of copolymer concentration. Therefore $PEO_{10}F5$ was not used in further investigations. . At higher concentrations (17.5, and 25 % w/v) both $PEO_{10}F9$, and $PEO_{10}F13$ copolymers showed shear rate dependency i.e. Slow increase (Shear thickening) in viscosity at low shear rates, followed by (shear thinning) gradual decrease in the viscosity at higher shear rates (see Fig.3.3). This behavior has been reported for PEO end-capped with either hydrogenated or fluorinated hydrophobes.[140,141] Shear thickening can be explained in terms of resistance of polymeric network to the stress applied. Stress in such a network system is slowly released with cooperative motion of the attached chains. At higher shear rate the chains will break and shear thinning occurs.

Oscillatory shear experiments were performed within the linear viscoelastic regime. The storage and the loss moduli as a function of frequency, ω, are plotted at different concentrations for three different copolymers. These copolymers differ in either hydrophobic block chain length ($PEO_{10}F9$, $PEO_{10}F13$) or hydrophilic block chain length ($PEO_{10}F9$ and $PEO_{20}F4$ has similar number of end hydrophobic chains but differ in chain length of middle hydrophilic block). For all the copolymers investigated, at the lower concentration 14 wt % for $PEO_{10}F9$, $PEO_{10}F13$ and at 2.5 wt % for $PEO_{20}F4$ in the entire frequency range studied
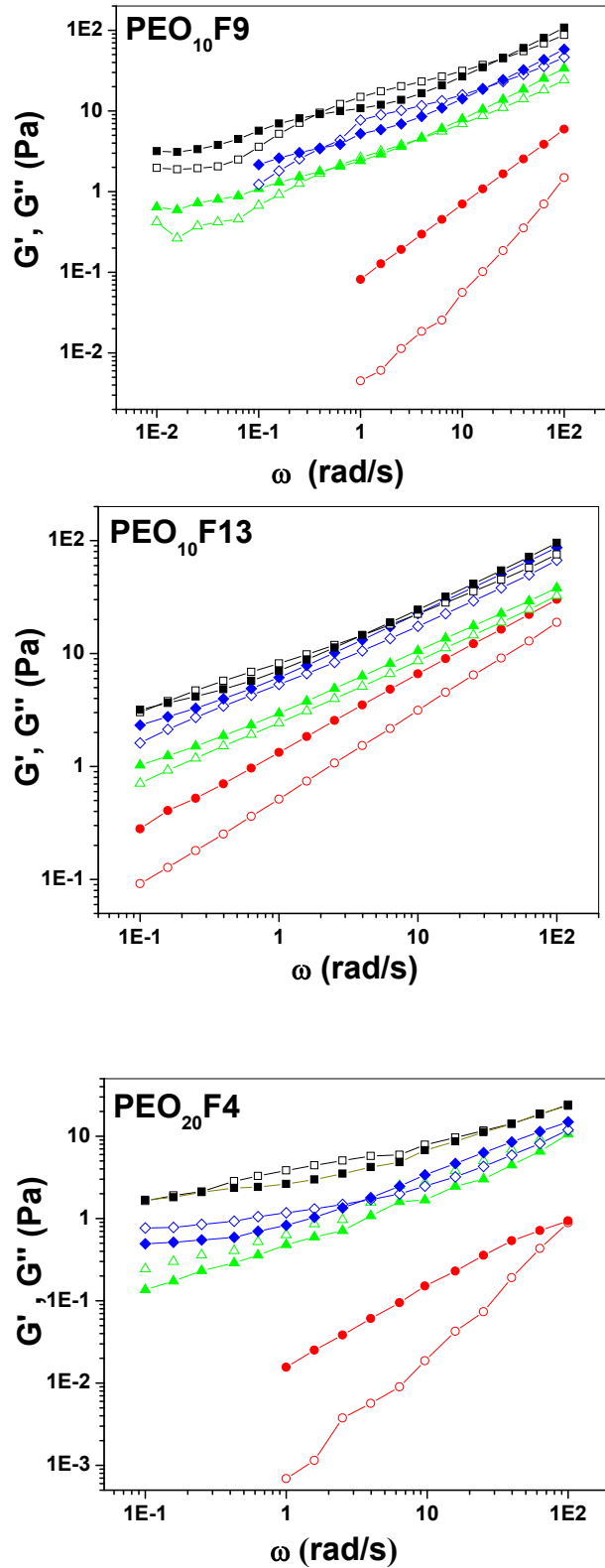
Figure 3.4. G' (ω)(open symbols), G'' (ω) (solid symbols) as function of frequency for $PEO_{10}F9$, $PEO_{10}F13$, at concentrations 14 wt% (●), 17.5 wt% (▲), 20 wt% (◆), and 25 wt % (■). $PEO_{20}F4$ at 2.5 wt% (●), 4 wt% (▲),5 wt% (◆), and 6 wt % (■).

(10^{-1} - 10^2 rad/s) G'', exceeds G' (see Fig. 3.4.) by about 1 order of magnitude and is virtually independent of ω, indicating that the solution behaves like a liquids.

At higher copolymer concentration for $PEO_{10}F9$ from 17.5 wt% and for $PEO_{20}F4$ starting from 4 wt% a crossover of G' (ω) over G'' (ω) is observed (see Fig.3.4.). Cross over of elastic modulus (G') value over viscous modulus (G'') indicates that at that particular concentration (17.5 % w/v of $PEO_{10}F9$, and 4 % w/v of $PEO_{20}F4$) copolymers are already hydrogels. In contrast for $PEO_{10}F13$ triblock copolymer no cross over was observed (see Fig.3.4.) even at 17.5 wt% and 20 wt%, However, based on the slope value for of the curve G' (ω) vs ω and G'' (ω) vs ω it can be said that $PEO_{10}F13$ shows solid like behaviour. (slope of the curve G' (ω) vs ω and G'' (ω) vs ω is less than 1[142]). Based on the results from oscillatory shear experiments, it can be stated that the sol – gel transition concentration lies in between 14 – 17 wt% for $PEO_{10}F9$ and $PEO_{10}F13$, 2.5 – 4 wt % for $PEO_{20}F4$. However, determination of gel-point from the crossover of the G' (ω) over G'' (ω) is difficult. Either more than one crossover points (crossover at high frequencies and low frequencies for $PEO_{10}F9$ and $PEO_{20}F4$) or no cross over for $PEO_{10}F13$ is observed (see Fig. 3.4.). In addition, Fig 3.4. shows a plateau for G' (ω) and G'' (ω) in low ω range. i.e. ω reaching to zero, the values of elastic and viscous modulus remained constant. This kind of behaviour was observed in various other physical gelling systems.[143] It is attributed to formation of ordered arrangement of hydrophobic domains in the gel network.

3.3.3. Determination of gel-point

From dynamic mechanical analysis, gel-point of the sol-gel transition system can also be determined by method known as frequency independence of tan δ. In this method the gel-point is determined from a multifrequency plot of tan δ vs concentration[144] and temperature[145] depending on the process which governs the gelation. Detailed mathematical description of

this method was explained in chapter -2. According to Winter and Chambon[85, 86] at the gel point

$$G'(\omega), G''(\omega) \propto \omega^n \qquad (2)$$

$$\text{Tan}\delta = G''/G' = \tan(n\pi/2) \qquad (3).$$

We have used the frequency independence of tan δ method to plot Tan δ vs concentration for different frequencies as shown in the Fig.3.5. for $PEO_{10}F9$, $PEO_{10}F13$ and $PE0_{20}F4$. All the curves in each figure pass through a point at a certain concentration. This concentration can be defined as critical gel concentration C_g.[143]

Table 3.1. Critical concentration for sol - gel transition and scaling
Component n determined for our triblock copolymers.

Block copolymer	C_{gel} wt%	Tan δ	n value
$PEO_{10}F9$	16.8	1.73	0.66
$PEO_{10}F13$	18.0	1.24	0.56
$PEO_{20}F4$	3.8	1.81	0.67

The critical exponent n was calculated using the relation in equation 3. The table 3.1 shows the value of C_g and n determined for our triblock copolymer systems. The low tan δ or n value represents the strength of network.[146] Intrestingly, the value of the n was found to be low for $PEO_{10}F13$ compared to the n value for $PEO_{10}F9$ and $PEO_{20}F4$ (see Table 3.1.). The n value of $PEO_{10}F13$ is 0.56 which is typical for solid like materials.[146] Lower n value for copolymer with greater hydrophobic chain length signifies the role of hydrophobic chain in the gel strength. The higher strength of network with increasing hydrophobic content is due to high density of micellar packing. $PEO_{10}F9$ and $PEO_{20}F4$ differ in hydrophilic block chain length. Lower C_g of $PEO_{20}F4$ compared to $PEO_{10}F9$ indicates the role of hydrophilic block length on the sol – gel transition concentration.
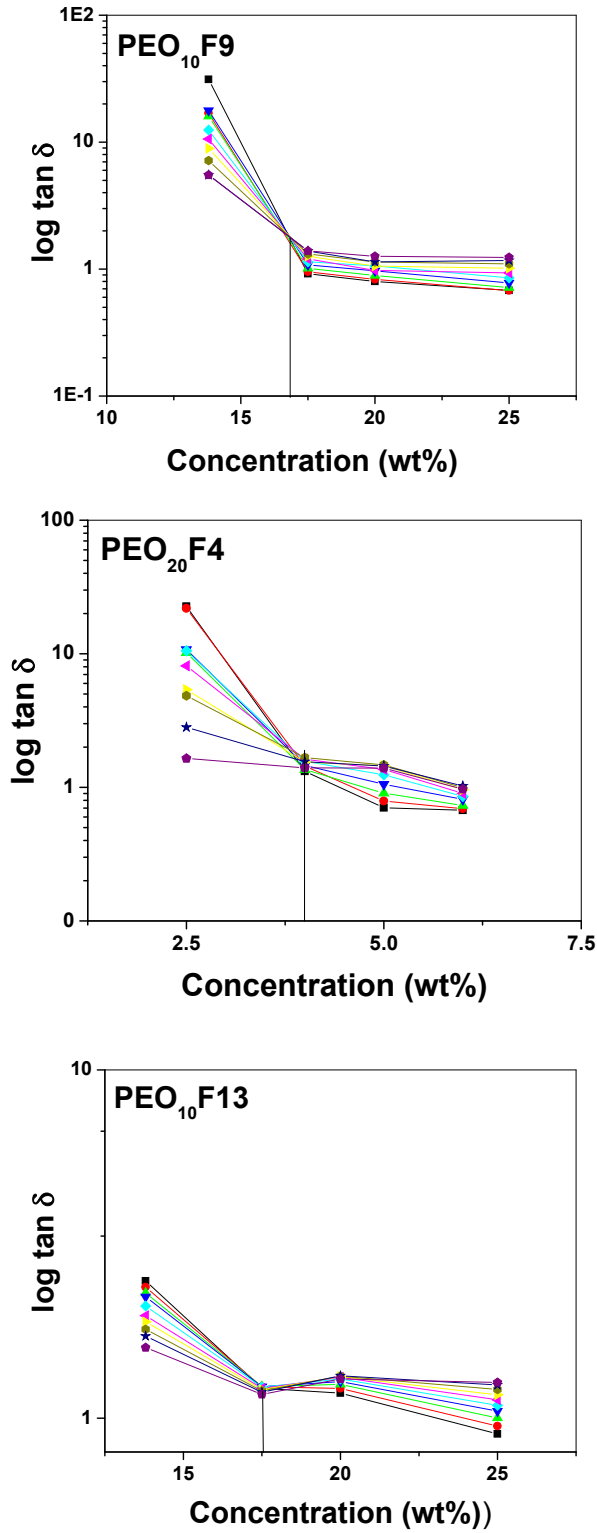
Figure 3.5. Tan δ vs concentration of different triblock copolymers at various frequencies.

3.3.4. Temperature dependence of G' and G"

Temperature dependence of G' (ω) and G" (ω) was measured for $PEO_{10}F9$ triblock copolymer at 25 wt%. It should be noted that our triblock copolymer systems in the measured concentration were clear by visual observation in the range of 25° - 50° C. We did not observe turbidity in this range. No macro phase separation (i.e. polymer rich and polymer poor phases) was observed in sol state as well gel state of the triblock copolymer. Here we are interested to know if G' and G" values will have some effect on the temperature as the PEO solubility is know to be decreased with increasing temperature. Fig.3.6. shows the plot of log of G' (ω) and G" (ω) vs log w. Data in the graph is shifted to avoid overlap in vertical direction with shifting factor X as indicated in the graphs. Typical gel plateau observed at temperature 25°C is not found in lower temperature measurements. With decreasing temperature PEO becomes more soluble, this makes the network more flexible. No ordered arrangement of micelles can be expected. Interestingly, with increasing temperature at 30°C at low ω plateau is not observed but the G' (ω) was found to be increased compared G" (ω). Further increase in temperature at 35°C G' (ω) value increases significantly and G' (ω), G" (ω) vs log ω curve becomes plateau over the entire frequency range. This is a typical behaviour of solid like gel systems. This can be attributed to decreased solubility of PEO in water.[147] With decreasing solubility PEO looses its flexibility in water; the micelles are fixed in their positions, which results in some ordering in the block copolymer physical gels.

SAXS data of $PEO_{20}F4$ at different concentrations was shown in Fig. 3.7. For the highest concentration (7.5 wt %) a significant peak was observed. Compared to the SAXS pattern for the low concentrated samples, the highly concentrated sample shows a sharper peak, and it is shifted to higher wave vector, q. (see Fig. 3.7.). Peak shift towards higher wave vector indicates long range structure formation.[148] Based on the SAXS pattern for the $PEO_{20}F4$

concentrated solutions, it appears that with increasing concentration of the block copolymer long range order is improved in our block copolymer hydrogels. The low frequency plateau in the storage modulus with increasing concentration (Fig. 3.4.) correlates with the formation of the ordered structure.
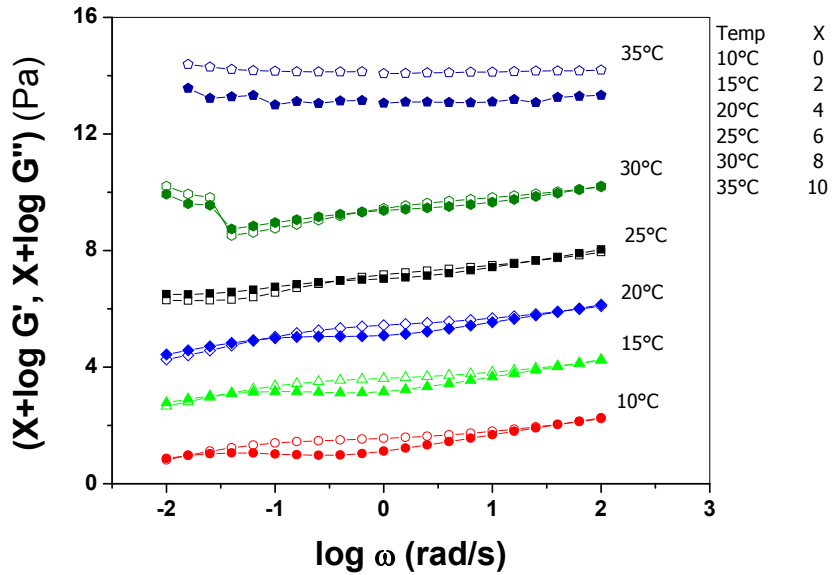

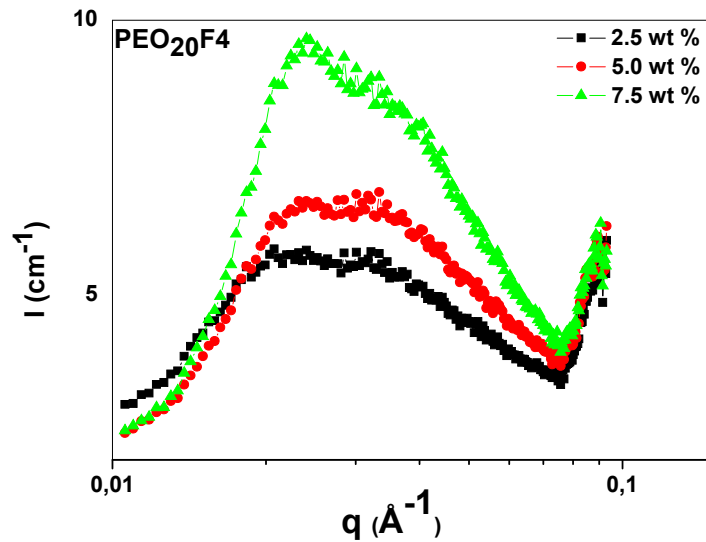**Figure 3.6**. Temperature dependency of G' (ω) and G" (ω) of $PEO_{10}F9$ block copolymer at 25 wt%

Figure 3.7. SAXS pattern for $PEO_{20}F4$ solutions at different concentrations.

3.4. Conclusions

DLS and rheology data showed that the perfluorinated ABA triblock copolymers can form physical gels. The hydrophobic block has effect on gel strength, whereas the hydrophilic block influences the critical gel concentration. SAXS data indicated improved longrange order with increasing concentration. Based on our results and literature information, we propose that in ABA triblock copolymers with hydrophilic middle block, network formation occurs with combination of open and closed association models. In open association model triblock copolymers aggregate without micelle formation, where as in closed association models micelles are formed at lower concentration and with increasing concentration micelles form aggregates and gradually develops into gels. Upon shear stress these loose networks will loss their connectivity and act as individually dispersed spheres. Fig.3.8. shows the schematic representation of infinite network formation in our triblock copolymer systems.
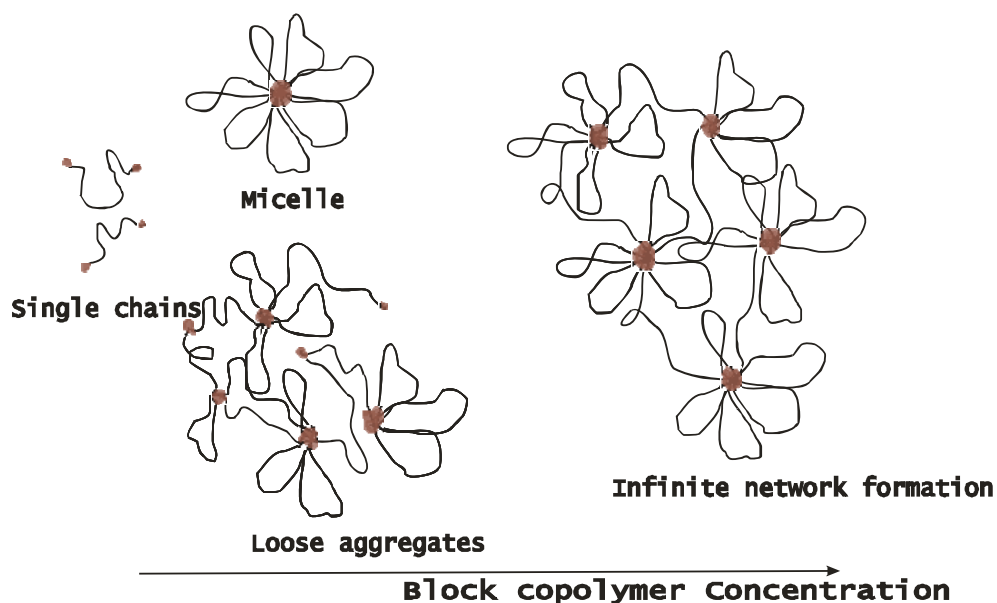

Figure 3.8. Schematic representation of network formation in ABA triblock copolymer systems.

Chapter 4

Langmuir Monolayer and Langmuir-Blodgett Films of Amphiphilic Triblock Copolymers with Water Soluble Middle Block

4.1. Introduction

Block copolymers are usually composed of mutually immiscible blocks. They are known to form self-assembled nanostructures of various morphologies in presence of selective solvents and surfaces.[149, 150] In particular, ordered structures of thin block copolymers films on solid surfaces are of considerable scientific interest as well as for their potential applications.[151] Such ordered structures can be obtained with the well-established Langmuir-Blodgett (LB) technique by transferring amphiphilic molecules from the water surface to solid substrates.[152] This technique has the advantage of controlling the molecular density and thus the phase behavior of the monolayer.

Numerous groups have reported on the monolayer behavior of amphiphilic block copolymers anchored at the air-water interface by neutron reflectivity,[153-158] light scattering studies[154] and by measuring the surface pressure versus the mean molecular area (π-mmA) at constant temperature, i.e. the surface isotherms, particularly for poly(ethylene oxide)-*block*-poly(styrene) (PEO-*b*-PS) based linear diblock[153-167] and star block copolymer systems.[168-172] In general, a characteristic rearrangement occurs with compression of the monolayer of block copolymers containing PEO as a hydrophilic block. Typically the Langmuir isotherms show three distinct regions with one phase-transition. This phase-transition was interpreted according to

scaling theories of Alexander et al.[173] as the formation of pancake-like structures at large molecular areas transforming into brushes at lower molecular areas with an intermediate plateau region corresponding to the dissolution of the PEO block. In contrast, in isotherms of PS-*b*-PEO with high PS content, the intermediate plateau region was reduced significantly[163] or completely disappeared[164,167]. For telechelic PEO copolymer systems Barentin et al.[172] have reported a phase-transition in the brush regime in addition to the described phase-transition. This transition was attributed to the dissolution of alkyl chains resulting in the loss of polymer into the subphase. Multiple transitions were observed in poly(styrene)-*block*-poly(alkyl acrylate) diblock copolymer monolayers.

Additionally, micelles were observed in anchored amphiphilic block copolymer chains after the transfer to a solid substrate by transmission electron microscopy, TEM, and atomic force microscopy, AFM.[173-183] Surface micelle formation and aggregation at the air water interface was found for PS-*b*-PEO linear diblock copolymer[162-166] for three-arm star block copolymer,[168, 170, 171] and for hetero arm star block copolymer[169] systems after the transfer at various surface pressures. Well-organized structures developed, when the microphase segregation of the polymer is driven through the choice of solvent and grafting density on the solids as a result of different initial surface pressures.[184] Three different mechanisms were reported to explain the domain formation in linear amphiphilic block copolymers after transfer from the liquid surface to the solid. According to Goncalves da Silva et al.[158] block copolymers form micelles in the spreading solution already. Upon spreading they form surface micelles, which become more densely packed with increasing surface pressure. In contrast, An et al.[174] and Israelachvili[175] suggested that the polymers were spread as unimers onto the subphase and aggregate upon compression. Cox et al.[163] stated that linear block copolymers deposit as a combination of both models. The different models, suggested for the formation of surface micelles, reflect the richness of block copolymers

under investigations. To get a deeper insight into the interrelation between micelle formation and pancake-to-brush transition the length of the anchor relative to the polymer block has to be changed systematically.

In this paper, we report on the phase behavior of monolayers from amphiphilic triblock copolymers of poly(ethylene oxide) (PEO) and poly(perfluorohexyl ethyl methacrylate) (PFMA) at the air-water and the air-silicon interface. Compared to the previously described systems, they contain a long hydrophilic middle block (PEO) with very short hydrophobic end blocks (PFMA). The PFMA block consists of a methacrylate backbone with non-fluorinated ethyl and perfluorinated n-hexyl side chains. These block copolymers are highly surface active and form micelles and clusters in aqueous solutions.[185] A clear aqueous solution is formed only, when the hydrophobic PFMA-part is less than 15 wt%.[185, 186] The phase behavior at the air-water interface was studied by means of Langmuir isotherms. The resulting morphology of the monolayers was investigated by AFM after the transfer to silicon wafers at different surface pressures. The PFMA block chain length is varied to study the influence on the brush formation in Langmuir monolayers and on the surface morphology of the LB films.

4.2. Experimental section

4.2.1. Surface pressure measurements

The surface isotherms of the copolymers at the air-water interface, i.e. the plots of pressure (π) versus the mean molecular area (mmA), were measured with a Teflon® Langmuir trough system (KSV Ltd, Helsinki, Finland) equipped with two moving barriers and a micro-roughened platinum Wilhelmy plate. The maximum available surface area of the Langmuir trough is 76800 mm^2 (compression ratio 8:1). As subphase distilled water was used, which was

subsequently passed through a water purification system from Purelab option system (ELGA Ltd., Celle, Germany) equipped with an organic removal cartridge (conductance 0.06 μS cm^{-1}). The purity of the bare water surface was checked before each measurement by a maximum compression ($\Delta\pi$<0.1 mN m^{-1}). The temperature of the water subphase was maintained at 23$\pm$0.5°C, using a circulating water bath system. Copolymers were dissolved (2 mg mL^{-1}) in HPLC grade chloroform (Sigma-Aldrich, Fluka, Seelze, Germany) and predetermined amounts were spread evenly on the subphase in 1-2 μL small drops using a Hamilton's digital microsyringe. The compression at a constant rate of 7.5 cm^2 min^{-1} was started after 20 min to ensure the full evaporation of solvent. To obtain the complete isotherm the copolymer solutions were spread upon different initial pressures and thus different parts of the isotherm were recorded. After copying into one plot they overlap within the experimental error. The experimental setup was enclosed in a box for constant humidity and minimization of surface contamination.

4.2.2. Substrate cleaning for Langmuir-Blodgett deposition

Silicon (111) wafers were cut into 3 x 1 cm substrates. They were cleaned using a modified Shiraki technique.[187] The silicon substrates were placed in a solution containing 4:1:1 (vol.) $H_2O/H_2O_2/NH_4OH$ at 80°C for 5 min, then rinsed in deionized water followed by washing at room temperature in a solution containing 3:1 H_2O/HF, and finally rinsed again in deionized water to remove residuals. This treatment results in a hydrophobic surface. Afterwards they were heated in a solution containing 5:1:1 (vol.) $H_2O/H_2O_2/HCl$ to 80°C for 5 min. After cooling they were rinsed in deionized water. The procedure was repeated with a dilute HF treatment until a contact angle with pure water of approximately 10° was achieved. The contact angle was

measured optically with OCA 20 (DataPhysics, Filderstadt, Germany). The cleaned substrates were stored under double distilled water until use. For Langmuir-Blodgett (LB) film preparation cleaned substrates were immersed into subphase prior to the monolayer deposition. The monolayer was compressed until the desired transfer surface pressure was reached, then allowed to equilibrate for 10 min. The monolayers were transferred onto the silicon substrates at constant surface pressure by a vertical upstroke through the film at a constant rate of 1 mm min^{-1} (hydrophilic transfer).

4.2.3. Atomic Force Microscopy (AFM)

The transferred films were allowed to dry in air for at least 24 h in a desiccator at room temperature. LB film surface morphology was studied using a Nanoscope multimode AFM in tapping mode (Digital Instruments, Santa Barbara, CA). The silicon cantilevers (NSC15/AlBS/15 µMasch, Spain) were 125 µm long with a resonance frequency of approximately 325 Hz and a tip radius < 10 nm (Force constant 40 N m^{-1}). The images were captured with lateral scan frequency of 1-2 Hz and a set point ratio of 0.95. The acquired images were flattened using a second order flattening routine in digital instruments software. The images from 3 different LB films for each sample were comparable, indicating reproducible depositions.

4.3. Results and Discussion

4.3.1. Monolayer behavior at the air-water interface

Figure 4.1. shows compression isotherms obtained for triblock copolymers with a low PFMA content, PEO$_{10}$F9 and PEO$_{20}$F4. The isotherms are similar to the isotherms of PS-*b*-PEO

diblock copolymers with a low PS content.[155, 157, 158] They show three different regimes. At high mmA the surface pressures increase gradually with compression. For $PEO_{10}F9$ and $PEO_{20}F4$ the first increase of the surface pressure is observed at mmA of approximately 160 nm^2 and 320 nm^2, respectively. With further compression a pseudo-plateau is observed at about 35 nm^2 and 8.4 mN m^{-1} or 70 nm^2 and 9.2 mN m^{-1}, respectively, where the surface pressure changes only slightly (8-10 mN m^{-1}). When compressed beyond the pseudo-plateau the surface pressure sharply increases until the film collapses at small mmA. The isotherms for $PEO_{10}F9$ and $PEO_{20}F4$ reflect the typical behavior of anchored PEO chains at the air-water interface. At low surface pressures a typical liquid expanded monolayer is observed, where the hydrophobic PFMA segment anchors the polymer chain to the surface, while the PEO adopts a flattened conformation at the interface due to its affinity to the water. According to Alexander, this phase can be described as a self-similar adsorbed layer (SSAL) or as pancake-like.[173] The shift of the isotherms to larger areas with an increasing PEO block length confirms the adsorption of PEO blocks at the air-water interface. As the film is compressed laterally, the surface pressure increases due to an increased surface density of PEO blocks. In the pseudo-plateau the PEO blocks extend into the subphase forming brushes. As a confirmation, the plateau coincides with the pseudo-plateau reported for homopolymer PEO systems.[172]
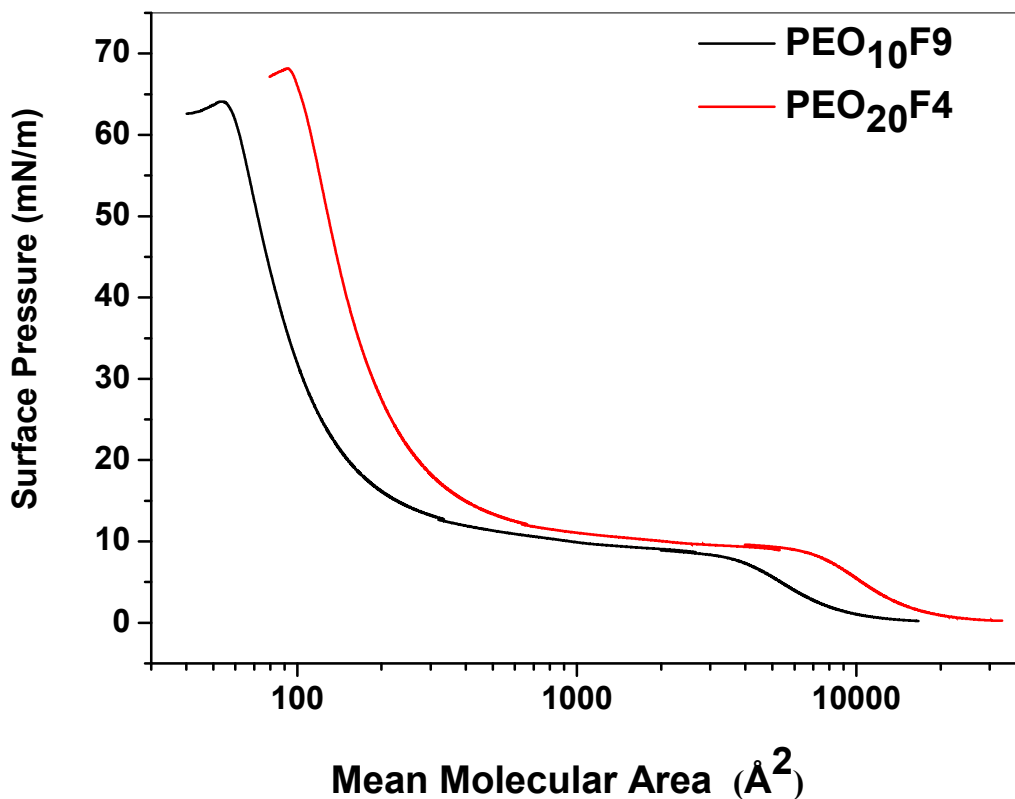
Figure 4.1. Surface pressure (π)–mean molecular area (mmA) isotherms of $PEO_{10}F9$ and $PEO_{20}F4$. The collapse area is 56 $Å^2$ for $PEO_{10}F9$ and 90 $Å^2$ for $PEO_{20}F4$. A pseudoplateau is observed at 8.4 mN m^{-1} for $PEO_{10}F9$, and at 9.2 mN m^{-1} for $PEO_{20}F4$. X-axis log scaled.

The height of the plateau is slightly dependent on the molar mass of the PEO chains. The same behavior was observed for PEO-*b*-PS copolymers with different PEO block lengths by Goncalves da Silva et al.[155] This plateau is indicative of a first-order pancake-to-brush transition and continued until either the PEO chains reach their limiting brush density or the anchoring block at the surface begin to overlap, resulting in the dissolution of PEO into the subphase. In

both cases the sharp increase of the surface pressure beyond the plateau indicates the brush regime.
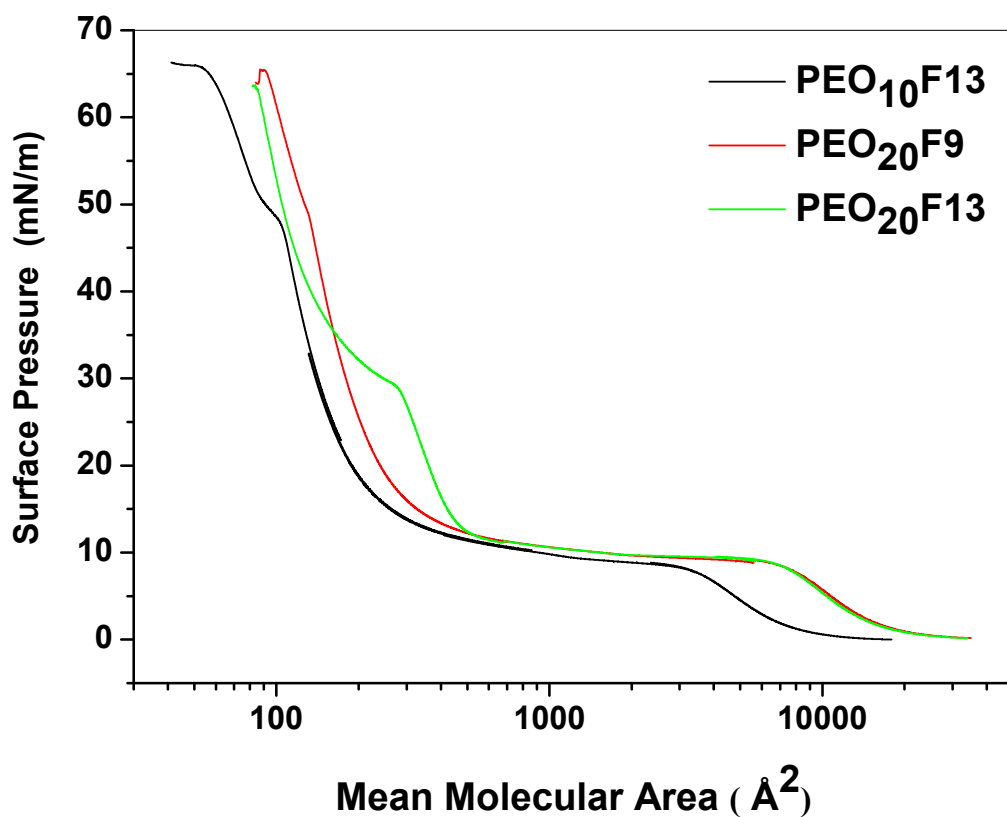
Figure 4.2. Surface pressure (π)–mean molecular area (mmA) isotherms of $PEO_{10}F13$, $PEO_{20}F9$, $PEO_{20}F13$. A change in the slope is apparent at surface pressures of ~ 47mN m^{-1}, ~ 47 mN m^{-1}, and ~ 30 mN m^{-1}, respectively. This transition corresponds to mmA of 101 Å^{2}, 131 Å^{2}, and 265 Å^{2}, respectively. X- axis log scaled.

Fig. 4.2 shows isotherms of the more hydrophobic block copolymers with a higher PFMA content i.e. for $PEO_{10}F13$, $PEO_{20}F9$, and $PEO_{20}F13$. The surface isotherms show two pseudo-plateaus. The one at large mmA is comparable to the phase-transition observed for the isotherms

of copolymers with low PFMA content. Thus it can be assigned to a pancake-to-brush transition. The limiting brush density, i.e. the left end of the pseudo-plateau region increases with increasing number of FMA units. In Fig. 4.3. the limiting brush area of the different triblock copolymers systems was plotted versus the number of FMA units.
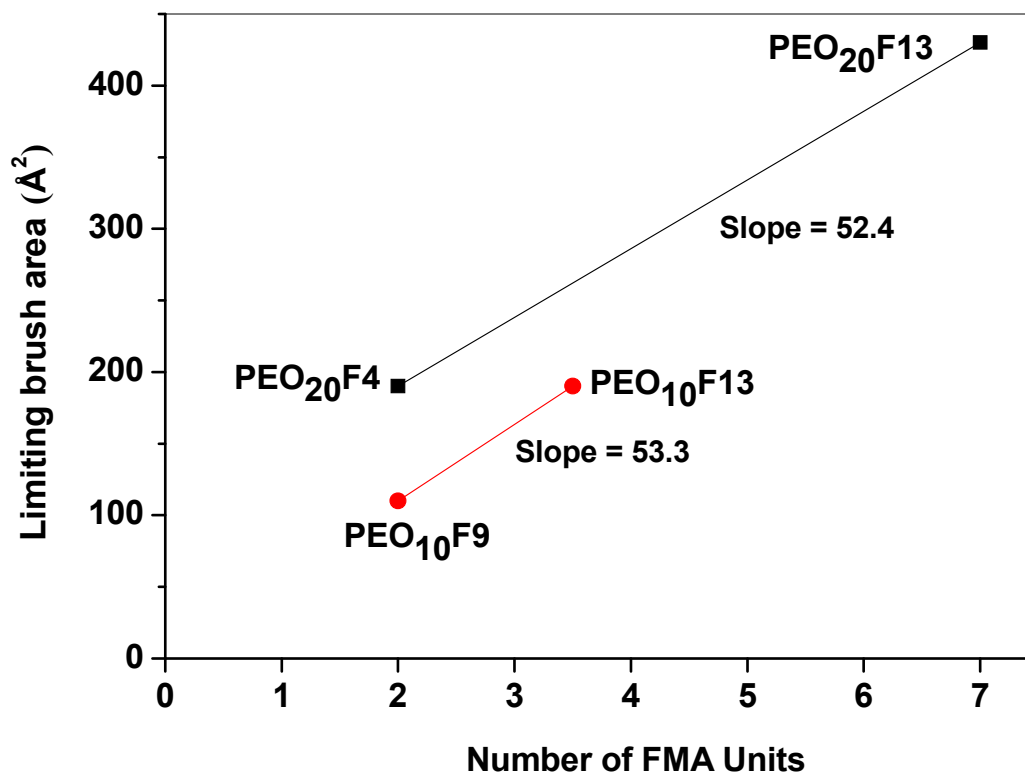

Figure 4.3. Limiting brush area over the number of FMA units in the respective block copolymers.

For both triblock copolymer systems the area per monomer obtained from the slope of a linear fit is 53.3 $Å^2$ in PEO10K and 52.2 $Å^2$ in PEO20K systems. This value agrees well with the value of 52 $Å^2$ found in the literature for fluorinated amphiphilic molecules.[187] The offset of the

linear fit of PEO10K systems equals zero. This implies that the anchored PEO chains can be compressed into a densely packed brush state at the end of the pancake-to-brush transition, which is just hindered by the per-fluorinated alkyl layer. In contrast, the offset obtained from the linear fit of the PEO20K systems is 104 $Å^2$. This is significantly higher than the cross-sectional area (30-40 $Å^2$) required for two neighbored EO units (the diameter of a EO monomer is 4.5 Å.[155] At this mean molecular area a putative loop structure can be expected for the PEO block within the subphase. This shows that the PEO block in the PEO20K system is too long to be compressed into a densely packed brush state at the end of the pancake-to-brush transition, even for a vanishing hydrophobic anchor. Most probably this is due to entropic repulsion between the PEO chains. A further increase in the surface pressure is needed to overcome this. These interpretations are confirmed by comparing the areas for the PEO10K and PEO20K systems at ~65 mN m^{-1}, the collapse pressure. The corresponding mmA are ~56 $Å^2$ and ~90 $Å^2$, respectively. For PEO10K this is roughly twice the cross-sectional area for looped PEO chains and similar to the area required for 2 FMA units in a highly condensed state.[187] Thus, the PEO block indeed is short enough to be compressed into a dense brush state. In contrast, the mmA at the collapse for PEO20K is higher and close to the offset from Fig. 4.3. This confirms that the longer PEO block in the PEO20K system counteracts the compression. Additionally it shows that even for the copolymers with low FMA content dissolution into subphase is unlikely; they are well anchored at the air-water interface.

A second pseudo-plateau or a kink occurs in the brush regime. The surface pressure at the inflection point of the plateau (Table 4.1.) depends on the number of FMA units but is independent from the length of the PEO chain. For $PEO_{10}F13$ and $PEO_{20}F9$ with nearly the same number of FMA units the plateau in the brush regime is observed at a surface pressure of approximately 47 mN m^{-1} at slightly different mmA. If this mmA is divided by the number of

FMA units per PEO chain, as received from ^{1}H NMR data (Table 4.1.), the resulting areas are around 30 $Å^2$ for one per-fluorinated n-hexyl side chain in the corresponding triblock copolymer. This is in good agreement with the reported cross-sectional area of 32 $Å^2$ per fluorocarbon side chain.[187, 188]

Table 4.1. Langmuir monolayer characteristic properties of different copolymers

Copolymer	M_n [a] g mol^{-1}	$n(EO)$ [b]	$n(FMA)$ [c]	MMA$_{ob}$ [d] ($Å^2$)	MMA$_{spt}$ [e] ($Å^2$)
PEO$_{10}$F9	10890	227	2	110	-----
PEO$_{10}$F13	11490	227	3-4	190	101
PEO$_{20}$F4	20834	455	2	209	-----
PEO$_{20}$F9	21978	455	4-5	230	133
PEO$_{20}$F13	22988	455	7	470	270

[a] The molar mass was calculated based on ^{1}H NMR data e.g. from Table 1 it is known that PEO$_{10}$F9 contains 9 wt% of PFMA block and 91 wt% of PEO block. The molar masses of PEO blocks in PEO10K and PEO20K systems were taken as 10000 and 20000 g mol^{-1}, respectively. From these data molar masses of triblock copolymers were calculated and used for Langmuir monolayer measurements.

[b] The number of EO units are calculated by dividing the molar mass of PEO in the copolymers with the EO molar mass.

[c] The PFMA block mass was calculated by deducting the PEO block mass from the overall block copolymer molar mass. The molar mass of a single FMA unit was taken as 432 g mol^{-1} in order to calculate the number of FMA units.

[d] Limiting brush area per molecule.

[e] Mean molecular area corresponding to the inflection point in the second phase-transition.

This suggests that the plateau indicates a phase-transition within the per-fluorinated alkyl chain layer to a closely packed FMA layer. Upon further compression the surface pressure increases smoother until the monolayer collapses. This might come from a rearrangement of the methacrylate backbone as has been reported in lipopolymer systems with very low PEO content.[189] A similar transition is observed in the brush region of different telechelic PEO copolymers.[172] This transition was attributed to the dissolution of the surface attached alkyl chains resulting in loss of polymer into the subphase. This effect should be the more pronounced, the lower is the content of PFMA in the block copolymers, in opposite to our observations. This is in contrast to our observations. Moreover, the expansion isotherms also show the phase-transition in the brush regime, like for compression. Therefore, dissolution of the surface attached alkyl chains into the subphase cannot account for the transitions we observed.

The phase-transition can be either due to crystallization of perfluorinated n-hexyl side-chains as observed in monolayers of perfluorinated amphiphiles[187] or due to the rearrangement of PFMA blocks at the air-water interface. Atsuhiro et al. observed a similar phase-transition in isotherms of amphiphilic 2-(perfluorodecyl)ethyl methacrylate.[187] It was interpreted as the result of crystallization of perfluorinated chains at higher surface pressure. The isotherms were not reversible due to crystallization. In contrast, our isotherms of PEO-PFMA triblock copolymers show reversibility. Thus a crystallization of perfluorinated n-hexyl side chains is unlikely here. With increasing PFMA content the second phase transition becomes more significant and is observed as a pronounced plateau in isotherms of $PEO_{20}F69$ copolymer.[190] A close analysis of the second phase-transition observed in this high PFMA content copolymer reveals that the plateau corresponds to both, the condensation of fluorinated alkyl chains and rearrangement of PFMA block. In $PEO_{20}F13$ copolymer isotherm the second phase transition begins at 285 $Å^2$ mmA which is higher than the area required for closed packed FMA units in the copolymer ($7 \times 32 Å^2 =$

224 Å^2) and ends at ~140 Å^2 mmA, which is smaller. Thus, with increasing FMA content a combination of condensation of FMA units and rearrangement of PFMA block might reflect the second phase transition. The minimum areas to which the monolayers can be compressed further supports our assumption that a vertical rearrangement of PFMA block takes place at low mmA. The block copolymers with at least 3-4 FMA units show a collapse area, which is lower than that for densely packed FMA units. Thus, a rearrangement of the FMA units must occur prior to the collapse. In contrast, the copolymers with a low PFMA content collapse at an area, which is the same or bigger than that for a densely packed FMA layer. Thus, rearrangement of PFMA block is not likely in these systems.

4.3.2. Morphology of the Langmuir-Blodgett films

A monolayer of PEO$_{10}$F13 copolymer was transferred at different surface pressures, 0.5 mN m^{-1}, 3 mN m^{-1}, 20 mN m^{-1}, and 35 mN m^{-1} onto silicon substrates by the LB technique. These surface pressures were chosen based on the plateaus observed in the monolayer, indicating a change in the copolymer organization at the air-water interface, i.e. a phase-transition. The transfer efficiency of the LB films can be measured by the transfer ratio. It is defined as the ratio of the area of monolayer removed from the air-water interface to that of the substrate to be deposited. In case of low molecular weight amphiphilic molecules it was found that the transfer ratio should be equal to 1.[152] In our triblock copolymer system, the LB films were transferred with high transfer ratios of 1.5 and 1.3 at 0.5 mN m^{-1} and 3 mN m^{-1}, respectively. In the brush regime (at high surface pressures 20 mN m^{-1}, and 35 mN m^{-1}) they were transferred with a transfer ratio of 1. Fig. 4.5a shows an AFM image of a PEO$_{10}$F13 LB-film transferred at 0.5 mN m^{-1} with the corresponding 3D image (Fig. 4.5b). A very thin layer (< 4 nm) with elevated white

appearing spots is observed in Fig. 4.5a. A zoom-in into Fig. 4.5a shows small domain structures projected towards the air-water interface in the size range of 50-100 nm. The height of these domains varies between 1.5 to 3 nm. The height of the domains is larger than a monolayer thickness, which implies aggregation of the triblock copolymer. Overall, the size of these domains is consistent with 2D micelles observed in LB film studies of PS-*b*-PEO by Zhu et al.[176-182] and Logan et al.[170, 171]

Figure 4. 5 a**)** AFM image of the PEO$_{10}$F13 triblock copolymer transferred at surface pressure of 0.5 mN m^{-1}. b) Corresponding 3D AFM image of PEO$_{10}$F13 triblock copolymer. Surface micelles projected towards the surface can clearly be seen.

They have observed micelle structures with elevated, white appearing PS cores above a dark appearing PEO corona. Due to the hydrophilic nature of silicon surfaces, the PEO block is oriented towards the silicon substrates and both silicon substrate and PEO repel the PFMA block.

This repulsion leads to aggregation. Thus, the entire domain, as observed in Fig.4.5b, illustrates a micellar structures with a PEO corona and PFMA blocks anchoring towards air-copolymer interface. Thus higher elevated parts of these domains can be assigned to PFMA. At this surface pressure the isotherms are similar to the PEO homopolymer isotherms in which isolated pancakes are expected. Since 3D micelles do not exist at the air-water interface, they must be formed during or after film transfer.
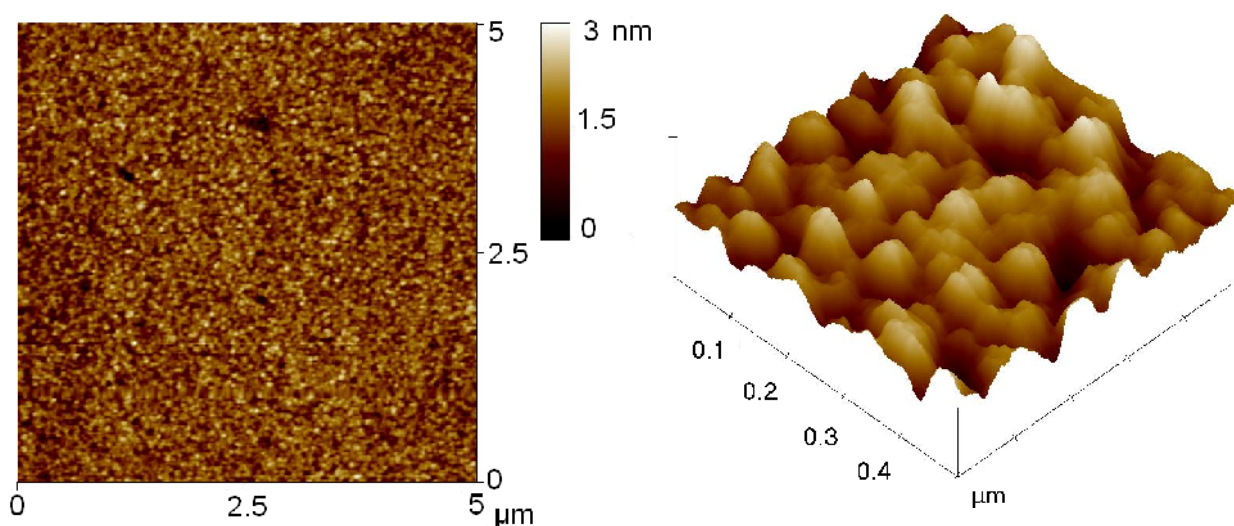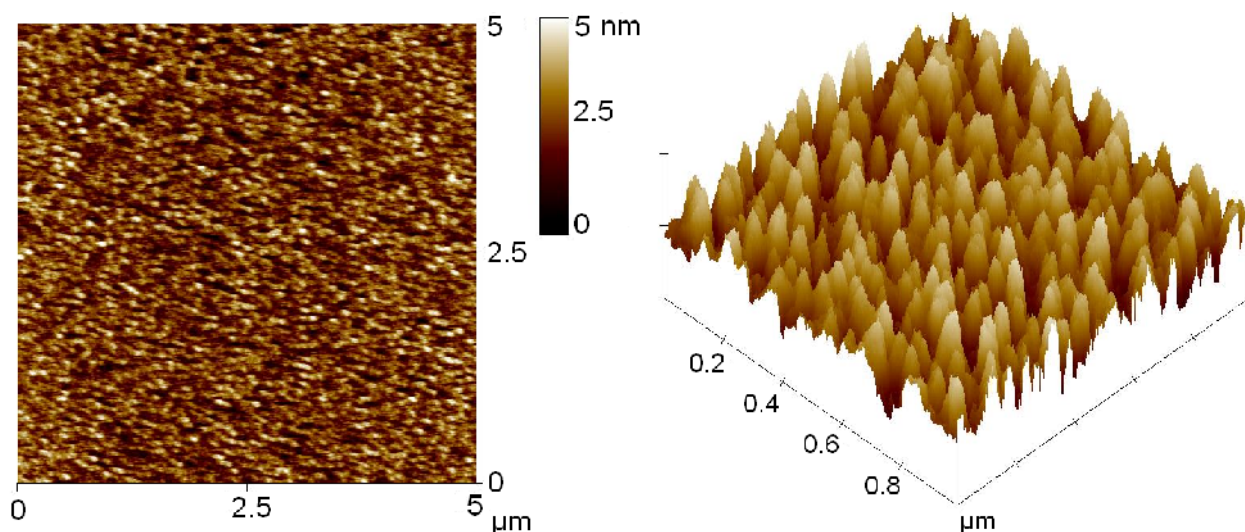

Figure 4. 6. a) AFM image of the $PEO_{10}F13$ triblock copolymer transferred at a surface pressure of 3 mN m^{-1}. b) Corresponding 3D AFM image the $PEO_{10}F13$ triblock copolymer. Surface micelles in the range of 50-100 nm size projected towards the surface are clearly visible.

Fig. 4.6a shows the morphology of the LB films of $PEO_{10}F13$ transferred at a surface pressure of 3 mN m^{-1}. The size of the surface micelles is similar to the size observed at the lower

surface pressure of 0.5 mN m^{-1}. In contrast, the height of the domain structures is considerably increased to 3-5 nm (see Fig. 4.6b). This can be assigned to stretching of PEO molecules into the water subphase upon compression prior to transfer.
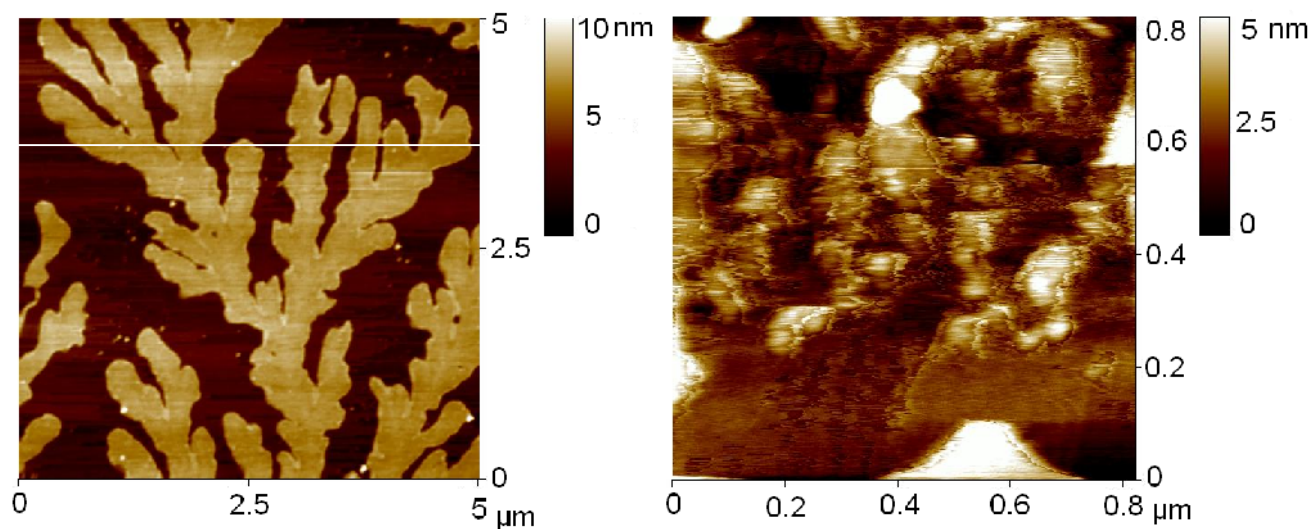
Figure 4.7. a) AFM image of the PEO$_{10}$F13 triblock copolymer at a surface pressure of 20 mN m^{-1}. b) Zoom-in into the space between the finger-like patterns from Fig. 4.7a. Irregularly shaped aggregates are observed.

Fig. 4.7a shows the AFM image of the LB film morphology of PEO$_{10}$F13 transferred at a surface pressure of 20 mN m^{-1}. It shows a finger-like morphology typical for crystallized PEO homopolymer monolayers in thin spin-coated films.[191-193] They are formed due to the conformational difference between the PEO chains adsorbed on the silicon surface and chains, which are not adsorbed. [191-193] This morphology can only be observed if the film is thick enough,

or only after significant supercooling to overcome the nucleation barrier.[194] Thus, we observe it only at a higher surface pressure, where the monolayer is in a condensed state with densely packed brushes and thus thick enough. Moreover, the $PEO_{10}F13$ copolymer contains 3 to 4 FMA units and the volume content of PFMA in $PEO_{10}F13$ copolymer is only 10 vol-%. This is very small compared to the volume fraction of the PEO block (the densities of 1.22 g cm^{-3} for PEO and 1.69 g cm^{-3} for PFMA are measured in a helium pycnometer). So the PFMA blocks have less effect on the PEO conformation on the silicon surface and the crystallization of PEO chains in not hindered. Fig. 4.7b shows a zoom-in into the transferred monolayer. Irregular domains with heights between 2 and 4 nm are visible between the finger-like patterns. This observation is in agreement with the assumption that upon transfer a monolayer covers the entire surface area of the silicon wafer. It further supports the assumption that the finger-like patterns are developed due to crystallization of the block copolymers after the film transfer.
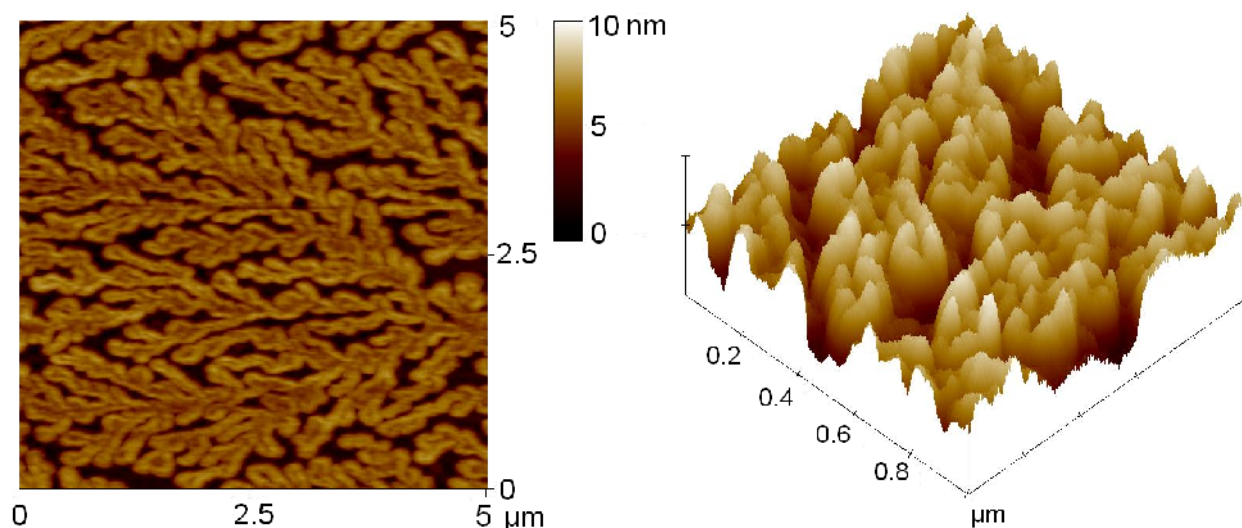
Figure 4.8. a) AFM image of the $PEO_{10}F13$ triblock copolymer transferred at a surface pressure of 35 mN m^{-1}. b) Zoom-in into the finger-like patterns in Fig 4.8a. Finger-like patterns are composed of surface micelles similar to that observed at lower surface pressures.

Fig. 4.8a shows an AFM image of LB film morphology of $PEO_{10}F13$ transferred at 35 mN m^{-1}. The surface area covered by the finger-like morphology is increased compared to the LB film morphology obtained at 20 mN m^{-1}. A closer look at these finger-like patterns reveals that these structures are composed of densely packed surface micelles as can be seen in the 3D AFM image Fig. 4.8b. These surface micelles are projected towards the surface, with similar size range as observed in Fig. 4.6b. This further supports our assumption that the formation of 3D micelles and of finger-like structures occurs during or after the transfer to the silicon substrate.
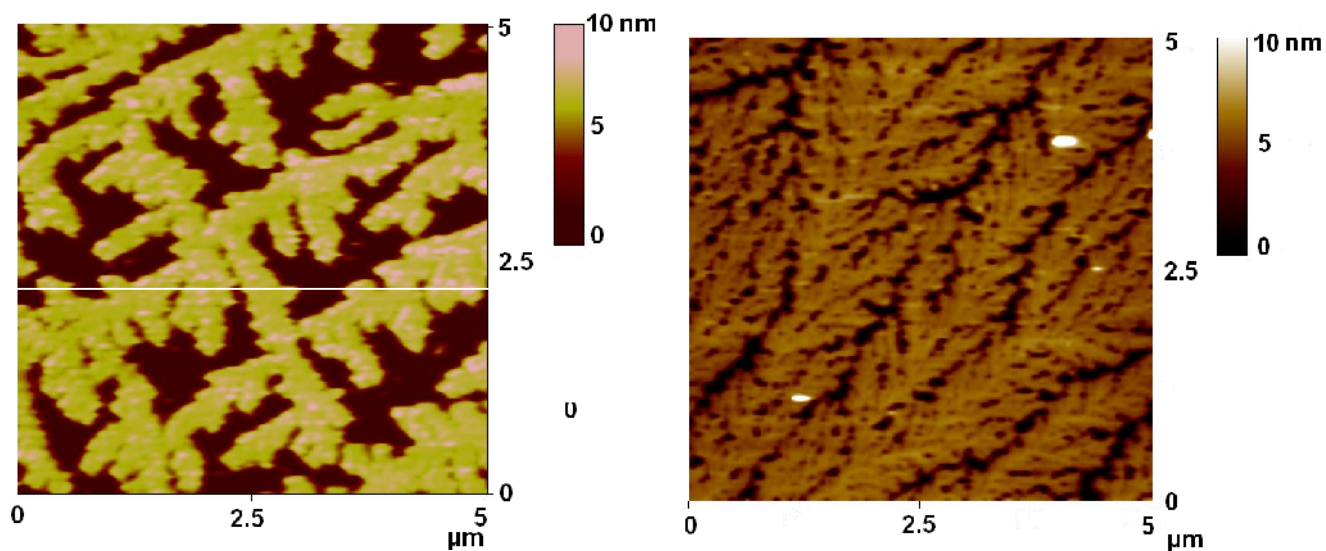
Figure 4.9. AFM image of the PEO$_{20}$F4 triblock copolymer transferred at surface pressure of (a) 20 mN m^{-1} and (b) 35 mN m^{-1}.
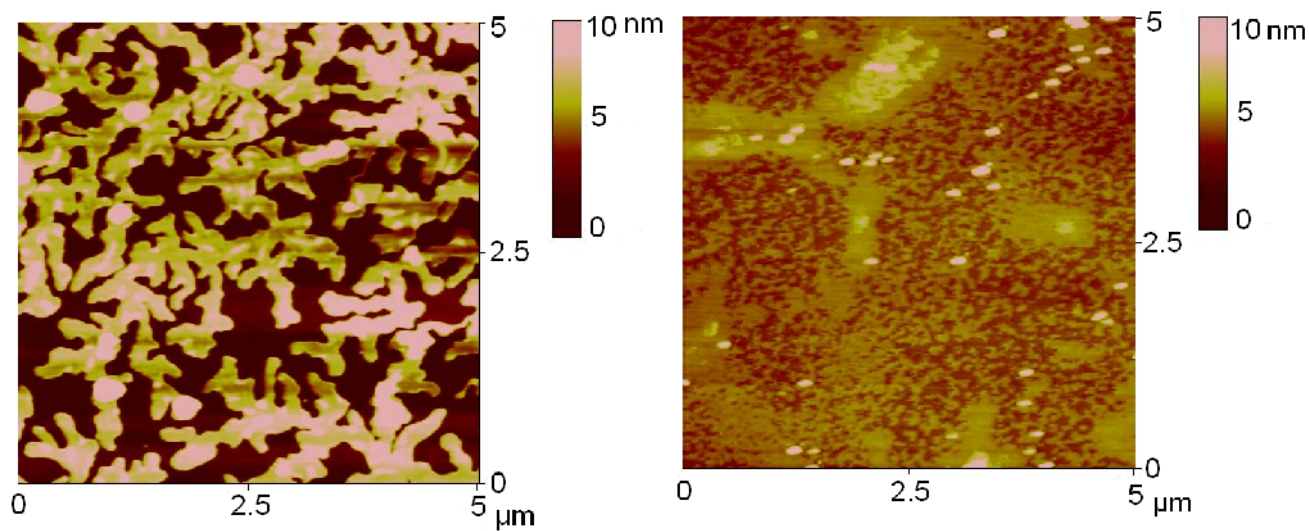
Figure 4.10. AFM image of the PEO$_{20}$F13 tri block copolymer transferred at a surface pressure of (a) 20 mN m^{-1} and (b) 35 mN m^{-1}

Figures 4.9 and 4.10 show AFM images of $PEO_{20}F4$ and $PEO_{20}F13$ copolymer LB films transferred at 20 mN m^{-1} and 35 mN m^{-1} respectively. Again finger-like patterns are observed for $PEO_{20}F4$ at both surface pressures with increasing density. Compared to $PEO_{20}F4$ LB film the crystallization of PEO is hindered in the $PEO_{20}F13$ copolymer LB film transferred at 20 mN m^{-1} (Fig 10a) or even missing at 35 mN m^{-1}. (Fig. 4.10b). This indicates that the PFMA content in $PEO_{20}F13$ is high enough to suppress the crystallization of PEO, as was discussed for bulk crystallization of block copolymers.[184] To discuss the role of the PEO middle block in detail, the AFM images of $PEO_{10}F13$ and $PEO_{20}F4$ LB films at surface pressure 20 mN m^{-1} are compared.
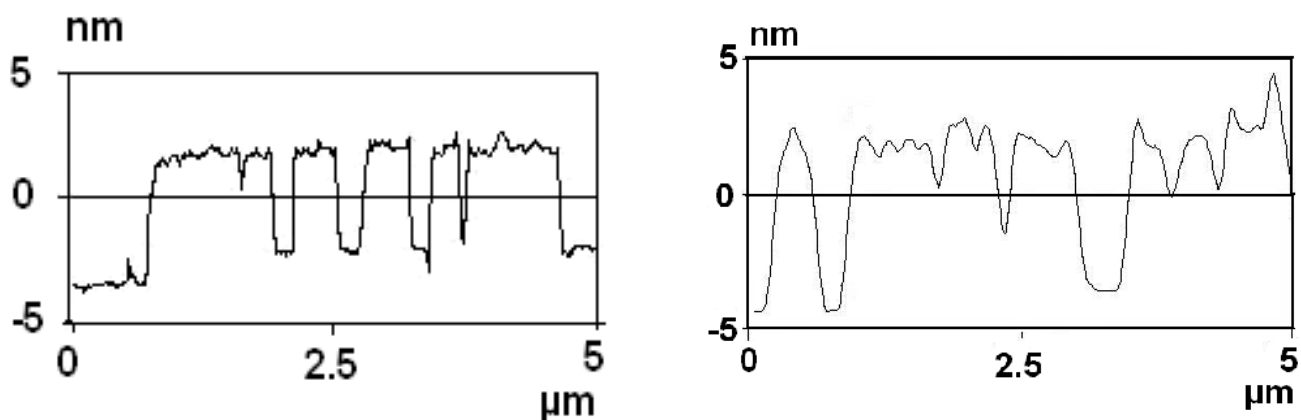
Figure 4.11 a) Height profile of $PEO_{10}F13$ copolymer film shown in Fig. 7a. b) Height profile of $PEO_{20}F4$ copolymer film shown in Fig. 9a. These height profiles are taken along the white lines in the respective figures

Fig. 4.11 shows the height profile of the LB films shown in Fig. 4.7a and Fig. 4.9a taken along the indicated lines. The height of the fingers is 3.8 nm and 6.5 nm for $PEO_{10}F9$ and

PEO$_{20}$F4, respectively. The increase in the height of the fingers for PEO20K copolymer can be related to the higher molar masses of the PEO middle block. According to Reiter et al.[191-193] the thickness or height of the fingers gives information about chain folding and thus about organization of polymer segments in the crystal. In our LB films the height of the finger-like patterns is significantly lower, when compared to a fully stretched molecule. For instance, the length *L* of fully stretched crystalline PEO10K and PEO20K molecules is 63 nm and 125 nm, respectively. (L = 0.2783 nm x (Mn^{PEO}/ Mn^{EO}) = 63 nm) (0.2783 nm is the ethylene oxide unit length).[194] This implies that polymer molecules are folded several times due to crystallization. These observations are in accordance with observations by Reiter et al. [191-193]

Figure 4.12. Schematic representation of triblock copolymer monolayer behavior at air-water interface.

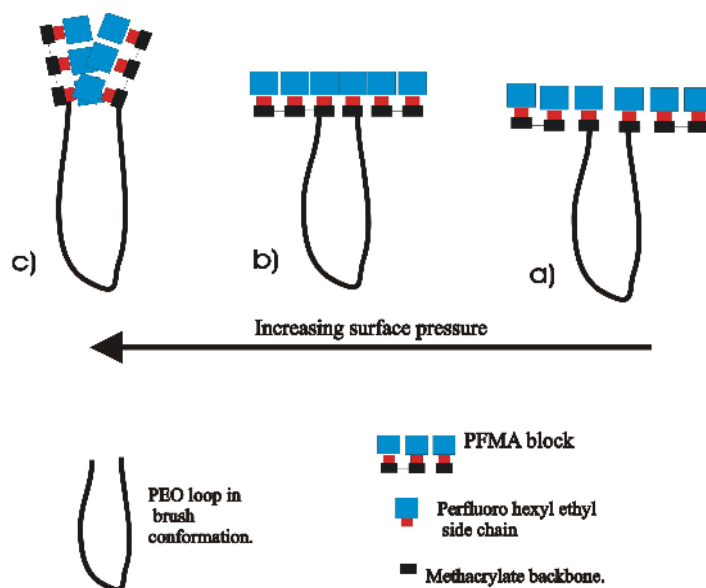Fig. 4.12 illustrates the molecular behavior of triblock copolymers with increasing surface pressure in the brush regime. At the limiting brush area (Fig. 12a) the PEO block extends into the subphase forming brushes, anchored by loosely packed PFMA blocks (overlapping region of PFMA blocks). Upon compression (Fig. 12b), at the inflection point of the phase-transition in the brush regime closely packed PFMA blocks are arranged with vertically oriented perfluoro n-hexyl ethyl side chains attached to the methacrylate backbone. Near the collapse (Fig. 12c), the whole PFMA blocks are arranged perpendicular to the aqueous subphase.

4.4. Conclusions

Amphiphilic triblock copolymers of PEO and PFMA form stable monolayers at air-water interface. It is observed that a small PFMA content (less than 13 wt% of the copolymer) can influence the brush formation of the PEO block. An extended plateau for all copolymers shows the typical phase-transition from pancake to brush for the PEO chains. An additional plateau in the brush regime is attributed to rearrangement of PFMA blocks from horizontal to vertical. The mean molecular area at the second plateau corresponds to the area of closely packed perfluorinated n-hexyl side chains of FMA block in the corresponding triblock copolymer system. Therefore, vertically oriented perfluorohexyl-ethyl side chains can be assumed (i.e. methacrylate backbone is arranged horizontally to aqueous subphase). Upon compression the whole PFMA block is rearranged perpendicular to the aqueous subphase. LB films transferred at low surface pressure show surface micelles. Triblock copolymer LB films with low PFMA transferred at high surface pressure show a typical crystalline morphology of PEO. This crystallization was hindered with increasing amount of PFMA content.

In this work, we have studied the monolayer properties of triblock copolymers with a PEO middle block at the air-water interface. Compared to the simple telechelic systems with non-fluorinated alkyl hydrophobic anchoring groups, fluorinated alkyl hydrophobic groups can anchor PEO more strongly at the air-water interface. Additionally, it is an ideal system to study the role of the length of PEO middle blocks on the phase-transition within the hydrophobic anchor group. With single anchoring groups at each end of the copolymer a rearrangement of anchoring group is impossible and the telechelic block copolymers behave like ordinary anchored PEO chains. In contrast, a rearrangement within the anchor groups is probable with an increasing number of anchoring groups (≥ 3 FMA units). The packing density of the anchoring groups also depends on the length of the middle block. PEO10K systems with 227 EO units form nearly dense brushes with molecular areas of 56 Å^2. For the longer PEO20K systems with 455 EO units the minimum area is 90 Å^2. Thus, the cross-sectional area of the hydrophobic anchor groups has to be larger than these limiting areas for a rearrangement of the anchor groups to be possible. .

Chapter 5

Water Surface covering of Fluorinated Amphiphilic Triblock Copolymers: Surface Pressure-Area and X-ray Reflectivity Investigations

5.1. Introduction

Amphiphilic block copolymers are known to form polymer brushes at high grafting densities on the water surface.[195,196] The copolymers are anchored by their water soluble blocks on the water surface with the hydrophobic blocks above the surface. Polymer brushes are interesting due to their potential applications such as colloidal stabilisation[197,198] or biological membranes.[199,200] In experiments on a Langmuir trough, the surface densities of polymer brushes and therefore the mean molecular area (mmA, the average area per polymer molecule on the surface) can be varied easily. X-ray and neutron reflectivity (XR and NR) studies have been found to be very useful techniques to study the developing surface structure at the air-water interface.[201-203] Typical hydrophobic blocks consist of poly(propylene oxide) (PPO),[204] poly(ethyl ethylene) (PEE),[205-207] poly(hydrogenated isoprene) (PhI),[208] poly(1,1-diethylsilabutane) (PdESB)[209] or poly(styrene) (PS)[210-215] and the hydrophilic part is formed e.g. by poly(styrenesulfonic acid) (PSSa),[207,208] poly(methacrylic acid) (PMAa),[209] and poly(ethylene oxide) (PEO).[204-206, 210, 212, 214-221]

Polymer monolayer systems at the air-water interface have been widely studied by NR[222-225] and XR[214,215, 226-230] techniques. For many polyelectrolytes [e.g. PEE-*b*-PSSa,[207] PhI-*b*-PSSa,[208] PdESB-*b*-PMAa[209]], the thickness of the hydrophilic brush depends - beside compression - also on the ion density, furthermore for some strongly ionic polyelectrolytes, the thickness of the

hydrophilic brush was found to be independent of the surface pressure in the osmotic brush phase. These polymer brushes were named as double layers or carpet like dense brush layers. In the case of PEO copolymer systems the behavior is different.[204-206, 210-215] PEO remains at low surface pressure near the surface ('pancake') and only at high grafting densities the brushes are stretched into the subphase due to excluded volume interactions between polymer chains. In such systems, the thickness or height of the brush was found to be increased with increasing surface pressure. Measuring the surface pressure depending on mmA, this pancake-to-brush transition can be observed at low surface pressure (~9 mN/m).

Monolayers of PEO systems with lipid headgroups[216-219] (lipopolymers) or with other short hydrophobic endgroups[220,221] (telechelic polymer) show additionally a second phase-transition at high surface pressure. In lipopolymer systems, this behavior was assigned for ordering of hydrophobic tails, whereas in PEO telechelic polymers it was assigned for dissolution of the polymer into the subphase. In PEO-*b*-PS systems (PS block is glassy at room temperature) the anchoring long PS block was found to be aggregated to form 2D micelles[210-213] at the air-water interface. In PEE-PEO diblock copolymer monolayers[205,206] (the hydrophobic PEE blocks behave like fluid at room temperature) large domain formation was observed in which PEE blocks are partly immersed into the water. The thickness of hydrophobic PEE blocks was found to be inversely proportional to mmA.

This study is based on water insoluble triblock copolymers, consisting of a hydrophilic PEO middle block and poly(perfluorohexyl ethyl methacrylate) (PFMA) as hydrophobic end blocks. The synthesis is described elsewhere.[231] It was also shown, that PFMA-*b*-PEO-*b*-PFMA amphiphilic triblock copolymers with very short PFMA block (e.g. a single FMA unit at the each end of a 227 units long PEO middle block) are water soluble[232,233] and that these copolymers sometimes show a second phase transition at the air-water interface which can be related to a

rearrangement of PFMA as in the case of lipopolymer systems.[234] Triblock copolymers with >2 FMA units per end block are water insoluble, but show always this second phase transitions in the isotherms. In this paper we correlate the phase transition limits with the characteristic length scales of the polymers and using XR measurements we prove that the phase transition in the brush region corresponds to rearrangement of the whole PFMA block from horizontal to perpendicular orientation with respect to the water surface. In the present work, monolayer behavior of 3 different block copolymers with different molecular architecture was studied using Langmuir trough experiments. X-ray reflectivity measurements were carried out on triblock copolymers as a function of surface pressure at the air-water interface on a Langmuir trough.

5.2. Experimental Section

5.2.1. Materials

PFMA-*b*-PEO-(*b*-PFMA) di- and triblock copolymers used in this study (see Figure 5.1.) were synthesized and characterized in accordance to the previously reported procedure.[231] In the abbreviation scheme PEO_xFy x represents the molecular weight of the PEO block (in kg/mol, according to the supplier) and y the PFMA content in wt%, based on NMR measurements. In case of diblock copolymers, an additional -D is added to the name. The PEO samples were converted into a macroinitiator and the PFMA blocks were added. Polydispersity of the polymerization products was measured using size exclusion chromatography (SEC), where the calibration is carried out using PEO standards. Due to the well known effect, that modified polymers can show a lower mass in SEC caused by a contraction of the chain, values for M_n were calculated via the PFMA content obtained from NMR measurements. The characteristic data of the polymers are given in Table. 5.1. From homopolymer samples, the bulk densities were measured in a helium pycnometer (PEO: 1.22 g/cm^3; PFMA: 1.69 g/cm^3)
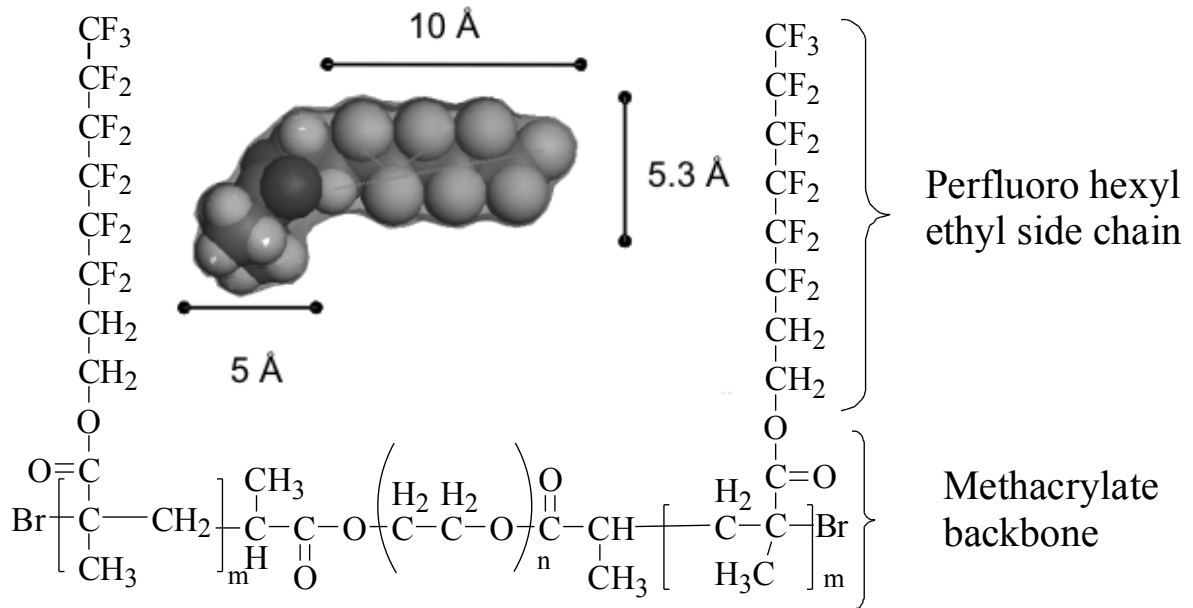
Figure 5.1. Chemical structure of PFMA-*b*-PEO-*b*-PFMA triblock copolymer. The inset shows the characteristic length scales of a FMA unit. The perfluoro hexyl ethyl side chain has a typical length of 10 Å and a thickness of 5.3 Å and the methacrylate backbone is approximately 5 Å thick.

Table 5.1. Characterization of the block copolymers

Copolymer	M_w/M_n [a]	n(EO) [b]	PFMA [c] wt.%	n(FMA) [d]	M_n [e] kg/mol
PEO$_5$F32-D	1.26	113	31.9	6	7.6
PEO$_{10}$F9	1.33	227	9	2	10.9
PEO$_{10}$F41	1.32	227	40.3	16	16.9
PEO$_{20}$F69	1.30	455	68.7	102	65

[a] SEC results measured in THF using PEO standards.

[b] number of EO units per chain obtained from initial macroinitiator mass (5, 10 and 20 kg/mol)

[c] ^{1}H NMR results.

[d] number of FMA units per polymer chain obtained from PFMA wt% and PEO macroinitiator molar mass

[e] molar mass obtained from PFMA wt% and PEO macroinitiator molar mass.

5.2.2. Surface pressure(π)-area (mmA) measurements

The surface isotherms (surface pressure (π) versus mmA) of the copolymers at the air-water interface, were measured with a Teflon® Langmuir trough system (KSV Ltd, Helsinki, Finland) equipped with two moving barriers and a micro-roughened platinum Wilhelmy plate. The maximum available surface area of the Langmuir trough is 76800 mm^2 (compression ratio 8:1). Distilled water was used as subphase, which was subsequently passed through a water purification system from Purelab option system (ELGA Ltd., Celle, Germany) equipped with an organic removal cartridge (conductance < 0.06 µS cm^{-1}). The purity of the bare water surface was

checked before each measurement by a maximum compression ($\Delta\pi<0.1$ mN/m). The temperature of the water subphase was maintained at 23±0.5°C, using a circulating water bath system. Copolymers were dissolved (2 mg/mL) in HPLC grade chloroform (Sigma-Aldrich / Fluka, Seelze, Germany) and predetermined amounts were spread evenly on the subphase in 1-2 μL small drops using a Hamilton's digital microsyringe. The compression at a constant rate of 7.5 cm^2/min was started after 20 min to ensure the full evaporation of solvent. To obtain the complete isotherm the copolymer solutions were spread upon different initial pressures and thus different parts of the isotherm were recorded. After combining them into one plot they overlap within the experimental error. The experimental setup was enclosed in a box for constant humidity and minimization of surface contamination.

5.2.3. X-ray reflectivity measurements

X-ray reflectivity measurements were carried out at the BW1 beam line at HASYLAB (DESY, Hamburg, Germany) using a liquid surface diffractometer with an incident wavelength of λ=1.3037 Å. A thermostated Langmuir trough equipped with a Wilhelmy film balance to measure surface pressure and a single barrier to change the surface area was mounted on the diffractometer. The instrumental details are given in an article by J. Als-Nielsen.[235] To avoid beam damage, the sample was displaced after several minutes of irradiation, i.e. a single profile was measured on four neighbored positions. The data were corrected for background scattering and the obtained reflectivity curves were fitted using the Parratt algorithm[236] embedded in a program by Mr. Braun ('Parratt-The Reflectivity Tool', kindly provided by HMI, Berlin[237]).

5.3. Results and Discussion

5.3.1. Monolayer behavior at the air-water interface (surface pressure–area measurements).

Fig.5.2. shows the compression isotherms for PEO_5F32-D, $PEO_{10}F41$, and $PEO_{20}F69$. For comparison, the isotherm of the water soluble $PEO_{10}F9$ is also given. Irrespective of the differences in their molecular architecture all three block copolymers show qualitatively similar behavior. At low compression (i.e. high mmA values), the molecules are separated at the surface and no significant change in surface pressure occurs during compression. The first increase of the surface pressure (indicated by number -1- in Fig. 5.2.) defines the limiting pancake area A_p. With further compression, the surface pressure increases until it reaches a pseudo plateau at ~9 mN/m - the pancake to brush transition. The transition starts at the upper limiting pancake to brush transition area A_{pb} (number -2-) and ends at the limiting brush area A_b (number -3-). With further compression, the surface pressure increases again until it reaches in case of the water insoluble polymers a second pseudo plateau or phase transition at ~28 mN/m. The upper and lower limits of this transition, A_{ust} and A_{lst}, are also indicated in Fig. 5.2 by -4- and -5-. Further compression after the second phase transition leads again to an increase in surface pressure until film collapse at A_{col} (-6-). The obtained data are summarized in Table II. Sample $PEO_{20}F69$ shows also an additional kink at 1000 $Å^2$ with a surface pressure of ~50 mN/m. At large mmA, until the limiting brush area, the isotherms for $PEO_{10}F41$ and $PEO_{20}F69$ are similar to the isotherms of block copolymers with low PFMA content, i.e. $PEO_{10}Fy$ (y=9, 13) and $PEO_{20}Fy$ (y=4, 9, 13) block copolymer isotherms respectively.[231] Fig. 5.3. shows a plot of the limiting pancake area A_p vs. the number of EO monomers. A_p increases linearly with the number of PEO monomers. The slope of the curve is 39 $Å^2$, which represents the area of a single EO unit in the pancake region. This value is in good agreement with literature values (40 $Å^2$- 48 $Å^2$) reported for PEO homopolymers.[238]

This indicates that at large mmA the block copolymer behavior at the air-water interface is determined only by the PEO block.
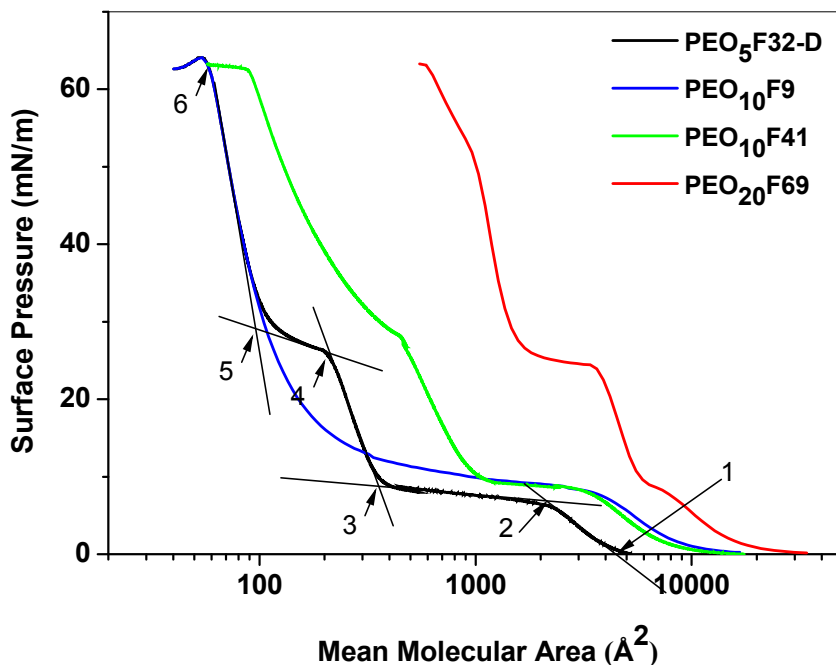
Figure 5.2. Surface pressure (π)–mean molecular area (mmA) isotherms of PEO$_5$F32-D, PEO$_{10}$F41, and PEO$_{20}$F69. For comparison, the isotherm of the water soluble PEO$_{10}$F9 without second transition is also given. The numbers and the lines in the graph describe the determination of limiting pancake area (1, A_p), upper limiting pancake to brush transition area (2, A_{pb}), limiting brush area (3, A_b), upper (4, A_{ust}) and lower (5, A_{lst}) limiting 2nd phase transition area and collapse area (6, A_{col})

Table 5.2. Characteristic mmA values.

Copolymer	A_p[a] ($Å^2$)	A_{pb}[b] ($Å^2$)	A_b[c] ($Å^2$)	A_{ust}[d] ($Å^2$)	A_{lst}[e] ($Å^2$)	A_{col}[f] ($Å^2$)
PEO$_5$F32-D	4360	2170	335	200	101	57
PEO$_{10}$F9	8700	3750	110	--	--	56
PEO$_{10}$F41	8270	3350	900	451	186	90
PEO$_{20}$F69	18300	7750	5560	3880	1490	510

[a] limiting pancake area per molecule

[b] upper limiting pancake to brush transition area per molecule

[c] limiting brush area per molecule

[d] upper limiting second phase-transition area per molecule

[e] lower limiting second phase-transition area per molecule

[f] collapse area per molecule

Under further compression, the pancake region is followed by the first pseudo-plateau with a surface pressure of ~9 mN/m for all block copolymers. This pseudo-plateau corresponds to pancake to brush transition of PEO block in the copolymer and is very well established. Polymer chains anchored at the air-water interface by one or two of their end points, have strong excluded volume interactions between neighboring polymer chains, which results in stretching of polymer chains towards subphase on compression of the monolayer. At very high grafting densities these are called polymer brushes. Therefore, the PEO parts remaining at the surface are now pressed into the water subphase and the hydrophobic PFMA block remains at the surface.
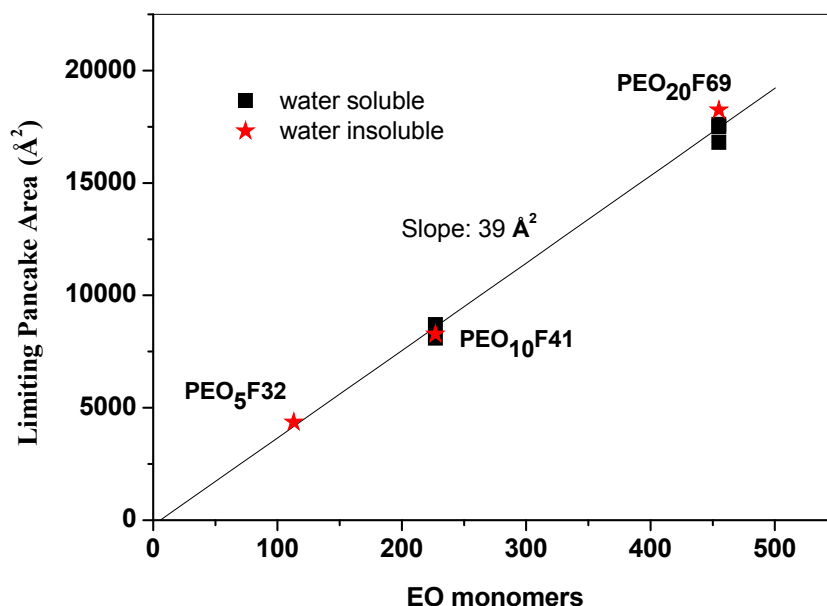
Figure 5.3. Limiting pancake area (A_{op}) vs the number of EO monomers of the respective copolymers. The values for water soluble species are also added (from ref. 234)

The plateau ends at the limiting brush area (A_b), when the area occupied by the hydrophobic parts at the surface is reached. Baker et al.[239,240] have shown, that the pancake-to-brush phase transition can be hindered if the area occupied by the hydrophobic anchoring (PS blocks) is similar to the pancake area of PEO blocks due to steric interaction between hydrophobic anchoring (PS) blocks and the repulsive interactions between hydrophobic (PS) and hydrophilic (PEO) blocks. For PEO-PS copolymer isotherms with 15.5 wt% of PEO[211] a small pseudo-plateau was observed, whereas the PEO-PS copolymer isotherm with only 7 wt% of PEO[213] did not show any pseudo-plateau corresponding to the pancake-to-brush transition of PEO block.

In PEO$_{20}$F69 copolymer isotherm length of the plateau corresponding to PEO pancake to brush transition is significantly reduced, but still observable. For the polymers under investigation, the limiting brush area was plotted against the number of FMA units (Fig. 5.4). Additional values for

water soluble polymers $PEO_{10}Fy$ and $PEO_{20}Fy$ with low PFMA content were taken from reference 234. There it was shown, that isotherms of $PEO_{10}F9$ triblock copolymer (being with approximately 1 FMA unit per end block more a hydrophobic endcapped PEO polymer than a real block copolymer) show no such pseudo plateau in the brush regime. Furthermore, the isotherms of $PEO_{20}F9$ and $PEO_{10}F13$ triblock copolymer (having approximately 2 FMA units per end block) show a kink in the brush regime as indication for a beginning plateau. Between the limiting brush area and the number of FMA units a linear dependence can be observed.
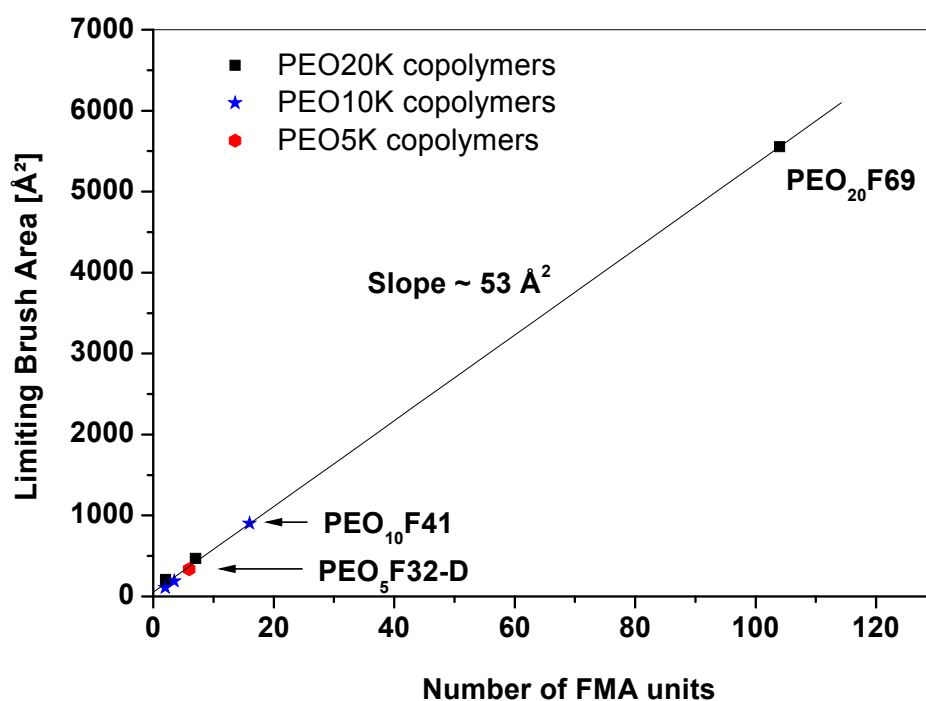

Figure 5.4. Limiting brush area per FMA unit vs. number of FMA units.

The limiting brush area is proportional to the number of FMA units of the polymer and from Fig. 5.4 a slope of 53 Å^2 per FMA unit can be obtained. This value corresponds to the sticky, fluorinated part (perfluoro hexyl, FH) of a flat lying FMA monomer unit (see inset in Fig. 5.1) with a typical length of ~10 Å and a diameter of ~5.3 Å and is in excellent agreement with the value of 52 Å^2 found in the literature for fluorinated amphiphilic molecules.[241] Therefore, the limiting brush area is determined by the length of the PFMA block. Under further compression, the hydrophobic PFMA blocks begin to overlap, and the surface pressure increased rapidly. This increase in surface pressure is therefore due to steric interactions between hydrophobic PFMA blocks and is not affected by the PEO block, which is continuously pushed into the water subphase.

With increasing compression, the FMA sidechains are tilting up. First, the surface pressure is increasing until it reaches a second pseudo-plateau at ~25 mN/m (see Fig. 5.2). The corresponding A_{ust} value (Table 5.2) divided by the number of respective FMA unit is for the PEO$_{20}$F69 and the PEO5F32-D polymer ~36 Å^2 and for PEO10F41 ~28 Å^2. This value has to be compared with the area of a flat lying FH unit (53 Å^2) and a standing FH/FMA unit, which corresponds to the molecular cross section of 28 Å^2 (obtained from poly(tetra fluoro ethylene)[242]). Investigations on poly(N-(polyfluoroalkyl) acrylamide)[243] (a system with comparable fluorinated but without a hydrophilic part) lead to a significant different behavior. At mmA values ~30 Å^2 the surface pressure increases as expected for dense packed fluorinated chains until the film collapse. Therefore, the value of 36 Å^2 could correspond to an expanded liquid state, when the FMA side chains are partly ordered and not in a condensed state, but that is not possible for the value of 28 Å^2, where the FMA chains would be already in the compressed state. To understand the origin of the different behavior, the mmA values at the end of the 2nd pseudo-plateau (A_{lst}, Table 5.2) have

also to be kept in mind. The area increases nearly linear with the FMA content- and an average

mmA value of 14.4 $Å^2$ per FMA unit can be found - just half of the expected value. Therefore, a

double layer of standing FMA side chains seems to be formed on the water surface. For instance,

in $PEO_{20}F69$ copolymer isotherm the second phase transition begins at 3880 $Å^2$ mmA (36 $Å^2$ per

FMA unit) and ends at ~1490 $Å^2$ mmA (14 $Å^2$ per FMA unit or 28 $Å^2$ for 2 FMA units). Thus, a

tilting of FMA units from horizontal mono- to a vertical double-layer until a liquid condensed

film is formed reflects the second phase transition. To prove these assumptions, X-ray reflectivity

measurements have been performed.

5.3.2. Monolayer behavior at the air-water interface (X-ray reflectivity measurements).

X-ray reflectivity measurements have been carried out on $PEO_{20}F69$ triblock copolymer

on a water filled Langmuir trough. The corresponding isotherm of $PEO_{20}F69$ was discussed in the

previous section. It shows a typical behavior of our triblock copolymers with >3 FMA units per

chain with a prominent 2nd pseudo-plateau. To compare the XR results, the same investigations

have been performed also with the water soluble $PEO_{10}F9$ triblock copolymer, which does not

show a 2nd pseudo plateau. The corresponding isotherm is given in Fig. 5.5. The polymers were

prepared as in the π/mmA measurements and at defined mmA values reflectivity measurements

were performed (see Fig. 5.5).

In most cases, the reflectivity could be calculated from a two-box model for electron density

profile (see Fig. 5.6), for simplicity, the 1st layer is called PFMA-layer and the 2nd one PEO-

layer, although such a rigorous assignment is not always permissible. The boundaries between

two layers/phases were smeared using a normal distribution (at each interface z_i, the electron

density is varied according to $\rho(z)=\rho_1+\Delta\rho(1+erf((z-z_i)/(\sigma_i\sqrt{2})))/2$, with the Gaussian width σ_i as a

roughness factor). The electron densities of the water subphase and air phase were fixed to 0.336 $\mathring{A}^{-3}$ and 0, respectively, while the other seven fitting parameters (thickness and electron density of both layers and the roughness of three interfaces) were kept variable. The results for the PFMA layer (thickness, electron density and roughness) are well determinable.
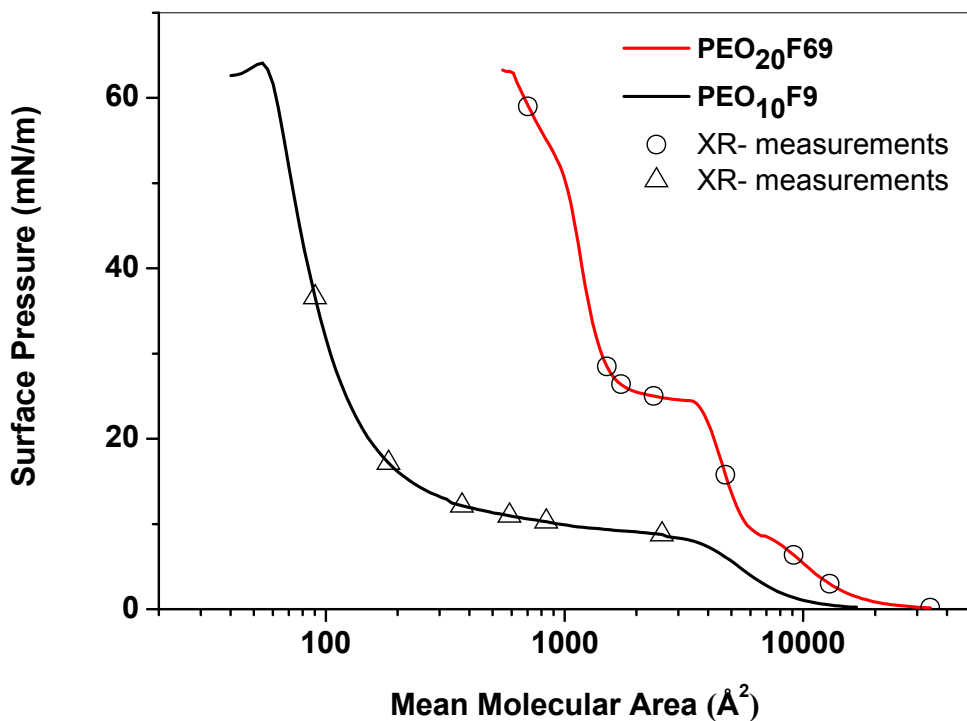
Figure 5.5. Surface pressure (π)–mean molecular area (mmA) isotherms of PEO$_{10}$F9 and PEO$_{20}$F69 with indicated positions for XR measurements.

To obtain an acceptable match between data and fit, a PEO layer must be present for all higher surface coverings. Though, in some cases it could not be distinguished, whether the electron density of the PEO layer is slightly smaller or larger than the water subphase electron density; both scenarios are possible, depending on the amount of water in the PEO layer. Therefore, a

detailed investigation of the PEO in subphase was not practical for our measurements (e.g. the brush density in the water subphase could not be calculated). In cases with a thick PEO layer, the roughness σ_{H2O} has nearly no influence on the fitting result (but must be nonzero), it was fixed then to 5 Å. Typical results for the interface roughness where either around 4 Å, i.e. quite sharp interfaces with surface capillary waves,[244] or at half the layer thickness, i.e. disordered interface[206]. The significance of the fit (typical χ^2 ~0.01-0.02) was good enough to obtain PFMA layer thickness and electron density with an accuracy of ~3%.

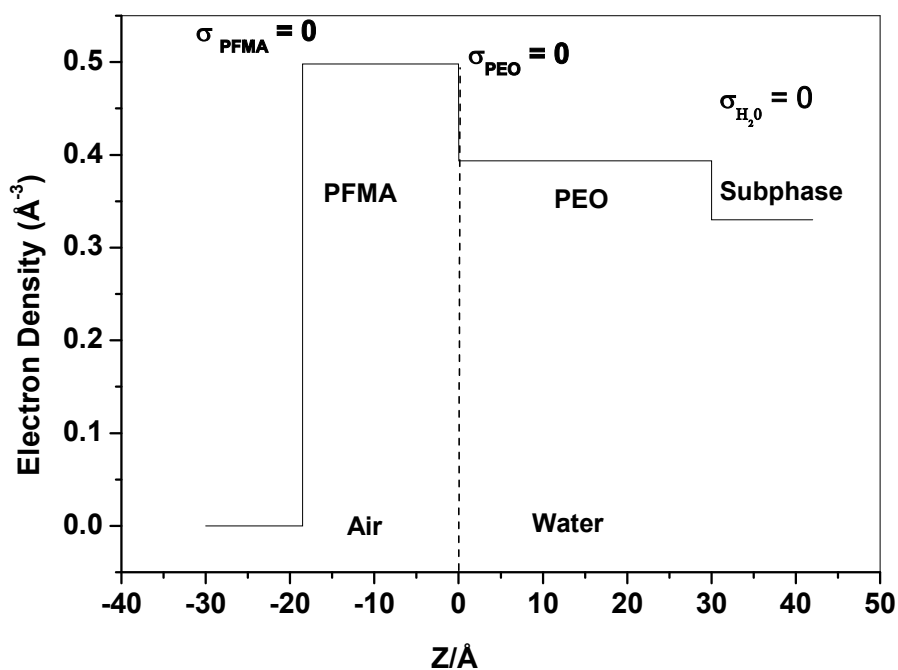**Figure 5.6.** Two box model used for X-ray analysis with sharp interfaces. The interface roughness is simulated by a normal distribution.

The obtained electron density profiles were tested with different conditions with respect to their consistency: (a) the reflectivity curve should be approximated good, (b) the thickness of each

layer should correspond to typical length scales (i.e. they should not be below 4 Å or above 100 Å), and (c) the calculated number of electrons per PFMA chain (electron density × mmA × PFMA layer thickness) should be in the range of the true value for the corresponding molecule. It is important to note that in our copolymer systems the length of the hydrophobic block is very small when compared to the PEO block length. The block copolymer with highest PFMA content ($PEO_{20}F69$) contains only ~52 FMA units at each end of a long (455 units) PEO middle block. As no water should be embedded in the PFMA phase, the expected electron density of a highly compressed film should be in the range of 0.5 $Å^{-3}$. PEO with low water content (above water surface, 'swimming', or dehydrated216[7]) should have a lower and water enriched PEO (below water surface) a slightly higher electron density than pure water.

XR of $PEO_{20}F69$ at the air-water interface

From Fig. 5.5 it can be seen, that XR measurements have been carried out at pancake region (at 38600 $Å^2$, 12900 $Å^2$ and 9000 $Å^2$), in the brush regime at 4800 $Å^2$, within and at the end of the second pseudo-plateau at 2400 $Å^2$, 1700 $Å^2$, and 1500 Å2, and at the collapse region at ~700 $Å^2$. (Remark: due to collapse of the film, the exact mmA value for the final measurement could not be determined from trough area. The more reliable value of mmA = 700 ± 50 $Å^2$ was obtained from surface pressure and XR results.) Fig. 5.7 shows the XR profiles of $PEO_{20}F69$ copolymers and the fitting curves, obtained from the electron density depth profiles given in Fig. 5.8 and Table 5.3. In the profiles, the line at z=0 indicates, that the total number of electrons counted at negative z is equal to the expected total number of electrons in the PFMA parts of the polymer for the given compression.
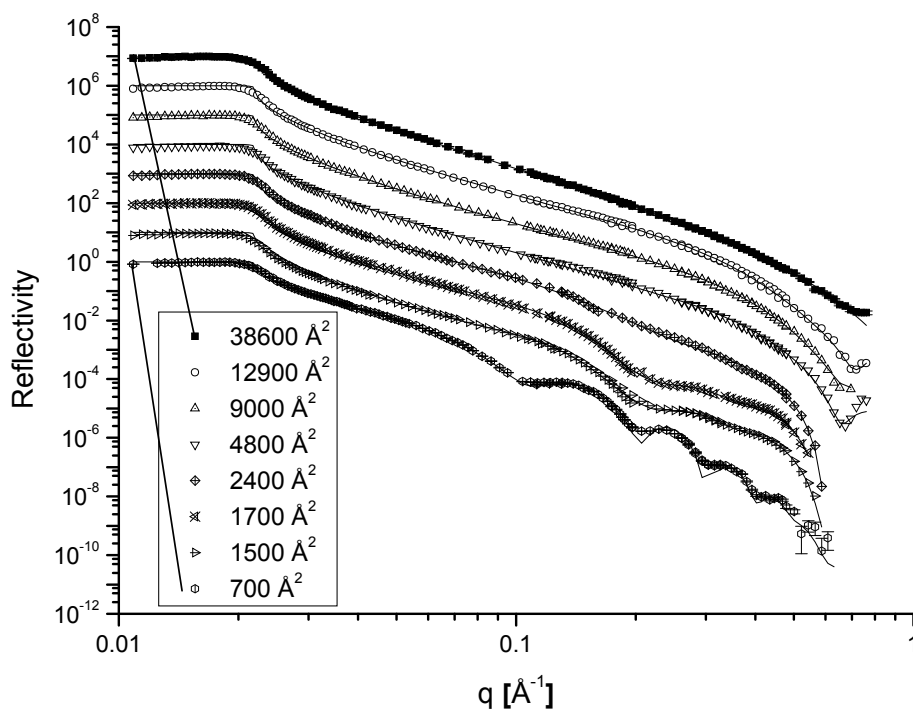
Figure 5.7. X-ray reflectivity data for a $PEO_{20}F69$ copolymer on a water surface at various surface pressures. The solid lines are the fit to the data using two box-models. The reflectivity data for 700 $Å^2$ are in scale, the other data are shifted upwards for clarity. The experimental error from counting statistics is typical smaller than symbol size, only at very low reflectivity it is significant, as indicated for the 700 $Å^2$ data.
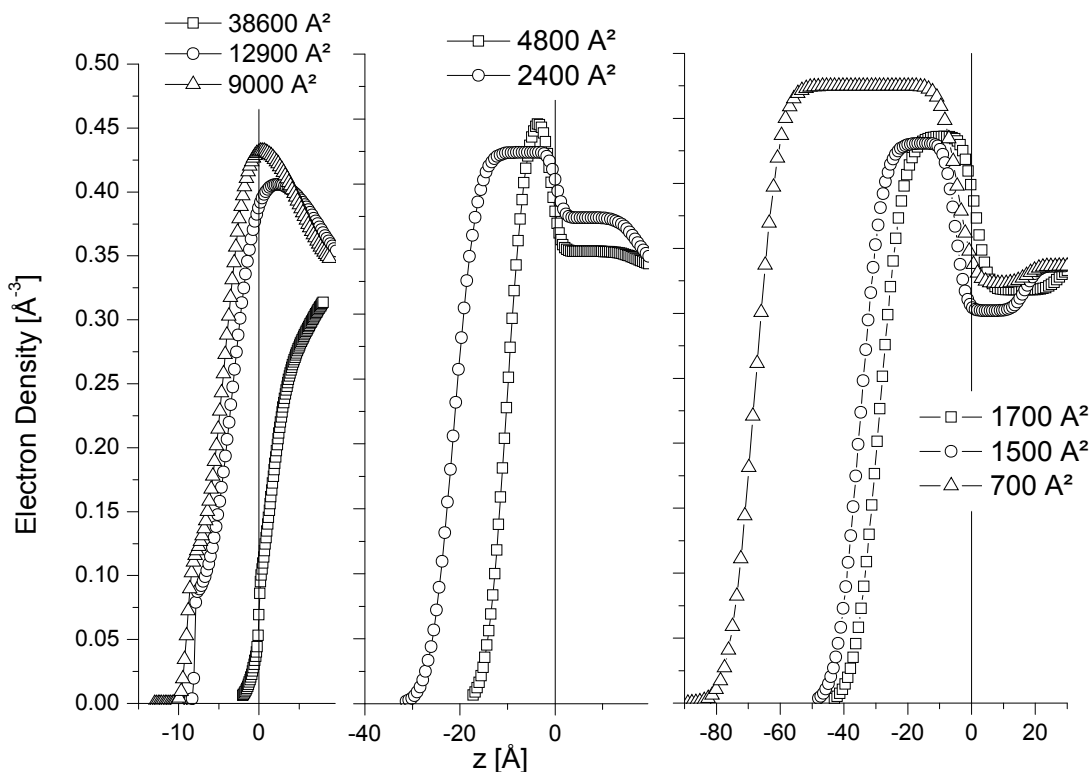
Figure 5.8. Electron density profiles for a $PEO_{20}F69$ copolymer on the water surface at various surface pressures. The vertical line at $Z = 0$ corresponds to the idealized hydrophobic (PFMA) - hydrophilic (PEO + water) interface.

At largest mmA (38600 $Å^2$), the polymer concentration is to small to give any significant change in the scattering profile compared to the pure water surface. At following mmA (12900 $Å^2$ and 9000 $Å^2$) the PFMA layer thickness (4.7 Å, 4.83 Å) corresponds to the typical diameter of a FMA unit, but the total number of counted electrons ($\sim$ 5000) is only a forth of the expected total number per chain (22.000 for PFMA part). On the other hand, the electron density of the PEO layer is much higher than expected. The profile is understandable, when assuming, that the FMA chains are partially tilted up and the second layer consists of a PFMA / PEO / water mixture, which cannot be solved in more detail. The idealized PFMA-PEO interface position (shown in

Fig. 5.8) indicates, that the real PFMA layer should have a typical thickness of ~10 Å and that the high electron density part of the second layer is still part of the real PFMA layer (within ~3 Å roughness). During the compression from 12900 Å^2 to 9000 Å^2 mmA, the thickness of the real PFMA layer above the idealized PFMA-PEO interface remains constant and the electron density of the first layer scales with the reciprocal area. This is typical for compression, when no reorientation of the FMA parts takes place. The observations coincide with the expected pancake like structures at the air-water interface above the first pseudo plateau. As already mentioned, the behavior of the PEO part cannot be obtained from the data.

Table 3: 2-Box model fit results for PEO$_{20}$F69 XR measurements

PEO layer			PFMA layer			
Thickness (Å)	e$^-$ρ (Å^{-3})	σ (Å)	Thickness (Å)	e$^-$ρ (Å^{-3})	σ (Å)	mmA (Å^2)
-	-	-	-	-	-	38600
10.76	0.410	2.1	4.7	0.0812	0.1	12900
9.31	0.440	1.9	4.8	0.109	0.5	9000
18.12	0.348	1.5	9.4	0.45	3.2	4800
17.5	0.374	11	21.6	0.42	3.2	2400
10.6	0.32	3	27.9	0.43	9	1700
26	0.30	3	30.3	0.436	5.8	1500
22	0.322	4	65	0.474	6	700

e$^-$ρ and σ are electron density and interface roughness of each layer, respectively

For all following measurements between 4800 Å^2 and 1500 Å^2 mmA, the thickness of the first layer coincides quite well with the PFMA layer thickness above the idealized PFMA-PEO

interface. At 4800 Å^2, the surface pressure is just between the pancake to brush transition and the second transition. The observed PFMA layer thickness of ~9.35 Å can be correlated to mainly 'standing' FMA side chains or to partially stapled lying FMA chains. With further compression, the PFMA layer reaches a thickness of 21.6 Å (2400 Å^2), 27.9 Å (1700 Å^2), and 30 Å (at 1500 Å^2), i.e. at the end of the second phase transition, the thickness of the PFMA layer can be explained as a staple of approximately six lying FMA units or a double layer of standing FMA units (2×10 Å for fluorinated parts and ~10 Å for nonfluorinated parts). The assumptions from the isotherm measurements are therefore confirmed, but as no reduced electron density at half the height of the layer, a pure double layer seems not to be the dominating species (at least not with a high ordering).

In contrast, at higher compressed states, there is no significant effect in thickness and electron density for the second layer during compression. The electron density of the water enriched PEO phase is in the range of the pure water phase, but from the measurements no clear decision can be made, whether the electron density is significantly higher or lower than the pure water phase.

The film was compressed until no further increase in surface pressure was observed (collapse region). As the compression was stopped after the collapse, the calculated mmA from the final trough area is smaller than the real collapse area. The surface pressure reached at collapse a maximum of ~ 57 mN/m (this value leads via the isotherm to an mmA of ~650 Å^2) and decreased afterwards again. As for all previous measurements, the idealized hydrophobic-hydrophilic interface agrees with the PFMA layer thickness, the corresponding mmA value can be calculated from layer thickness and electron density to be in the range of 700 Å^2. The obtained thickness of 65 Å of PFMA blocks is comparable to the height of 12-13 stapled FMA units - just a forth of the total number of FMA units at each end of the polymer. As the thickness of a FMA unit (~5.3 Å) is twice the value of the monomer unit length at the PFMA backbone (~2.6 Å), we can assume

that every second FMA unit contributes to the same staple, i.e. the PFMA side blocks are standing perpendicular on the water surface, forming two staples of FMA side chains (alternating left and right) and at half the block length, the chain is folded back. The observed electron density of 0.47 $Å^{-3}$ value is close to the calculated electron density 0.5 $Å^{-3}$ of dense packed PFMA block.

Assuming a single backfolding of the PFMA chain at ~700 $Å^2$ and a triple backfolding at ~1500 $Å^2$ mmA, then a double backfolding can be expected at ~1100 $Å^2$ - slightly above the value of the observed kink in the π/A isotherm. Unfortunately no XR results are available in this region to confirm the results. The calculated fitting parameters for the measured XR profiles at various surface pressures are in agreement with our assumption of copolymer organization at the air-water interface. Excellent agreement between the calculated mmA (with 216 electrons per FMA unit) from the area under the electron density profile curves obtained from the XR profiles in the brush region and the mmA from the isotherm validates fitting parameters.

XR of PEO$_{10}$F9 at the air-water interface

The water soluble PEO$_{10}$F9 copolymer shows no second pseudo-plateau in the isotherm and the XR measurements should therefore differ significantly from the PEO$_{20}$F69 results. XR measurements for this sample were carried out at several compressions between 2530 $Å^2$ and 85 $Å^2$, i.e. at first pseudo plateau and higher compression (indicated in Fig. 5.5). The XR profiles and the fitting curves are shown in the Fig. 5.9. For this polymer, there is no significant change in the reflectivity curves observable during compression. Also, none of the XR profiles show local minima, therefore no significantly layered structure seems to occur. From the electron density profiles (not shown here) no correlation between shape and idealized hydrophobic (PFMA) - hydrophilic (PEO+water) interface can be found, as it was possible for the PEO$_{20}$F69 series. The electron densities are comparable to those of the PEO$_{20}$F69 sample at the first pseudo plateau

(between 9000 and 4800 Å²), without having a significant enrichment of FMA units. That means, even if we compress the PEO$_{10}$F9 below the limiting brush area, no PFMA layer is formed at the surface. Therefore, most of the FMA blocks are immersed in the water subphase.
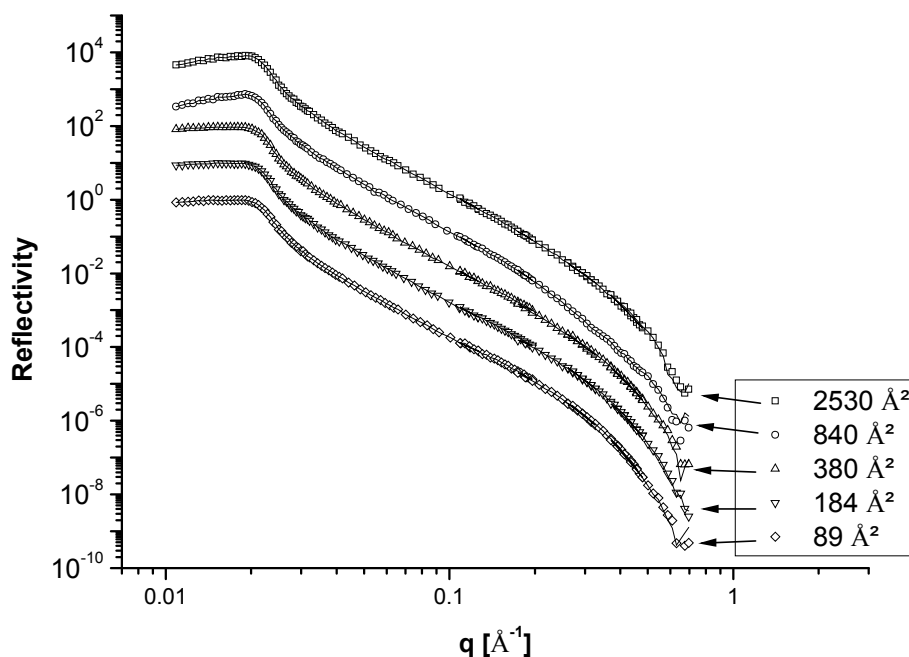
Figure 5.9. X-ray reflectivity data for a PEO$_{10}$F9 copolymer on a water surface at various surface pressures. The solid lines are fit to the data using two box-models. The reflectivity data for 89 Å² (lowest data in the graph) are in scale. The other data are shifted upwards for clarity.

The suggested monolayer behavior for water insoluble PFMA-PEO-PFMA triblock copolymers is shown in Fig. 5.10: Scheme (a) shows the pancake like structures at large mean molecular area. Both PEO and PFMA block are on the water surface and the chains are separated from each other. Scheme (b) shows the behavior in the brush regime near the limiting brush area. PEO blocks are pushed into the water subphase (due to steric interaction between PFMA chains)

forming bulb like structures (putative loops) and they are anchored by loosely packed hydrophobic PFMA blocks. Scheme (c) describes the polymer arrangement in the second plateau region. The PEO block is solved in the water subphase but still anchored by close packed FMA units at the air-water interface. The PFMA blocks form a double layer of standing FMA units. In scheme (d) it is shown, that for polymers with a higher number of FMA units per block (a rough guess gives at least 12 FMA units per block) another reorientation can take place, where the PFMA blocks are vertically oriented on the water surface.
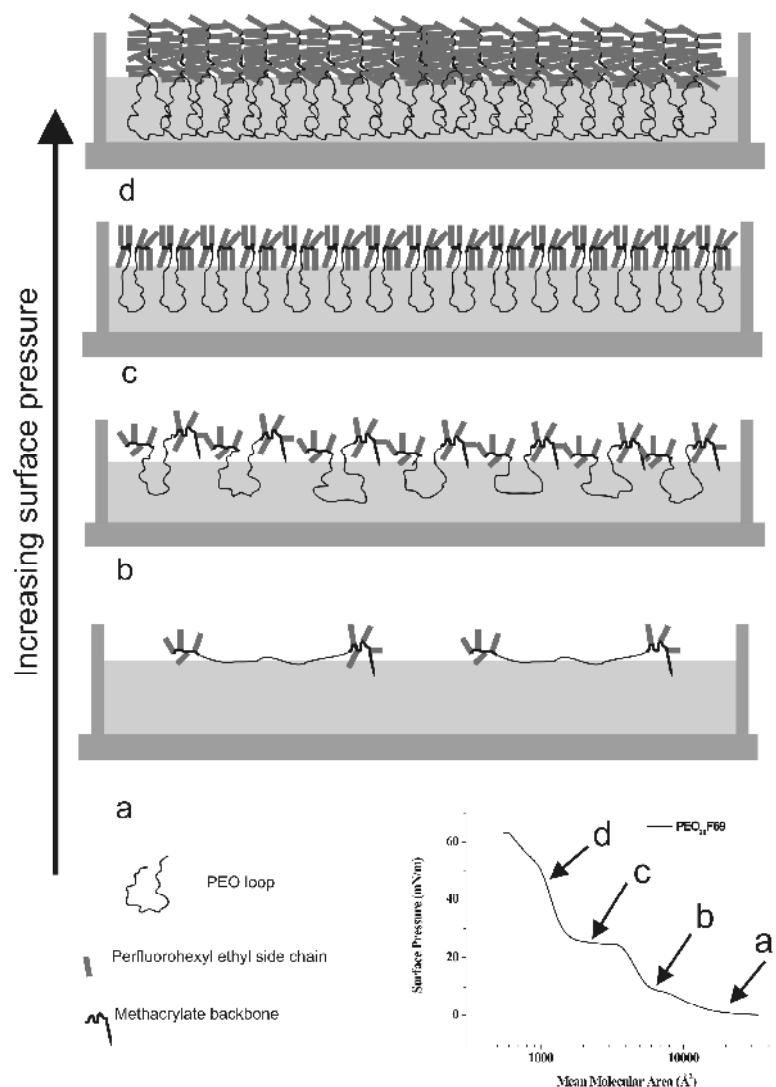
Figure 5.10. Schematic drawing of suggested monolayer of water insoluble PFMA-b-PEO-b-PFMA triblock copolymer behavior at the air-water interface. For clarity, the length of the PEO part is strongly reduced compared to the PFMA length. (a) pancake regime - separate chains on surface, (b) pancake to brush transition - overlapping chains but still PFMA parts separate, (c) 2nd transition - brush formation of PFMA part, (d) reorientation for polymers with high fluorine content.

5.4. Conclusions

We have investigated the monolayer behavior of AB, and ABA amphiphilic triblock copolymers with hydrophobic end blocks poly(perfluoro hexyl ethyl methacrylate)-*b*-poly(ethylene oxide)-*b*- poly(perfluoro hexyl ethyl methacrylate) at the air-water interface using surface pressure-area and XR measurements. Surface pressure-area isotherms of di- and triblock copolymers (containing more than 2 FMA units per PFMA block) show two pseudo-plateaus. The plateau observed at high mean molecular area is consistent with the one reported for PEO homopolymers and PEO copolymers. The plateau observed in the brush regime was assigned for horizontal to perpendicular rearrangement of flexible hydrophobic PFMA chain at the air-water interface. The water soluble $PEO_{10}F9$ triblock copolymer shows no second pseudo plateau in the isotherm and no enrichment of FMA parts could be observed at the air-water interface during compression.

Chapter 6

Perfluorinated block copolymer interaction with lipid monolayer

6.1. Introduction

Amphiphilic block copolymers used in biomedical applications have been shown to influence the interactions with biological environments and consequently influence the efficiency of system being used.[245-247] It has been shown that physical characteristics such as molecular architecture, hydrophobicity, hydrophilicity, and surface charge of these polymers can significantly influence their interactions with lipids.[248-250] Among the different block copolymer pluronics have been used extensively in a variety of pharmaceutical formulations.[251] Pluronics are known to interact with cell membranes. In cell culture studies, certain pluronics have been shown to cause pronounced chemosensitization of tumor cells that exhibit drug resistance to anticancer drugs.[252-254] This effect was attributed to inhibition of the P-glycoprotein responsible for drug efflux by interacting with the membrane lipids surrounding this protein. Both Pluronic bulk hydrophobicity and the chemical microstructure of the copolymer determine its membrane-disturbing ability. Pluronic F68 was found to be effective in sealing permeabilized cell membranes both in vitro and in vivo. However, when the membrane was restored at high SP, Pluronic F68 was expelled out of the lipid monolayers.[255]

Langmuir monolayers of lipid are excellent model systems for the cell membrane, the mimic the out layer of the cell bilayer.[256] The Langmuir lipid monolayers are very well-defined, stable, homogeneous bidimensional system with planar geometry.[257-259] In addition, various parameters such as lipid composition, subphase, and temperature can be chosen to imitate biological

conditions. They provide an excellent model system for investigating the interactions between polymers and the lipid of the cell membrane.[260-264] They also used to study of ordering processes in two dimensions, especially because physical parameters, such as lateral pressure, area per molecule, temperature, salt concentration, and subphase composition can be easily controlled. Additional information about the morphology of the monolayer domains can be obtained by using modern biophysical techniques, such as atomic force microscopy, fluorescence microscopy. High resolution information about two-dimensional ordering on the nanometer scale can be obtained by using synchrotron-sourced specular XR studies.[265-270]   These methods provide information on the molecular organization and structure of lipid monolayers. Furthermore, this information can also be used to obtain information on lipid–polymer interactions.

In this study, we have investigated membrane sealing capability of perfluorinated block copolymer using Langmuir film balance and insitu XR. We have chosen $PEO_{20}F9$ as representative block copolymer, and DPhPC as model lipid. Comparision of pure DPhPC isotherm with $PEO_{20}F9$ penetrated DPhPC isotherm showed that the block copolymer could penetrate into fully expanded lipid monolayer and remained in the lipid monolayer until SP 25 mN/m. Further compression, leads to expulsion of the block copolymer from the lipid monolayer. Insitu XR data confirmed the conclusions based on the Langmuir studies.

6.2. Experimental

6.2.1 Materials

1,2-diphytanoyl-*sn*-glycero-3-phosphocholine (DPhPC) was purchased from

Avanti Polar Lipids (Alabaster, Alabama, USA). It was used without further purification. Block

copolymer characteristic properties were provided in Table 2.1.

6.2.2. Surface pressure(π)-area (mmA) measurements

The surface isotherms (surface pressure (π) versus mmA) of the DPhPC lipid and

DPhPC/PEO$_{20}$F9 at the air-water interface, were measured with a Teflon$^{®}$ Langmuir trough

system (KSV Ltd, Helsinki, Finland) equipped with two moving barriers and a micro-roughened

platinum Wilhelmy plate. The maximum available surface area of the Langmuir trough is 76800

mm^2 (compression ratio 8:1). Distilled water was used as subphase, which was subsequently

passed through a water purification system from Purelab option system (ELGA Ltd., Celle,

Germany) equipped with an organic removal cartridge (conductance < 0.06 μS cm^{-1}). The purity

of the water surface was checked before each measurement by a maximum compression ($\Delta\pi<0.1$

mN/m). The temperature of the water subphase was maintained at 23±0.5°C, using a circulating

water bath system. DPhPC lipid was dissolved (2 mg/mL) in HPLC grade chloroform (Sigma-

Aldrich / Fluka, Seelze, Germany) and predetermined amounts were spread evenly on the

subphase in 1-2 μL small drops using a Hamilton's digital microsyringe. The compression at a

constant rate of 7.5 cm^2/min was started after 20 min to ensure the full evaporation of solvent.

6.2.3. X-ray reflectivity measurements

X-ray reflectivity measurements were carried out at the BW1 beam line at HASYLAB

(DESY, Hamburg, Germany) using a liquid surface diffractometer with an incident wavelength

of λ=1.3037 Å. A thermostated Langmuir trough equipped with a Wilhelmy film balance to

measure surface pressure and a single barrier to change the surface area was mounted on the diffractometer. The instrumental details are given in an article by J. Als-Nielsen.[271] To avoid beam damage, the sample was displaced after several minutes of irradiation, i.e. a single profile was measured on four neighbored positions. The data were corrected for background scattering and the obtained reflectivity curves were fitted using the Parratt algorithm[272] embedded in a program by Mr. Braun ('Parratt-The Reflectivity Tool', kindly provided by HMI, Berlin[273]).

6.3. Results and Discussion

6.3.1. Block copolymer penetration into lipid monolayers by surface pressure measurements
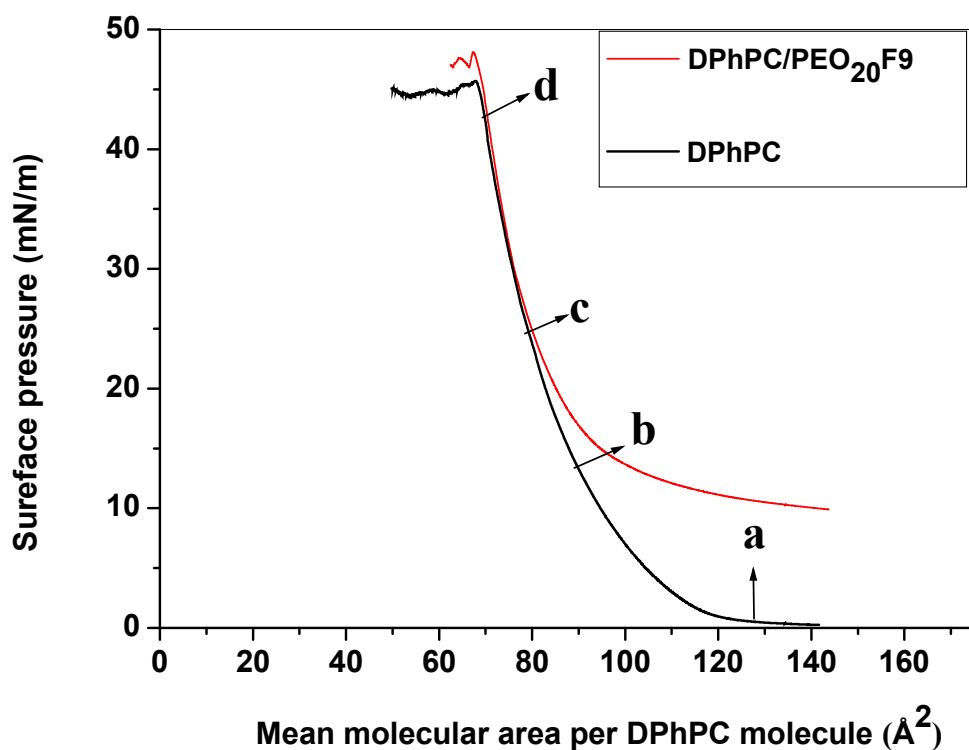
Figure 6.1. Surface pressure (π)–mean molecular area (mmA) isotherms of DPhPC and DPhPC/PEO$_{20}$F9 on pure water subphase. To get DPhPC/PEO$_{20}$F9 isotherm, compression was started after 30 min following PEO$_{20}$F9 injection into the subphase. A 200 μL of 2 mg/mL PEO$_{20}$F9 was injected under fully expanded DPhPC film prior to compression.

Figure 6.1. shows the π/A isotherms of a pure DPhPC film and PEO$_{20}$F9 block copolymer penetrated DPhPC films on the water surface. In pure DPhPC isotherm, compression of the monolayer leads to a phase transition from liquid-expanded phase to liquid condensed phase, followed by collapse of the monolayer at $\pi \sim 45$ mN/m and $A \sim 67$ Å^2 per molecule. Following

the injection of the polymer solution into the subphase under a fully expanded DPhPC film, a shift toward a higher area/molecule in the isotherms can be seen. It is a clear indication of the block copolymer chain penetration into the DPhPC monolayer. A considerable increase in surface pressure of the fully expanded DPhPC film is observed with the injection of the copolymer solution into the water subphase. At high surface pressures (at $\pi \sim 25$ mN/m), the isotherms (Fig. 6.1) of the pure DPhPC and the polymer-penetrated DPhPC overlap, indicating the expulsion of the polymer chains from the lipid film. Similar behavior of the isotherms has been reported by hussaain et al[274] and for a poloxamer (triblock copolymer of PEO and PPO) inserted lipid monolayer systems.[275-277] At high surface pressures, the isotherms of the block copolymer penetrated lipid monolayer reverted to that of the pure lipid, and it was attributed to the expulsion of the copolymer chains from the lipid monolayer.

6.3.2. Block copolymer penetration into lipid monolayers by X-ray reflectivity.

To confirm our hypothesis, penetration of the block copolymer at fully expanded phase of DPhPC followed by expulsion at SP 25 mN/m (cell membrane bilayer equivalent SP), we carefully monitored structures of the DPhPC monolayers before and after the block copolymer injection by in situ XR as a function of surface pressure. The X-ray reflectivity data was collected before and after squeeze-out SP. The squeeze-out SP is the surface pressure at which the isotherm of $PEO_{20}F9$ penetrated DPhPC overlaps with pure DPhPC isotherm. It is determined from the surface pressure-area measurements. The XR data was analyzed using a model for the electron density profile that consists of two boxes sandwiched between bulk water and bulk air.[278] One box represents the average electron density for the head group region of the lipids and the other box represents the electron density in the tail group region. The XR data of DPhPC, $DPhPC/PEO_{20}F9$ ($PEO_{20}F9$ penetrated DPhPC) on a water surface was fitted using parratt

algorithm.[279] While fitting the XR data the following rules were followed. The electron density of water was fixed to the theoretical value 0.334 Å^{-3} and the electron density of air was set to zero. In addition, the electron density of head group region was restricted between 0.322 Å^{-3} and 0.45 Å^{-3} (0.322 Å^{-3} calculated electron density value for PC head group using reference 2. 0.45 Å^{-3} the maximum electron density value for hydrated DPPC head group obtained from literature[280]) and the length of head group was restricted 7.4 Å and 10.5. The minimum and the maximum values reported for Phosphocholine (PC) head group.[281,282]

Fig. 6.2 shows idealized electron density profiles for condensed DPhPC monolayer. The electron density for tail region is calculated using scattering length density calculator[283] with assumed mass density of 1g/cm^3, whereas electron density of head group region was taken as 0.42.[284] The values obtained at the 42.2 mN/m for the headgroup and tail group are considered as thickness values, the roughness at the 3 interfaces was set to zero. Each box is characterized by a constant electron density ρ throughout its thickness.
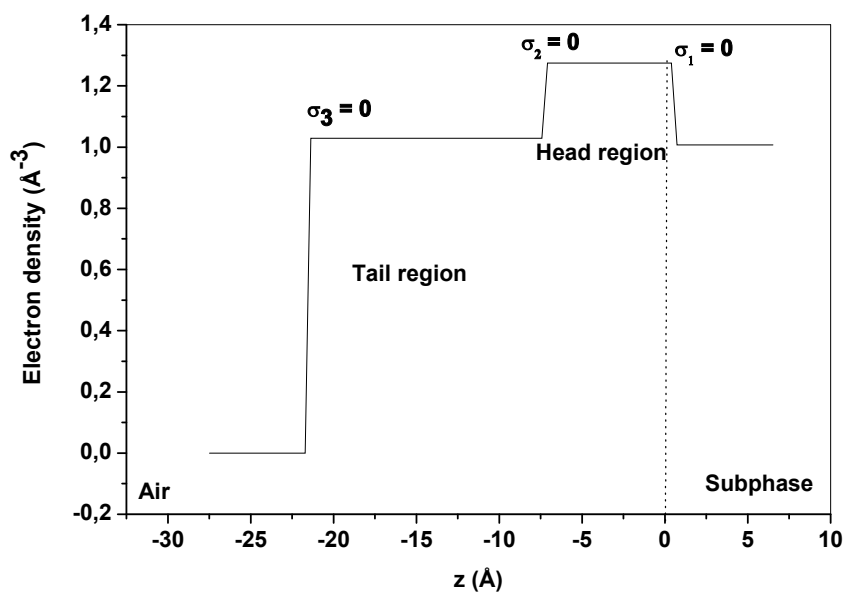
Figure 6. 2. Idealized electron density profile when roughness at every interface is set to zero.

A separate measurement of pure water showed an interfacial roughness of the water surface of 3Å, which is in good agreement with literature values.[285] It is attributed to thermal fluctuations of the water surface.
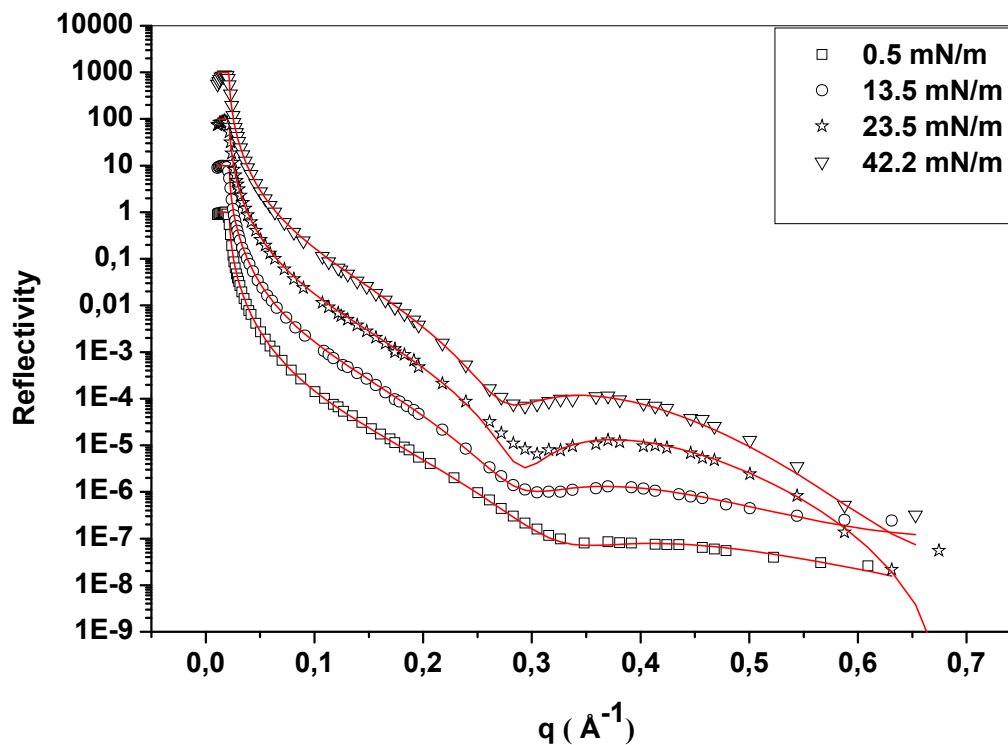
Figure 6.3. X-ray reflectivity data for a DPhPC monoloayer on a water surface at various surface pressures. The solid lines are fit to the data using two box-models. The reflectivity data for 0.5 mN/m (lowest data in the graph) is in scale. The other data were shifted upward for clarity.

Table 6.1. Fitting parameters of XR data of DPhPC monolayer on pure water at different mmA

Head group region				Tail region			
Thickness (Å)	$e^-\rho$ ($Å^{-3}$)	σ_1 (Å)	σ_2 (Å)	Thickness (Å)	$e^-\rho$ ($Å^{-3}$)	σ_3 (Å)	mmA ($Å^2$)
9.04	0.403	6.06	2.92	9,62	0.143	2.06	120
7.6	0.409	5.81	2.90	11.25	0.257	2.46	90
7.97	0.396	1.77	2.61	12.52	0.323	3.48	80
7.29	0.401	2.26	3.25	14.2	0.330	4.50	68

Fig. 6.3 shows the XR profiles of DPhPC at various surface pressures as indicated in the figure. The agreement between experimental XR profile and the calculated profile is very good for all the data. The reflectivity curve differed slightly with increasing SP. XR curve for 0.5 mN/m SP shows the first minimum at 0.35 $°A^{-1}$ whereas at higher SP (42.2 mN/m) the first minimum (0.25 $Å^{-1}$) is shifted to a lower q-region, indicating that the total film thickness increases slightly (Fig. 6.3). The best fit parameters were given in the Table 6.1. To the best of our knowledge structural parameters of DPhPC monolayers are being discussed for the first time using in-situ x-ray reflectivity measurements. However, the structural parameters for the lipids with similar head group such as 1,2-dipalmitoyl-sn-glycero-3-phosphocholine (DPPC), 1-palmitoyl-2-oleoyl-sn-glycero-3-phosphocholine(POPC),1,2-dioleoyl-sn-glycero-3-phosphocholine (DOPC), and 1-Stearoyl-2-oleoyl-sn-glycero-3-phosphocholine (SOPC) were discussed more extensively.[286-288] The total thickness value for DPhPC monolayers at different surface pressure ranges between 18.66 A° at 0.5 mN/m and 21.49 A° at high surface pressures 42.2 mN/m. These values are in consistent with the value reported by Vogel et al.[289] and Malkova et al.[290] Vogel reported thickness value of 39 A° for POPC bilayer corresponding to monolayer thickness of 19.5 A°. Malkova et al.[290] studied the monolayer of SOPC lipids using XR

techniques and he reported a value of 21 A°. The high electron density corresponding to the head

group region is due to hydration of head groups at the air-water interface. DOPC, DPPC, and

POPC bilayers were studied by Liu and Nagle, Nagle and Tristam- Nagle and Pabst et al.

respectively. The headgroup thickness determined by these studies was 9 A° , which is

slightly higher than the value we report here. The lower thickness of the tail group region at low

SP and the electron density in this region, indicate that the acyl chains are disordered. The high

electron density in the headgroup region is due to the presence of the phosphate group. The total

thickness of the monolayer adds up to 21 A° consistent with the dimensions of a phospholipid

monolayer.[294,295]
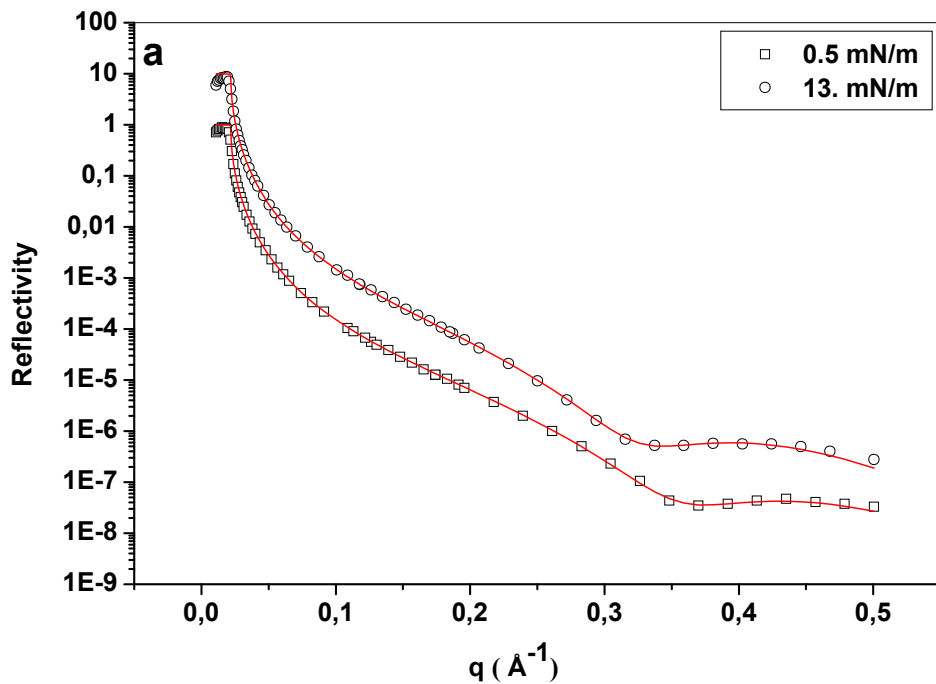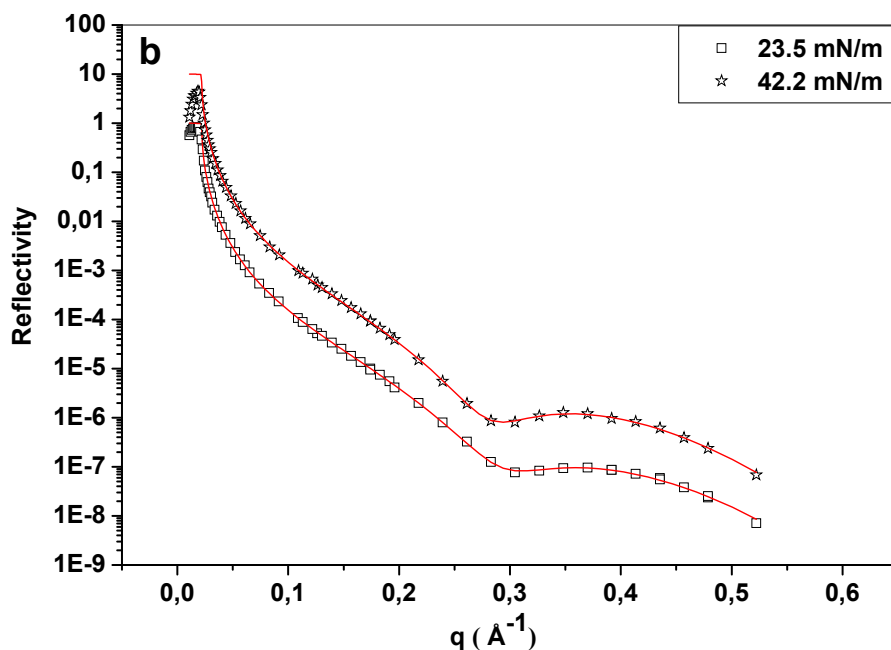
Figure 6.4. X-ray reflectivity data for $PEO_{20}F9$ penetrated DPhPC monoloayer on water before squeeze out SP (a), after squeeze out SP (b). The solid lines are fit to the data using two box-models. The reflectivity data for 0.5, 23.5mN/m (lowest data in the graph (a) and (b) respectively) is in scale. The other data were shifted upward for clarity.

Table 6.2. Fitting parameters of XR data of $PEO_{20}F9$ penetrated DPhPC monolayer on pure water at different mmA

Head group region				Tail region			
Thickness (Å)	e⁻ρ (Å⁻³)	σ_1 (Å)	σ_2 (Å)	Thickness (Å)	e⁻ρ (Å⁻³)	σ_3 (Å)	mmA (Å²)
7.85	0.399	1.22	7.58	10.2	0.301	3.55	120
7.31	0.386	1.37	2.65	11.42	0.325	3.82	90
7.81	0.392	2.68	2.79	12.59	0.319	4.04	80
6.8	0.395	1.70	3.32	14.19	0.318	4.33	68

Fig. 6.4 shows the XR profiles of $PEO_{20}F9$ penetrated DPhPC before (Fig. 6.4a) and after (Fig 6.4b) squeeze out SP. The agreement between experimental XR profile and the calculated profile is very good for all the data. The best fit parameters were given in the Table 6.2. Before squeeze out SP the electron density values for the $PEO_{20}F9$ penetrated DPhPC tail region are significantly higher (at 0.5 mN/m is 0.301 $Å^{-3}$ and at 13 mN/m 0.325 $Å^{-3}$) compared to pure DPhPC monolayers (at 0.5 mN/m is 0.143 $Å^{-3}$ and at 13 mN/m 0.257 $Å^{-3}$). Higher electron density signifies the penetration of $PEO_{20}F9$ fluorinated hydrophobic chains into the DPhPC monolayer tail region. Thus, XR data clearly demonstrated the penetration of $PEO_{20}F9$ into fully expanded DPhPC monolayer. As the lipid density is restored, XR data shows that the $PEO_{20}F9$ is squeezed-out of the lipid monolayer, which has been qualitatively suggested by isotherm data. Upon compression beyond squeeze out SP (that is similar to the bilayer equivalent pressure in cell membrane) XR profiles from pure and the $PEO_{20}F9$ treated DPhPC film at 42.2 mN/m are practically identical, confirming the removal of $PEO_{20}F9$ from the film. Comparison between the electron density values for the pure DPhPC and $PEO_{20}F9$ treated DPhPC shows that with the expulsion of $PEO_{20}F9$ above squeeze out SP all structural parameters revert to those of pure DPhPC.

6.4. Conclusions

$PEO_{20}F9$ penetrates when the lipid packing density is low. Assuming that the lipid monolayer at low lipid packing density mimics the damaged cell bilayer, the penetration of block copolymers helps the damaged membrane to regain barrier control. At higher lipid density, the block copolymer was squeezed out of the DPhPC lipid monolayer. This extraordinary ability of block copolymer to selectively insert when needed and leave once the membrane regained its structural integrity are major features that promise perfluorinated block copolymer ($PEO_{20}F9$) to be a good therapeutic agent for various biomedical applications.

Chapter 7

Summary and perspectives

My thesis research focused primarily on investigating the self assembly of perfluorinated block copolymer in water, at the air-water interface, on solid substrates and potential biomedical application. I have used diblock and triblock perfluorinated amphiphilic block copolymer: poly(ethyleneoxide)-*b*-poly(pefluoro hexyl ethyl methacrylate) (PEO-PFMA) with different molecular parameters. The triblock copolymers consist of water soluble PEO in the middle with hydrophobic PFMA outer blocks. Self assembling behavior of these block copolymers was studied using dynamic light scattering (DLS), rheology, Langmuir film balance, atomic force microscopy (AFM), and most advanced X-ray scatterings methods such as SAXS and XR.

Self assembly of PEO-PFMA triblock copolymers in water was investigated using DLS, rheology, and SAXS. We have studied effect of concentration, hydrophobic, hydrophilic block chain length on the association of block copolymers in water. In dilute concentration regime; at particular concentration of triblock copolymer in water no significant difference was found in micelle size and cluster size with respect to hydrophobic and hydrophiphilic (middle block) block length. However, all triblock copolymers under investigation showed strong influence of concentration on cluster size. The rheological measurements were carried out to investigate the sol-to-gel transition of block copolymers with high concentration. Effect of block copolymer chain length and middle block chain length was observed on hydrogels. The hydrophobic block has effect on gel strength whereas the hydrophilic block influences the critical gel concentration

i.e. block copolymers $PEO_{10}F9$, $PEO_{20}F4$ has same number of hydrophobic units, they differ in hydrophilic block chain length. With increasing PEO block length critical gel concentration (cgc) was found to be decreased $\sim$ 4 times. $PEO_{10}F9$ and $PEO_{20}F4$ cgc are 16.8 %, 3.8 % w/v respectively. Effect of temperature on rheological properties, of block copolymer gels in water was studied with changing temperature. At 35 ºC a typical solid like gel behaviour was observed. The G' (ω) value increased significantly and G' (ω), G" (ω) vs log ω curve became plateau over the entire frequency range. SAXS measurements were employed to investigate the nanostructures in the block copolymer hydrogels. SAXS data indicated improved long-range order with increasing concentration of block copolymer in water.

Self assembly of water soluble perfluorinated triblock copolymers at air-water interface and on solid substrates was studied using surface pressure-area measurements and atomic force microscopy (AFM). The triblock copolymers are composed of long water soluble poly(ethylene oxide) PEO chains as middle block with very short poly(perfluorohexyl ethyl methacrylate) PFMA end blocks. The surface pressure-area isotherms show phase-transitions in the brush regime. This phase-transition is due to a rearrangement of PFMA block at the air-water interface. It becomes more significant with increasing PFMA content in the copolymer. LB films transferred at low surface pressures from the air-water interface to hydrophilic silicon substrates show surface micelles in the size range of 50-100 nm. A typical crystalline morphology of the corresponding PEO homopolymer is observed in LB films of copolymers with very short PFMA blocks, transferred in the brush region at high surface pressure. This crystallization was found to be hindered with increasing PFMA content in the copolymer

Summary and perspectives

Highly fluorinated block copolymer self assembly at the air-water interface was investigated using surface pressure-area and X-ray reflectivity (XR) measurements. The triblock copolymers are composed of long poly(ethylene oxide) PEO middle blocks with poly(perfluorohexyl ethyl methacrylate) PFMA end blocks. These block copolymer are not soluble in water. The surface pressure-area isotherms show two pseudo-plateaus. The plateau at low surface pressure is consistent with pseudo-plateau observed for PEO copolymers in the literature. The plateau in the brush region can be assigned to the horizontal to vertical rearrangement of whole PFMA chains at the air-water interface, which was followed by XR measurements. For water soluble species with a very low amount of PFMA no (significant) second pseudo-plateau and no enrichment of PFMA at the air water interface was observed.

Amphiphilic block copolymers are known for their various biomedical applications such controlled drug delivery systems, stabilisation of emulsion systems etc. We have studied the sealing capability of our triblock copolymer systems using lipid monolayers as model membrane system. Penetration of lipid monolayers by amphiphilic triblock copolymers was investigated by surface pressure-area measurements, and XR. $PEO_{20}F9$ penetrates when the lipid packing density is low. Assuming that the lipid monolayer at low lipid packing density mimics the damaged cell bilayer, the penetration of block copolymers helps the damaged membrane to regain barrier control. At higher lipid density, the block copolymer was squeezed out of the DPhPC lipid monolayer. This extraordinary ability of block copolymer to selectively insert when needed and leave once the membrane regained its structural integrity are major features that promise perfluorinated block copolymer ($PEO_{20}F9$) to be a good therapeutic agent for various biomedical applications.

Future Perspectives

In order to fully exploit these perfluorinated block copolymers, the future works should be focused on the following.

1. Detailed investigation on structure formation in hydrogels using neutron and synchrotron x-ray scattering techniques.

2. Self assembly of block copolymer thin films using AFM, neutron and small angle X-ray diffraction techniques

3. To investigate the chemosensitizing effect on multidrug resistance cancer cells.

4. To investigate block copolymers applicability as artificial oxygen carriers.

Chapter 8

References

1. G. M. Whitesides and B. A. Grzybowski, *Science*, **2002**, 295, 2418.

2. G. M. Whitesides and M. Boncheva, *Proc. Natl. Acad. Sci*. USA, **2002**, 99, 4769.

3. H. Ringsdorf and J. Simon, *Nature*, **1994**, 371, 284.

4. F. S. Bates and G. H. Fredrickson, *Annu. Rev. Phys. Chem.* **1990**, 41, 525.

5. M. W. Matsen, *J. Phys. Condens. Matter,* **2001**, 14, R21.

6. I. W. Hamley, *J. Phys.: Condens. Matter,* **2001**, **13,** R643.

7. I. W. Hamley, *The Physics of Block Copolymers* (Oxford: Oxford University Press), **1998**.

8. N. Hadjichristidis, S. Pispas, G. Floudas, *Block Copolymers. Synthetic Strategies, Physical Properties and Applications* (New York: Wiley), **2003.**

9. L. Leibler, H. Benoit, *Polymer*, **1981,** 22, 195.

10. L. Leibler, *Macromolecules* **1980**, 13, 1602.

11. F. S. Bates and G. H. Fredrickson, Phys. Today, **1999**, 52, 32.

12. K. M. Hong, J. Noolandi, Polym. Commun. **1984**, 25, 265.

13. S. B. Darling, *Prog. Polym. Sci.* **2007,** 32, 1152.

14. I. W. Hamley, *Nanotechnology,* **2003**, 14**,** R39.

15. Y. Tsori, D. Andelman, C-Y. Lin, M. Schick, *Macromolecules,* **2006**, 39, 289.

16. S. Lecommandoux and R. Borsali, *Polym. Int.* **2006,** 55, 1161.

17. G. Riess, *Prog. Polym. Sci.* **2003**, 28, 1107.

18. M. Szware, M. Levy, R. Milkovich, *J. Am. Chem. Soc.* **1956**, *78*, 2656.

19. T. P. Lodge, *Macromol. Chem. Phys*. **2003**, *204*, 265.

20. J. R. Quintana, M. Villacampa, I. Katime, *Polymeric Material Encyclopedia*, J. C. Salamone (Ed.), CRC Press, Boca Raton, FL, 1996, p. 815.

21. G. Riess, *Prog. Polym. Sci.* **2003**, *28*, 1107.

22. T. Liu, Z. Zhou, C. Wu, V. M. Nace, B. Chu, *J. Phys. Chem. B,* **1998**, *102*, 2875.

23. Z. Tuzar, *Solvents and Self-Organization of Polymer*, NATO ASI series, E: applied sciences, Kluwer Academic Publisher, Dordrecht, **1996**, vol. 327, p. 1.

24. T. Annable, R. Buscall, R. Ettelaie, D. Whittlestone, *J. Rheol.* **1993**, *37*, 695.

25. B. Nystrom, H Walderhaung, F.K Hansen, *J.Phys.Chem*. **1993**, *97* 7743.

26. Y. W. Wang , Z Yang, ZK. Zhou, D. Attwood, C. Booth, *Macromolecules,* **1996**, *29,* 670.

27. E. J Amis, N. hu, T.A.P Seary, T.E. hogen-Esch, M. Yassini, F. Hwang, *Adv.Chem.Ser.* **1996**, *248*, 279.

28. P. Alexandridis and B. Lindman, **(2000)** *Amphiphilic Block Copolymers: Self-assembly and Applications,* Elsevier, Amsterdam.

29. A. J. Ryan, S.-M. Mai, J. Patrick, A. Fairclough, I. W. Hamley and C. Booth, *Phys. Chem. Chem. Phys*, **2001**, *3*, 2961.

30. C. Booth and D. Attwood, *Macromol. Rapid Commun*., **2000**, *21*, 501.

31. V. M. Nace, J. Am. Oil Chem. Soc., 1996, 73, 1. 5 G.-E. Yu, Y.-W. Yang, Z. Yang, D. Attwood, C. Booth and V. M. Nace, *L angmuir*, **1996**, *12*, 3404.

32. Y.-Z. Luo, C. V. Nicholas, D. Attwood, J. H. Collett, C. Price and C. Booth, *Colloid Polym. Sci*., **1992**, *270*, 1094.

33. A. D. Bedells, R. M. Arafeh, Z. Yang, D. Attwood, J. C. Padget, C. Price and C. Booth, *J. Chem. Soc., Faraday T rans.*, **1993**, *89*, 1243.

34. F. S. Bates, G. H. Fredrickson, *Annu. Rev. Phys. Chem.* **1990**, *41,* 525.

35. M. J. Fasolka, A.M. Mayes *Annu. Rev. Mater. Res.* **2001,** *31,* 323.

36. I. W. Hamley 1998 *The Physics of Block Copolymers* (Oxford: Oxford University Press).

37. I. W. Hamley, E.L. Hiscutt, Y. W. Yang, C. Booth C, *J. Colloid Interface Sci.* **1999** *209,* 255.

38. R. Limary, P.F. Green, *Langmuir,* **1999,** *15***,** 5617.

39. A. Boker, A.H.E Müller, G. Krausch, *Macromolecules,* **2001,** *34***,** 7477.

40. P. Müller-Buschbaum, J.S. Gutmann, M. Stamm *Phys. Chem. Chem. Phys.*   **1999,** *1,* 3857.

41. G. Kim, M. Libera *Macromolecules,* **1998***, 31,* 2670.

42. Zhu J, Eisenberg A, Lennox RB, *Langmuir,* **1991,** 7, 1579.

43. Raju F, Andrew MS, Stephen RC, Jennifer LL, Royale SU, Stephanie ADT,   Yves G, Randolph SD, *Macromolecules,* **2002,** 35, 6483.

44. Peleshanko S, Jeong J, Gunawidjaja R, Tsukruk VV *Macromolecules,* **2004,** *37,* 6511.

45. L. L. Jennifer, M. Pascal, D. Brian, M.S. Andrew, S.S. Sergei, F. Raju, T. Daniel, G. Yves, S.D. Randolph, *Langmuir,* **2005,** *21* 3424.

46. L. L. Jennifer, M. Pascal, T. Daniel, G. Yves, S.D. Randolph, *Langmuir* **2005,** *21* 7380.

47. A. Ulman. An Introduction to Ultrathin Organic Films from Langmuir-Blodgett to Self-Assembly, **1991,** Academic Press, NewYork.

48. T. P. Lodge, *Macromol. Chem. Phys.* **2003**, *204*, 265. J. R. Quintana, M. Villacampa, I. Katime, *Polymeric Material Encyclopedia*, J. C. Salamone (Ed.), CRC Press, Boca Raton, FL, 1996, p. 815.

49. Riess, *Prog. Polym. Sci.* **2003**, *28*, 1107.

50. T. Liu, Z. Zhou, C. Wu, V. M. Nace, B. Chu, *J. Phys. Chem. B,* **1998**, *102*, 2875.

51. Z. Tuzar, *Solvents and Self-Organization of Polymer*, NATO ASI series, E: applied sciences, Kluwer Academic Publisher, Dordrecht, **1996**, vol. 327, p. 1.

52. T. Annable, R. Buscall, R. Ettelaie, D. Whittlestone, *J. Rheol.* **1993**, *37*, 695.

53. B. Nystrom, H Walderhaung, F.K Hansen, *J.Phys.Chem.* **1993**, *97* 7743.

54. Y. W. Wang , Z Yang, ZK. Zhou, D. Attwood, C. Booth, *Macromolecules,* **1996**, *29,* 670.

55. E. J Amis, N. hu, T.A.P Seary, T.E. hogen-Esch, M. Yassini, F. Hwang, *Adv.Chem.Ser.* **1996**, *248*, 279.

56. P. Alexandridis and B. Lindman, **(2000)** *Amphiphilic Block Copolymers: Self-assembly and Applications,* Elsevier, Amsterdam.

57. A. J. Ryan, S.-M. Mai, J. Patrick, A. Fairclough, I. W. Hamley and C. Booth, *Phys. Chem. Chem. Phys*, **2001**, *3*, 2961.

58. C. Booth and D. Attwood, *Macromol. Rapid Commun.*, **2000**, *21*, 501.

59. V. M. Nace, J. Am. Oil Chem. Soc., 1996, 73, 1. 5 G.-E. Yu, Y.-W. Yang, Z. Yang, D. Attwood, C. Booth and V. M. Nace, *L angmuir*, **1996**, *12*, 3404.

60. Y.-Z. Luo, C. V. Nicholas, D. Attwood, J. H. Collett, C. Price and C. Booth, *Colloid Polym. Sci.*, **1992**, *270*, 1094.

61. A. D. Bedells, R. M. Arafeh, Z. Yang, D. Attwood, J. C. Padget, C. Price and C. Booth, *J. Chem. Soc., Faraday T rans.*, **1993**, *89*, 1243.

62. F. S. Bates, G. H. Fredrickson, *Annu. Rev. Phys. Chem.* **1990**, *41,* 525.

63. M. J. Fasolka, A.M. Mayes *Annu. Rev. Mater. Res.* **2001,** *31,* 323.

64. I W Hamley 1998 *The Physics of Block Copolymers* (Oxford: Oxford University Press).

65. I. W. Hamley, E.L. Hiscutt, Y. W. Yang, C. Booth C, *J. Colloid Interface Sci.* **1999** *209,* 255.

66. R. Limary, P.F. Green, *Langmuir,* **1999,** *15,* 5617.

67. A. Boker, A.H.E Müller, G. Krausch, *Macromolecules,* **2001,** *34,* 7477.

68. P. Müller-Buschbaum, J.S. Gutmann, M. Stamm *Phys. Chem. Chem. Phys.* **1999,** *1,* 3857.

69. G. Kim, M. Libera *Macromolecules,* **1998***, 31,* 2670.

70. Zhu J, Eisenberg A, Lennox RB, *Langmuir,* **1991,** 7, 1579.

71. Raju F, Andrew MS, Stephen RC, Jennifer LL, Royale SU, Stephanie ADT,   Yves G, Randolph SD, *Macromolecules,* **2002,** 35, 6483.

72. Peleshanko S, Jeong J, Gunawidjaja R, Tsukruk VV *Macromolecules,* **2004,** *37,* 6511.

73. L. L. Jennifer, M. Pascal, D. Brian, M.S. Andrew, S.S. Sergei, F. Raju, T. Daniel, G. Yves, S.D. Randolph, *Langmuir,* **2005,** *21* 3424.

74. L. L. Jennifer, M. Pascal, T. Daniel, G. Yves, S.D. Randolph, *Langmuir* **2005,** *21* 7380.

75. A. Ulman. An Introduction to Ultrathin Organic Films from Langmuir-Blodgett to Self-Assembly, **1991,** Academic Press, NewYork.

76. Z. Tuzar, *Solvents and Self-Organization of Polymer*, NATO ASI series, E: applied sciences, Kluwer Academic Publisher, Dordrecht, **1996**, vol. 327, p. 1.

77. T. Annable, R. Buscall, R. Ettelaie, D. Whittlestone, *J. Rheol.* **1993**, *37*, 695.

78. B. Nystrom, H Walderhaung, F.K Hansen, *J.Phys.Chem*. **1993**, *97* 7743.

79. Y. W. Wang , Z Yang, ZK. Zhou, D. Attwood, C. Booth, *Macromolecules,* **1996**, *29,* 670.

80. E. J Amis, N. hu, T.A.P Seary, T.E. hogen-Esch, M. Yassini, F. Hwang, *Adv.Chem.Ser.* **1996**, *248*, 279.

81. P. Alexandridis and B. Lindman, **(2000)** *Amphiphilic Block Copolymers: Self-assembly and Applications,* Elsevier, Amsterdam.

82. B. Nystrom, H Walderhaung, F.K Hansen, *J.Phys.Chem*. **1993**, *97* 7743.

83. Y. W. Wang , Z Yang, ZK. Zhou, D. Attwood, C. Booth, *Macromolecules,* **1996**, *29,* 670.

84. H. Hussain, H. Budde, S. Höring, K. Busse, J. Kressler, *Macromol Chem Phys* **2002** *203,* 2103.

85. R. Buttgereit, Michael Marth, Tobias Roths, Josef Honerkamp Macromol. Symp **2000** *162,* 173.

86. A.J.F Siegert, Massachussets Institute of Technology, Rad .Lab Rep. No 465, **1943**

87. F. Chambon, H. H. Winter *Polym. Bull.* **1985**, *13*, 499.

88. H. H Winter, F. Chambon *J. Rheol.* **1986**, *30*, 367.

89. A. Izuka, H. H Winter, T. Hashimoto *Macromolecules* **1992**, *25*, 2422

90. K. Te Nijenhuis, H. H Winter, *Macromolecules* **1989**, *22*, 411.

91. L. Li, Y. Aoki, *Macromolecules* **1997**, *30*, 7835.

92. Choi, J. H.; Ko, S.-W.; Kim, B. C.; Blackwell, J.; Lyoo, W. S. *Macromolecules* **2001**, *34*, 2964.

93. M. A Van Dijk, R. van den Berg, *Macromolecules* **1995**, *28*, 6773.

94. G. Binnig, C. F. Quate, Ch. Gerber, *Phy. Rev. lett*. **1986**, *56*, 930.

95. www.di.com

96. R. J. Roe, **2000** *Methods of X-ray and Neutron scattering in Polymer science.* Oxford university press. New York.

97. B. D. Cullity, **1978,** *Elements of X-Ray Diffraction*, 2nd edn. 555 pp.

98. Ulman A **1991** *An Introduction to Ultrathin Organic Films from Langmuir-Blodgett to Self-Assembly.* Academic Press, NewYork

100. A. Lavasanifar, J. Samuel, G. S. Kwon, *Adv. Drug. Delv. Rev*. **2002**, 54, 169.

101. M. F. Francis, L. Lavoie, F. M. Winnik, J. C. Leroux, Eur. *J. Pharm. Biopharm*. **2003**, 56, 337

102. A. V. Kabanov, E. V. Batrakova, V. Y. Alakhov, *J. Control. Release.* **2003**, 91, 75.

103. M. L. Adams, A. Lavasanifar, G. S. Kwon, *J. Pharm Sci* **2003***, 92,* 1343.

104. C. Nardin, J. Widmer, M. Winterhalter, W. Meier, *Eur. Phys. J. E,* **2000,** *4*, 403.

105. R. S. Kane, S. Takayama, E. Ostuni, D. E. Ingber, G. M. Whitesides, *Biomaterials* **1999**, 20, 2363.

106 . D. T. Chiu, N. L. Jeon, S. Huang, R. S. Kane, C. J. Wargo, I. S. Choi, D. E. Ingber, G. M. Whitesides, PNAS **2000**, 97, 2408.

107. J.Z. Hilt, A.K. Gupta, R. Bashir , N.A. Peppas, *Biomed. Microdevices*, **2003**, *5*, 177.

108. V.Castelletto, I.W. hamley, X-F. Yuan, A.kelarakis, C.Booth, *Softmatter,* **2005,** *1***,** 138.

109. J.Patrick, A.Fairclough, A. I. Norman, *Annu. Rep. Prog. Chem.,,* **2003**, *99*, 243.

110. S. Dai, P. Ravi, C. Y. Leong, K. C. Tam, L. H. Gan, *Langmuir* **2004,** *20,* 1597.

111. I. W. Hamley, *Phil. Trans. R. Soc. Lond,* **2001,** *359*,1017.

112. V. M. Nace, *Nonionic Surfactants: Polyoxyalkylene Block Copolymers*; Marcel Dekker: New York, **1996**.

113. P. Alexandridis, T.A. Hatton, *Colloids Surf,* **1995**, *96*, 1.

114. M. J. Park, K. Char, *Macromol. Rapid Commun.* **2002**, *23*, 688.

115. K. Mortensen, W. Brown, B. Norden, *Phys. Rev. Lett.* **1992**, *68*, 2340.

116. K. Mortensen, J. S. Pedersen, *Macromolecules* **1993**, *26*, 805.

117. B. Jeong, M. R. Kibbey, J. C. Birnbaum, Y. Y. Won, A. Gutowska, *Macromolecules* **2000**, 33, 8317.

118. G. N. Tew, N. S. DeLong, S. K. Agrawal, S. R. Bhatia, *Softmatter*, **2005**, *1*, 253.

119. Z. Zhong, P.J. Dijkstra, J. Feijen, Y.M. Kwon, Y. H. Bae, S.W.Kim, *Macromol. Chem. Phys.* **2002**, *203*, 1797.

120. Winnik, M. A.; Yekta, A. *Curr. Opin. Colloid Interface Sci.* **1997**, *2*, 424.

121. J. P. Kaczmarski, J. E. Glass, *Macromolecules* **1993**, *26*, 5149.

123. G. Tae, J. A. Kornfield, J. A. Hubbell, *Biomaterials*, **2005**, *26*, 5259.

124. H.Hussain, H. Budde, S.Höring, K.Busse, J.Kreßler, *Macromol, Chem, Phys* **2002**, 203, 2103.

125. H. Hussain, K. Busse, J. Kressler *Macromol, Chem, Phys.* **2003**, *204*, 936.

126. C. M. Flanigan, A. J. Crosby, K.R. Shull, *Macromolecules***, 1999,** *32***,** 7251**.**

127. T. Annable, R. Buscall, R. Ettelaie. *Colloid Surf* ,**1996**, *112*, 97.

128. K.C. Tam, R.D. Jenkins, M.A. Winnik, D.R. Bassett. *Macromolecules*, **1998**, *31*,4149.

129. D. Lairez, M. Adam, J.P. Carton, E. Raspaud. *Macromolecule,* **1997,** *30*, 6798.

130. H. Watanabe, T. Sato, K. Osaki. *Macromolecules,* **2000,** *33,* 2545.

131. K. Inomata, D. Nakanishi, A. Banno, E. Nakanishi, Y. Abe, R. Kurihara, K

Fujimoto, T. Nose, *Polymer***, 2003,** *44***,** 5303**.**

132. C. Li, Y. Tang, S. P. Armes**,** *Biomacromolecules,* **2005**, *6*, 994.

133. T. Mukose , T. Fujiwara , J. Nakano , I. Taniguchi, M. Miyamoto , Y. Kimura , I. Teraoka , C. W Lee, *Macromolecular Bioscience,* **2004**, *4*, 361.

134. V. Castelletto, I. W. Hamley, Y. Ma, X. Bories-Azeau, S. P. Armes, A. L. Lewis**,** *Langmuir,* **2004,** *20***,** 4306.

135. F. Tanaka. *Polym J* , **2002**, *34*, 479.

136. F. Tanaka, S.F. Edwards. *Macromolecules,* **1992**, 25, 1516.

137. A.J.F Siegert, Massachussets Institute of Technology, Rad .Lab Rep. No 465, **1943**

138. Bo Nystöm, H. Walderhaug, F. K. Hansen, *J. Phys Chem*. **1993**, 97, 7743.

139. L. Li, Y. Aoki, *Macromolecules* **1997**, *30*, 7835.

140. Choi, J. H.; Ko, S.-W.; Kim, B. C.; Blackwell, J.; Lyoo, W. S. *Macromolecules* **2001**, *34*, 296.

141. F. Chambon, H. H. Winter *Polym. Bull.* **1985**, *13*, 499.

142. H. H Winter, F. Chambon *J. Rheol.* **1986**, *30,* 367.

143. Xu R, Winnik MA, Hallett FR, Riess G, Croucher MD (1991) Macromolecules 24:87

144. Tuzar Z, Kratochvil P (1976) Adv Colloid Interfaces Sci 6:201

145. Koutsos V, van der Vegte EW, Pelletier E, Stamouli A, Hadziioannou G (1997) Macromolecules 30:4719

146. Ulman A (1991) An Introduction to Ultrathin Organic Films from Langmuir-Blodgett to Self-Assembly. Academic Press, NewYork

147. Goncalves da Silva AM, Filipe EJM, Oliveira JMR, Martinho JMG (1996) Langmuir 12:6547

148. Sauer BB, Yu H, Tien CF, Hager DF (1987) Macromolecules 20:393

149. Goncalves da Silva AM, Filipe, EJM (1996) Langmuir 12:6547

150. Gragson DE, Jensen JM, Baker SM (1999) Langmuir 15:6127

151. Faure MC, Bassereau P, Carignano MA, Szleifer I, Gallo Y, Andelman D (1998)

Eur Phys J B 3:365

152. Faure MC, Bassereau P, Lee LT, Menelle A, Lheveder C (**1999**) Macromolecules
     32:8538

153. Goncalves da Silva AM, Simoes Gamboa AL, Martinho JMG (1998) Langmuir
     14:5327

154. Dewhurst PF, Lovell MR, Jones JL, Richards RW, Webster JRP (1998)
     Macromolecules 31:7851

155. Robert BC, Matthew GM (2005) Langmuir 21:5453

156. Bijsterbosch HD, de Haan VO, de Graaf AW, Mellema M, Leermakers FAM,
     Cohen Stuart MA, van Well AA (1995) Langmuir 11:4467

157. Baker SM, Leach KA, Devereaux CE, Gragson DE (2000) Macromolecules 33:5432

158. Cox JK, Constantino B, Yu K, Eisenberg A, Lennox RB (1999) Langmuir 5:7714

159. Gragson DE, Jacob MJ, Baker SM (1999) Langmuir 15:6127

160. Devereaux CA, Baker SM (2002) Macromolecules 35:1921

161. Cox JK, Yu K, Eisenberg A, Lennox RB (1999) Phys Chem Chem Phys 18:4417

162. Raju F, Andrew MS, Stephen RC, Jennifer LL, Royale SU, Stephanie ADT, Yves G,
     Randolph SD (2002) Macromolecules 35:6483

163. Peleshanko S, Jeong J, Gunawidjaja R, Tsukruk VV (2004) Macromolecules
     37:6511

164. Jennifer LL, Pascal M, Brian D, Andrew MS, Sergei SS, Raju F, Daniel T, Yves G,
     Randolph SD (2005) Langmuir 21:3424

165. Jennifer LL, Pascal M, Daniel T, Yves G, Randolph SD (2005) Langmuir 21:7380

166. Barentin C, Muller P, Joanny JF (1998) Macromolecules 31:2198

167. Alexander S (1977) J Phys 38:983

168. An SW, Su TJ, Thomas RK, Baines FL, Billingham NC, Armes SP, Penfold J
     (1998) J Phys Chem B 102:387

169. Israelachvili J (1994) Langmuir 10:3774

170. Zhu J, Eisenberg A, Lennox RB (1991) Langmuir 7:1579

171. Zhu J, Eisenberg A, Lennox RB (1991) J Am Chem Soc 113:5583

172. Zhu J, Eisenberg A, Lennox RB (1992) J Phys Chem 96:4727

173. Zhu J, Eisenberg A, Lennox RB **(1992**) Macromolecules 25:6547

174. Zhu J, Eisenberg A, Lennox RB **(1992**) Macromolecules 25:6556

175. Li S, Hanley S, Khan I, Eisenberg A, Lennox RB (1993) Langmuir 9:2243

176. Li Z, Zhao W, Quinn J, Rafailovich MH, Sokolov J, Lennox RB, Eisenberg A, Wu XZ, 177. Kim M W, Sinha SK, Tolan M (1995) Langmuir 11:4785

178. Li S, Clarke CJ, Lennox RB, Eisenberg A (1998) Colloid Surf 133:191

179. Karim A, Slawecki TM, Kumar SK, Douglas JF, Satija SK, Han CC, Russell TP, Liu Y, Overney R, Sokolov J, Rafailovich MH (1998) Macromolecules 31:857

180. Hussain H, Busse K, Kressler J (2003) Macromol Chem Phys 204:936

181. Hussain H, Kerth A, Blume A, Kressler J (2004) J Phys Chem B 108:9962

182. Hussain H, Budde H, Höring S, Busse K, Kressler J (2002) Macromol Chem Phys 203:2103

183. Chunhung W, Tianbo L, Henry W, Benjamin C (2000) Langmuir 16:656

184. Atsuhiro F, Tohru A, Hiro N (2002) J Colloid Interface Sci 247:351

185. Aminuzzaman M, Kado Y, Mitsuishi M, Miyashita T (2003) Polymer J 35:785

186. Kuhl TL, Majewski J, Howes PB, Kjaer K, von Nahmen A, Lee K YC, Ocko B,

187. Israelachvilli JN, Smith GS (1999) J AmChem Soc 121:7682

188. Chiranjeevi P, Busse K, Kressler J manuscript in preparation.

189. Reiter G, Sommer JU (2000) J Chem Phys 112:4376

190. Reiter G, Sommer JU (2000) J Chem Phys 112:4384

191. Reiter G (2003) J Poly Sci 41:1869

193. Reiter G, Castelein G, Sommer JU, Röttele A, Thurn-Albrecht T (2001) Phys Rev Lett 87:226101

194. Kovacs AJ, Straupe C (1980) J Cryst Growth 48:210

195. S. T. Milner, S. T. *Science* **1991**, 251, 905.

196. H. D. Bijsterbosch, V. O. d. Haan, A. W. d. Graaf, M. Mellema, F. A. M. Leermakers, M. A. C. Stuart, A. A. Well, *Langmuir* **1995**, 11, 4467-4473.

197. D. D. Lasic, *Nature* **1996**, 380, 561.

198. M. Woodle, D. D. Lasic, *Biochim. Biophys. Acta* **1992**, 1113, 171.

199. S. Zalipsky, J. M. Harris, In *Poly(ethylene glycol): Chemistry and Biological*

Applications, Harris, J. M., Zalipsky, S., Eds., American Chemical Society: Washington, DC, **1997**, p 1.

200. J. D. Andrade, V. Hlady, S. I. Jeon, In *Hydrophilic Polymer*, Glass, J. E., Ed., *American Chemical Society:* Washington, DC, **1996**, p 51.

201. J. Daillant, A. Gibaud, A., Eds. X-ray and Neutron Reflectivity: Principles and Applications, Springer: New York, **1999**.

202. M. Tolman, Ed, X-ray Scattering from Soft Matter Thin Films, Springer: New York, **1999**.

203. H. Matsuoka, E. Mouri, K. Matsuomoto, *Rigaku J.* **2001**, 18, 54.

204. G. M. Mercedes, M. Francisco, O. Francisco, G. R. Ramon, L. Dominique, *Langmuir,* **2000**, 16 1083.

205. A. Wesemann, R. Steitz, H. Ahrens, S. Forster, C. A. Helm, *Langmuir* **2003**, *19*, 709-716.

206. A. Wesemann, H. Ahrens, S. Förster, C.A. Helm, *Langmuir* **2004**, *20*, 11528-11535.

207. H. Ahrens, S. Forster, C. A. Helm, *Macromolecules* **1997**, *30*, 8447.

208. P. Kaewsaiha, K. Matsumoto, H. Matsuoka, *Langmuir* **2004**, *20*, 6754.

209. E. Mouri, K. Matsumoto, H. Matsuoka, *J. Polym. Sci., Part B* **2003**, *41*, 1921.

210. J. R. Lu, T. J. Su, R. K. Thomas, J. Penfold, R. W. Richards, *Polymer* **1996**, *37*, 109.

211. E. P. K. Currie, F. A. M. Leermakers, M. A. C. Stuart, G. J. Fleer, *Macromolecules* **1999**, *32*, 487.

212. S. A. M. Goncalves, E. J. M. Filipe, J. M. R. Oliveira, J. M. G. Martinho, *Langmuir* **1996,** 12, 6547.

213. M. C. Faure, P. Bassereau, L. T. Lee, A. Menelle. C. Lheveder, *Macromolecules* **1999**, 32, 8538.

214. Z. Xu, B. H. Nolan, E. M. Roger, *Langmuir* **2001**, *17,* 377.

215. T. R. Baekmark, G. Elender, D. D. Lasic, E. Sackmann, *Langmuir* **1995**, *11*, 3975-3987, Correction **1996**, *12*, 4980.

216. H. Ahrens, T. R. Baekmark, R. Merkel, J. Schmitt, K. Graf, R. Raiteri, C. A. Helm, *Chem. Phys.Chem*. **2000**, *1*, 101.

217. H. Ahrens, K. Graf, C. A. Helm, *Langmuir* **2001**, *17*, 3113.

218. C. Barentin, P. Muller, J. F. Joanny, *Macromolecules* **1998**, *31*, 2198.

219. C.Barentin, J. F. Joanny, *Langmuir* **1999**, *15*,

220. T. J. Su, D. A. Styrkas, R. K. Thomas, F. L. Baines, N. C. Billingham, S. P. Armes, *Macromolecules* **1996**, 29, 6892.

221. S. W. An, T. J. Su, R. K. Thomas, F. L. Baines, N. C. Billingham, S. P. Armes, J. J. Penfold, *Phys.Chem. B* **1998**, 102, 387.

222. S. W. An, T. J. Su, R. K. Thomas, F. L. Baines, N. C. Billingham, S. P. Armes, J. J. Penfold, *Phys. Chem. B* **1998**, 102, 5120.

223. Y. Tran, P. Auroy, L. T. Lee, *Macromolecules* **1999**, 32, 8952.

224. Y. Tran, P. Auroy, L. T. Lee, M. Stamm, *Phys. Rev. E* **1999**, 60, 6984.

225. E. Mouri, C. Wahnes, K. Matsumoto, H. Matsuoka, H. Yamaoka, *Langmuir* **2002**, 18, 3865.

226. E. Mouri, K. Matsumoto, H. Matsuoka, *J. Appl. Crystallogr*. **2003**, 36, 722.

227. E. Mouri, Y. Furuya, K. Matsumoto, H. Matsuoka, *Langmuir* **2004**, 20, 8062.

228. E. Mouri, P. Kaewsaiha, K. Matsumoto, H. Matsuoka, N. Torikai, *Langmuir* **2004**, 20, 10604.

229. E. Mouri, H. Matsuoka, *Encyclopedia of Nanoscience and Nanotechnology*, Marcel Dekker: New York, **2004**, pp 2519-2529.

230. C. Peetla, K. Graf, J. Kressler, *Colloid and Polymer Science* **2006.**

231. B.B. Sauer, H. Yu, *Macromolecules,* **1989**, 22, 786.

232. S. M. Baker, K. A. Leach, C. E. Devereaux, D. E. Gragson, *Macromolecules* **2000**, 33, 5432-5436.

233. C. A. Devereaux, S. M. Baker, *Macromolecules* **2002**, 35, 1921-1927.

234. F. Atsuhiro, A. Tohru, N. Hiro, *J Colloid Interface Sci*. **2002**, 247:351

235. J. E. Mark, Ed *Physical properties of Polymers Handbook*, AIP press, Woodbury (NY), **1996**.

236. X. Li, A. Aoki, T. Miyashita, *Langmuir* **1996**, 12, 5444.

237. L. G. Parratt, *Phys. Rev.* **1954**, 95, 359.

238. Braslau, A., Deutsch, M., Pershan, P.S., Weiss, A.H., Als-Nielsen, J., Bohr, J. *Phys. Rev. Lett*. **1985**, 54, 114–117.

239. V. M. Nace, J. Am. Oil Chem. Soc., 1996, 73, 1. 5 G.-E. Yu, Y.-W. Yang, Z. Yang, D. Attwood, C. Booth and V. M. Nace, *L angmuir*, **1996**, *12*, 3404.

240. Y.-Z. Luo, C. V. Nicholas, D. Attwood, J. H. Collett, C. Price and C. Booth, *Colloid Polym. Sci*., **1992**, *270*, 1094.

241. A. D. Bedells, R. M. Arafeh, Z. Yang, D. Attwood, J. C. Padget, C. Price and C. Booth, *J. Chem. Soc., Faraday T rans.*, **1993**, *89*, 1243.

242. F. S. Bates, G. H. Fredrickson, *Annu. Rev. Phys. Chem.* **1990**, *41,* 525.

243. M. J. Fasolka, A.M. Mayes *Annu. Rev. Mater. Res.* **2001,** *31,* 323.

244. I. W. Hamley 1998 *The Physics of Block Copolymers* (Oxford: Oxford University Press).

245. I. W. Hamley, E.L. Hiscutt, Y. W. Yang, C. Booth C, *J. Colloid Interface Sci.* **1999** *209,* 255.

246. R. Limary, P.F. Green, *Langmuir,* **1999,** *15***,** 5617.

247. A. Boker, A.H.E Müller, G. Krausch, *Macromolecules,* **2001,** *34***,** 7477.

248. P. Müller-Buschbaum, J.S. Gutmann, M. Stamm *Phys. Chem. Chem. Phys.* **1999,** *1,* 3857.

249. G. Kim, M. Libera *Macromolecules,* **1998***, 31,* 2670.

250. Zhu J, Eisenberg A, Lennox RB, *Langmuir,* **1991,** 7, 1579.

251. Raju F, Andrew MS, Stephen RC, Jennifer LL, Royale SU, Stephanie ADT, Yves G, Randolph SD, *Macromolecules,* **2002,** 35, 6483.

252. Peleshanko S, Jeong J, Gunawidjaja R, Tsukruk VV *Macromolecules,* **2004,** *37,* 6511.

253. L. L. Jennifer, M. Pascal, D. Brian, M.S. Andrew, S.S. Sergei, F. Raju, T. Daniel, G. Yves, S.D. Randolph, *Langmuir,* **2005,** *21* 3424.

254. L. L. Jennifer, M. Pascal, T. Daniel, G. Yves, S.D. Randolph, *Langmuir* **2005,** *21* 7380.

255. A. Ulman. An Introduction to Ultrathin Organic Films from Langmuir-Blodgett to Self-Assembly, **1991,** Academic Press, NewYork.

256. T. P. Lodge, *Macromol. Chem. Phys*. **2003**, *204*, 265. J. R. Quintana, M. Villacampa, I. Katime, *Polymeric Material Encyclopedia*, J. C. Salamone (Ed.), CRC Press, Boca Raton, FL, 1996, p. 815.

257. Riess, *Prog. Polym. Sci*. **2003**, *28*, 1107.

258. T. Liu, Z. Zhou, C. Wu, V. M. Nace, B. Chu, *J. Phys. Chem. B,* **1998**, *102*, 2875.

259. Z. Tuzar, *Solvents and Self-Organization of Polymer*, NATO ASI series, E: applied sciences, Kluwer Academic Publisher, Dordrecht, **1996**, vol. 327, p. 1.

260. T. Annable, R. Buscall, R. Ettelaie, D. Whittlestone, *J. Rheol*. **1993**, *37*, 695.

261. B. Nystrom, H Walderhaung, F.K Hansen, *J.Phys.Chem*. **1993**, *97* 7743.

262. Y. W. Wang , Z Yang, ZK. Zhou, D. Attwood, C. Booth, *Macromolecules,* **1996**, *29,* 670.

263. E. J Amis, N. hu, T.A.P Seary, T.E. hogen-Esch, M. Yassini, F. Hwang, *Adv.Chem.Ser.* **1996**, *248*, 279.

264. P. Alexandridis and B. Lindman, **(2000)** *Amphiphilic Block Copolymers: Self-assembly and Applications,* Elsevier, Amsterdam.

265. A. J. Ryan, S.-M. Mai, J. Patrick, A. Fairclough, I. W. Hamley and C. Booth, *Phys. Chem. Chem. Phys*, **2001**, *3*, 2961.

266. C. Booth and D. Attwood, *Macromol. Rapid Commun*., **2000**, *21*, 501.

267. V. M. Nace, J. Am. Oil Chem. Soc., 1996, 73, 1. 5 G.-E. Yu, Y.-W. Yang, Z. Yang, D. Attwood, C. Booth and V. M. Nace, *L angmuir*, **1996**, *12*, 3404.

268. Y.-Z. Luo, C. V. Nicholas, D. Attwood, J. H. Collett, C. Price and C. Booth, *Colloid Polym. Sci*., **1992**, *270*, 1094.

269. A. D. Bedells, R. M. Arafeh, Z. Yang, D. Attwood, J. C. Padget, C. Price and C. Booth, *J. Chem. Soc., Faraday T rans.*, **1993**, *89*, 1243.

270. F. S. Bates, G. H. Fredrickson, *Annu. Rev. Phys. Chem*. **1990**, *41,* 525.

271. M. J. Fasolka, A.M. Mayes *Annu. Rev. Mater. Res.* **2001,** *31,* 323.

272. I W Hamley 1998 *The Physics of Block Copolymers* (Oxford: Oxford
University Press).

273. I. W. Hamley, E.L. Hiscutt, Y. W. Yang, C. Booth C, *J. Colloid Interface Sci.*
1999 *209,* 255.

274. R. Limary, P.F. Green, *Langmuir,* **1999,** *15***,** 5617.

275. A. Boker, A.H.E Müller, G. Krausch, *Macromolecules,* **2001,** *34***,** 7477.

276. P. Müller-Buschbaum, J.S. Gutmann, M. Stamm *Phys. Chem. Chem. Phys.*
1999, *1,* 3857.

277. G. Kim, M. Libera *Macromolecules,* **1998***, 31,* 2670.

278. Zhu J, Eisenberg A, Lennox RB, *Langmuir,* **1991,** 7, 1579.

279. Raju F, Andrew MS, Stephen RC, Jennifer LL, Royale SU, Stephanie ADT, Yves
G, Randolph SD, *Macromolecules,* **2002,** 35, 6483.

280. Peleshanko S, Jeong J, Gunawidjaja R, Tsukruk VV *Macromolecules,* **2004,**
37, 6511.

281. L. L. Jennifer, M. Pascal, D. Brian, M.S. Andrew, S.S. Sergei, F. Raju, T.   Daniel,
G. Yves, S.D. Randolph, *Langmuir,* **2005,** *21* 3424.

282. L. L. Jennifer, M. Pascal, T. Daniel, G. Yves, S.D. Randolph, *Langmuir* **2005,**
21 7380.

283. A. Ulman. An Introduction to Ultrathin Organic Films from Langmuir-
Blodgett to Self-Assembly, **1991,** Academic Press, NewYork.

284. Z. Tuzar, *Solvents and Self-Organization of Polymer*, NATO ASI series, E: applied
sciences, Kluwer Academic Publisher, Dordrecht, **1996**, vol. 327, p. 1.

285. T. Annable, R. Buscall, R. Ettelaie, D. Whittlestone, *J. Rheol.* **1993**, *37*, 695.

286. B. Nystrom, H Walderhaung, F.K Hansen, *J.Phys.Chem.* **1993**, *97* 7743.

287. Y. W. Wang , Z Yang, ZK. Zhou, D. Attwood, C. Booth, *Macromolecules,* **1996**,
29, 670.

288. E. J Amis, N. hu, T.A.P Seary, T.E. hogen-Esch, M. Yassini, F. Hwang, *Adv.Chem.Ser.* **1996**, *248*, 279.

289. G. Kim, M. Libera *Macromolecules,* **1998***, 31,* 2670.

290. Zhu J, Eisenberg A, Lennox RB, *Langmuir,* **1991,** 7, 1579.

291. Raju F, Andrew MS, Stephen RC, Jennifer LL, Royale SU, Stephanie ADT, Yves G, Randolph SD, *Macromolecules,* **2002,** 35, 6483.